Different in vitro experimental approaches to treat breast cancer: from combination treatment of olaparib, oxaliplatin and PI3K inhibitor to targeting the mitochondria with a novel Mito-CP derivative HO-5114

PhD Thesis

Kitti Andreidesz

Department of Biochemistry and Medical Chemistry
University of Pécs, Medical School

Interdisciplinary Doctoral School of Medicine
Molecular and Cellular Biochemistry Program
Doctoral School leader and Program leader: Prof. Dr. Ferenc Gallyas
Supervisor: Dr. Krisztina Kovács

2022

CONTENTS

1. ABBREVIATIONS

ANOVA	analysis of variance
ATP	adenosine triphosphate
Bad	Bcl-2 antagonist of cell death
Bcl-2	pro-apoptotic B-cell lymphoma 2
BRCA	breast cancer susceptibility gene
carboxy-H2DCFDA	6-carboxy-2',7'-dichlorodihydrofluorescein diacetate
CDK	cyclin-dependent kinase
CREB	cyclic AMP response element-binding protein
ECAR	extracellular acidification rate
ER	estrogen receptor
ETC	electron transport chain
FBS	fetal bovine serum
FCCP	carbonyl cyanide 4-(trifluoromethoxy)phenylhydrazone
FDA	Food and Drug Administration
FITC	fluorescein isothiocyanate
GSK3	glycogen synthase kinase-3
HER2	human epidermal growth factor 2
HIF	hypoxia-inducible factor
HKII	hexokinase II
HO-5114	hexadecyl (1-oxyl-2,2,5,5-tetramethyl-2,5-dihydro-1H-pyrrol-3-yl) diphenyl phosphonium bromide
HR	hormone receptor
IARC	International Agency for Research on Cancer
IKK	IκB kinase
IRS-1	insulin-receptor substrate-1
JC-1	5,5′,6,6′-tetrachloro-1,1′,3,3′tetraethylbenzimidazolylcarbocyanine iodide
KO	gene knockout
mito-CP	mito-carboxy proxyl
mTOR	mammalian target of rapamycin
MTT	3-(4,5-dimethylthiazol-2-yl)-2,5-diphenyl tetrazolium bromide
NAC	n-acetyl cysteine
NF-κB	nuclear factor kappa-light-chain-enhancer of activated B cells

OCR	oxygen consumption rate
PARP	poly (ADP-ribose) polymerase
PBS	phosphate buffered saline
PDK1	phosphoinositide-dependent kinase-1
PDK2	phosphoinositide-dependent kinase-2
PI	propidium iodide
PI-3,4,5-P3	phosphatidylinositol-3,4,5-trisphosphate
PI-4,5-P2	phosphatidylinositol-4,5-bisphosphate
PI3K	phosphatidylinositol 3-kinase
PKB	protein kinase B
PR	progesterone receptor
PS	phosphatidylserine
PTEN	phosphatase and tensin homolog
RTCA	xCELLigence Real-Time Cell Analysis
ROS	reactive oxygen species
SEM	standard error of mean
SRB	sulforhodamine B
TCA	trichloroacetic acid
TNBC	triple-negative breast cancer
TPP	triphenylphosphonium
VDAC	voltage-dependent anion channel
VEGF	vascular endothelial growth factor

2. INTRODUCTION

Cancer is a leading cause of death worldwide. Based on the GLOBOCAN 2020 estimates of cancer incidence and mortality produced by the International Agency for Research on Cancer (IARC): Worldwide, approximately 19.3 million new cancer cases and 10 million cancer deaths occured in 2020.

In healthy tissues organized signal transduction keeps cell division and apoptosis in balance to maintain the normal function of organs. On the contrary, cancer cells grow and proliferate, while they ignore signals that stop dividing in healthy cells or ignore signals that cause programmed cell death. Cancer is a disease in which some of the body's cells grow uncontrollably forming a malignant tumor. This is possible through the aberrant modification of their secondary signal transduction pathways. While healthy cells stop growing when they encounter other cells, cancer cells can invade nearby areas and spread to other areas of the body. Furthermore, cancerous nodules can express vascular endothelial growth factors (VEGF) that develop blood vessels to grow toward tumors. These blood vessels supply tumors with oxygen and nutrients and remove waste products from tumors, also enabling tumors to rapidly increase in size. When a malignant tumor reaches the fascia and grows out of it, it can spread to other parts of the body. Hence it can invade the vascular system and through the bloodstream some tumorparts can reach other organs forming secondary tumors.

2.1 Steps of tumor formation

In 1988 Bert Vogelstein's studies of various stages of colorectal cancers led him to propose a specific model for human tumorigenesis. He suggested that 'cancer is caused by sequential mutations of specific oncogenes and tumor suppressor genes' (Fearon ER 1987, Fearon ER 1990, Vogelstein B 1988). According to clinical and histopathological studies most malignant colorectal tumors (carcinomas) were previously monoclonal benign tumors (adenomas) (Fearon ER 1990; Fearon ER 1987) derived from a single pocket of epithelial stem cells through clonal expansion. (Healthy colonic epithelium is polyclonal, having arisen from numerous stem cells.) Thus, tumor progenitor pockets are mostly a group of monoclonal cells, however later further mutations may occur leading to variable genetic features of tumor cells (Ponder BA 1986).

To understand the molecular basis for clonal expansion, we need to study the somatic alterations present at various stages of colorectal tumor formation. Neoplastic alteration provides the cell proliferation advantage, allowing it to outgrow other neoplastic cells within the tissue to become

the predominant cell type constituting the neoplasm. The genetic alteration in neoplastic cells or individual tumor arises coincidentally and may grow further in addition with another changes that manisfest selective growth advantage. However, the same genetic alteration may be presented in many different tumors too (Greaves M 2012).

Generally speaking the first step of carcinogenesis is called initiation. During initiation tumor suppressor gene(s) are losing their function due to KO mutation (Scott RE 1984). The most important tumor suppressor gene is p53. However by the time, later or even preceding initiation the promotion can occur. During promotion proto-oncogenes gain oncogen activating mutations, which cause constitutive active overexpression of those genes, for example Ras, Myc, Myb oncogenes. These key gene expressions are also induced by chemical carcinogens (Budan F 2008, Budan F 2009).

Mutated p53 in mice (Jenkins JR 1984, Eliyahu D 1984, Parada LF 1984; Hinds P 1989) can cooperate with Ras to transform primary rodent cells in vitro, even though the rat cells express wild-type p53 too. Therefore, at the cellular level, p53 gene mutations function as dominant negative (Herskowitz I 1987) rather than recessive mutations. This dominant negative effect is explained by oligomerization of the p53 gene products (Eliyahu D 1988, Kraiss S 1988) while a mutant p53 gene product may inactivate the wild-type gene product by distorting its function (Eliyahu D 1988).

Mitochondrial pathway, as the central executioner of apoptosis, can be hindered by the overexpression of the Bcl-2 protein family that controls mitochondrial membrane permeabilization. Also in the absence of tumor suppressor protein p53 the mitochondrial apoptosis is reduced (Estaquier J 2012). Those two antiapoptotic mutations are also important in the malignant process.

Ultimately, if initiation and promotion occurs in the same cell, then that cell gains the ability to form malignant tumors. This process develops according to the aforementioned further steps, namely progression, invasion and metastasis formation (Fearon ER 1990).

Immune evasion develops during tumor progression. Inflammatory biomarkers are playing a crucial role in this process as well as further mutations of cell surface biomarkers (Gonzalez H 2018).

In summary, in each cancer development both clonal expansion and several mutations take part in malignant transformation, which are corresponding to aberrant secondary signal transduction pathways of an initialized cell. Therefore several therapeutic approaches may be applied, theoretically by influencing each signal transductor factor to normalize cell functions.

2.2 Breast cancer statistics

Previously, lung cancer was the most commonly diagnosed cancer, but it was surpassed by female breast cancer this year with 2.3 million new cases. Although lung cancer remained the leading cause of cancer death with 18 % of the total cancer deaths, female breast cancer increased to 6.9 % (Sung H 2021). Worldwide, breast cancer is the most common cancer in women, accounting for about 30 % of female cancers and has a 15 % mortality-to-incidence ratio (Loibl S 2021, Waks AG 2019).

In total, over 1 800 000 cancer cases was estimated for the year 2020 in the USA, from that the more than 279 000 characterized as breast cancer. The expected number of cancer deaths was estimated to be above 606 000, where breast cancer accounts for more than 42 000 deaths (Siegel RL 2020).

In Hungary approximately 32 000 people died of cancer in 2020. From that around 2 000 was caused by breast cancer. With this number it is the second most common cancer death in the country after lung cancer. There are around 8 000 new cases each year (GLOBOCAN 2020 pdf).

Breast cancer incidence is higher in high-income regions (highest in Western Europe and the US) than in lower income regions (lowest in Africa and Asia). These data reflect the use of breast cancer screening and the higher prevalence of breast cancer risk factors which includes obesity, alcohol intake, low physical activity, smoking, use of menopausal hormone therapy, high total lifetime number of menstrual cycles and use of oral contraceptives (Torre LA, 2016). Although the trend line of the incidence is rising or stable in different countries, mortality rates have been decreasing in many high-income regions since 1990, but it continues to increase in lower-income countries. It is likely due to the fact that in high-income countries there are an increased awareness and screening possibilities which means an early diagnosis, but in low-income regions breast cancer is often diagnosed at a later stage due to limited access to early detection program and treatment and for this reason, it is associated with poorer survival (Allemani C 2015).

The 5-year survival rate varies from 80 % or more in developed countries, while in low-income regions it can be less than 40 %. Survival rate is also influenced by the stage of the cancer, the age of the patient and the early detection as well (Maajani K 2019).

In general, a significant increase in breast cancer mortality rate in the world during the past 25 years occured due to increase in incidence and prevalence of this cancer. The increasing trend is an alarm for health policy makers in all countries, especially in developing countries and low-

income regions which experienced sharp slopes of breast cancer mortality rate (Azamjah, 2019).

2.3 Molecular pathology of breast cancer

Breast cancer classification systems have been based on histopathological assessment but nowadays these systems are augmented with the status of estrogen receptor (ER) and progesterone receptor (PR) expression and human growth factor receptor 2 (HER2) amplification (Vuong D 2014).

ER, PR and HER2 are the only three biomarkers used in routine pathological assessment of breast cancer. ER was identified in the 1960s and its status has been used since the mid-1970s to predict tumor responsiveness to endocrine therapy. Estrogen acts through its receptor and starts a cascade which ends in the dimerisation and translocation of estrogen responsive elements in gene promoter regions and modulates transcription thereby it can enhance cell survival and proliferation. Growth factors such as HER2 and cyclin/CDK complexes influence the action of ER. ER positive (ER+) tumors account for about 75 % of all breast cancer cases (Voung D 2014, Rakha EA 2010).

As PR is an estrogen-regulated gene, its expression indicates a functioning ER pathway. PR+ tumors account for 55-65 % of breast cancer cases and around 40 % of ER+ tumors are PR negative (PR-) (Rakha EA 2010).

Tumors with expression of either ER or PR in at least 1 % of tumor cells are categorized as hormone receptor positive (HR+) (Hammond ME 2010). The molecular pathogenesis of HR+ breast cancer is mediated by ER which activates oncogenic growth pathways (for example phosphatidylinositol 3-kinase (PI3K) - protein kinase B (Akt) pathway, extracellular-signal-regulated kinase (ERK) signaling pathway) (Chen GG 2008, Collins P 1999). HR+ represents about 70 % of all cases (Waks AG 2019).

HER2 is a transmembrane receptor tyrosine kinase in the epidermal growth factor (EGF) receptor family. HER2 signaling activates different pathways such as the RAS pathway, the PI3K-Akt pathway and mitogen-activated protein kinase (MAPK) pathway, indicating the activation of proliferation, cell survival and metastasis (Harbeck 2019). HER2 protein occurs with an amplified gene pattern in 15 – 20 % of the cases (Waks AG 2019). HER2 amplification was associated with disease relapse as a predictor of poor prognosis (Rakha EA 2010), but since the development of anti-HER2 targeted therapy, HER2+ cases show better prognosis (Buonomo OC 2017). About half of HER2+ tumors are also HR+ (Waks AG 2019).

Triple negative breast cancer (TNBC) is characterized by the lack of expression of ER, PR and HER2 genes and it represents about 15 % of all cases (Yao H 2017). TNBC is associated with poorer prognosis and limited targeted therapeutic options compared to the HR+ subtype (Masoud V 2017). Nevertheless nowadays, according to my best knowledge, the molecular pathogenesis of TNBC is poorly understood.

2.4 Treatment options of breast cancer

Management of early (nonmetastatic) and advanced (metastatic) breast cancer are different (Waks AG 2019). In case of the former, women who are deemed operable undergo surgery. Therapeutic options are based on tumor burden and subtype (Harbeck N 2019). The primary systemic therapy for HR+/HER2- breast cancer is endocrine therapy for 5 years. Tamoxifen has been the gold standard for endocrine treatment for more than 25 years. It is a selective estrogen receptor modulator that inhibits the binding of estrogen to its receptor. Aromatase inhibitors are also applied, they act by inhibiting the conversion of androgens to estrogen (Joshi H 2018). In some cases endocrine therapy is augmented with chemotherapy. Anthracycline-taxane sequence or docetaxel and cyclophosphamide are the options. Triple-negative breast cancer is treated with chemotherapy only, with anthracycline and taxanes, with or without carboplatin (Loibl S 2021). In the management of HER2+ breast cancer most patients receive trastuzumab plus pertuzumab, in addition to doxorubicin-cyclophosphamide followed by taxane, or in addition to docetaxel-carboplatin. Trastuzumab and pertuzumab are monoclonal antibodies. The former targets the extracellular domain of HER2, the latter the HER2 dimerization domain. Radiation therapy can be part of the treatment, it may be delivered to the whole breast, a portion of the breast, the chest wall and the regional lymph nodes (Harbeck N 2019, Loibl S 2021, Waks AG 2019).

Management options for metastatic HR+/HER2- breast cancer are endocrine therapy incorporated with cyclin-dependent kinase (CDK) 4/6 inhibitors and if resistance develops chemotherapy is applied. In metastatic triple-negative breast cancer the only option is chemotherapy if patients don't have germline BRCA1/2 mutations. PARP inhibitors are additional therapy options in HR+/HER2- and triple-negative breast cancer patients with BRCA1/2 mutations. In HER2+ metastatic breast cancer it is crucial to continue blocking the HER2 pathway with trastuzumab and pertuzumab and chemotherapy is also part of the treatment (Maughan KL 2010, Harbeck 2019).

2.5 PARP inhibition and olaparib

The first poly(ADP-ribose) polymerase enzyme was discovered over 50 years ago. By 1980 it was known that PARP-1 is activated by DNA damage and has an important role in the repair of DNA single-strand breaks (SSB) via the base-excision repair/single-strand break repair (BER/SSBR) pathway (Benjamin RC 1980, Drew Y 2015). Today 17 members of the PARP family are known and in DNA repair PARP-1 and PARP-2 play crucial roles. Beside DNA repair they have essential functions in replication, gene expression and maintenance of genomic instability (Drew Y 2015).

PARP catalyzes the transfer of ADP-ribose of NAD^+ to a wide range of proteins. Nowadays more than 30 substrates of PARP have been identified. It binds to specific DNA sequences, and by self-ADP-ribosylation, it recruits repair machinery to the site of DNA damage (Morales J 2014).

The development of PARP inhibitors started in the 1980s with 3-aminobenzamide (3-AB) (Purnell MR 1980). The first idea was to use it as a chemosensitizer with methylating agent and expecting an enhanced cytotoxic effect (Durkacz 1980). Olaparib (Lynparza) is the most widely used PARP inhibitor in clinical therapy nowadays. In 2014 the Food and Drug Administration (FDA) approved its application as a single agent in the treatment of germline breast cancer susceptibility gene (BRCA)-mutated advanced ovarian cancer that has received three or more prior lines of chemotherapy. In 2018 olaparib was approved for the treatment of germline BRCA-mutated metastatic breast cancer. In 2019 the PARP inhibitor was approved for the maintenance treatment of adults with germline BRCA-mutated metastatic pancreatic adenocarcinoma (Turk AA 2018).

The reason for using a PARP inhibitor for BRCA-mutated cancer is that in cells lacking homologous recombination repair (HRR) - those with BRCA mutations - DNA breaks will be left unrepaired if PARP inhibitor is applied resulting in cell death. However in cells with functional HRR PARP inhibition won't result in cell death (Drew Y 2015).

2.6 Platinum analogs including oxaliplatin

Cisplatin, carboplatin and oxaliplatin are the currently used platinum analogs in chemotherapy. Cisplatin was discovered through an observation that neutral platinum complexes inhibited division and filamentous growth of *Escherichia coli* (Rosenberg B 1965). FDA approval of cisplatin was given in 1978 for the treatment of advanced testicular, ovarian and bladder cancers. Later studies showed that this platinum compound has major antitumor activity in a

broad range of tumors, including cervix, head and neck, non-small cell and small cell lung cancer (Riddell IA 2018). However there are certain toxic side effects of cisplatin including nephrotoxicity, ototoxicity, peripheral sensory neuropathy and nerve dysfunction (Dasari S 2014).

Several platinum agents were synthesized and investigated to develop less toxic compounds. A second-generation platinum agent, carboplatin was approved by the FDA in 1989, and similarly to cisplatin, it is used in the treatment of a wide range of tumors including bladder cancer, breast cancer, ovarian cancer and non-small cell and small cell lung cancer. Carboplatin exhibits less renal toxicity compared to cisplatin, but it has other side effects: myelosuppression and hepatic dysfunction (Ho GY 2016, Riddell IA 2018).

To reduce the toxicity even more other platinum compounds were synthesized and researched. Oxaliplatin, a third-generation platinum analog, was approved by the FDA in 2002 in the therapy of metastatic colorectal cancer (Wheate NJ 2010). Studies prior showed that colon cancer didn't respond to cisplatin treatment, however response to oxaliplatin was significantly higher (de Gramont A 2000). Other clinical applications of oxaliplatin are in the treatment of gastroesophageal cancer and pancreatic cancer. Side effects of oxaliplatin include myelosuppression and peripheral sensory neuropathy. The mechanism of action and clinical pharmacology of oxaliplatin are identical to those of cisplatin and carboplatin, however tumors that are resistant to cisplatin and carboplatin are not resistant to oxaliplatin. This might explain its effect in the treatment of colorectal cancer (Riddell IA 2018).

Their mechanism of action: once inside the cell these compounds are transported into the nucleus or the mitochondria (Jamieson ER 1999) where they bind at the most nucleophilic sites on DNA and distort and unwind the duplex DNA, triggering cell death (Todd RC 2009). Beside the inhibition of DNA synthesis they can bind to cytoplasmic and nuclear proteins as well, contributing to their cytotoxic effects (Riddell IA 2018).

2.7 Phosphatidylinositol 3-kinase/Akt pathway and PI3K inhibitor LY294002

The phosphatidylinositol 3-kinase (PI3K) signaling pathway plays a key role in the regulation of cell survival and proliferation and they are also involved in differentiation and intracellular trafficking (Grandage VL 2005, Yuan TL 2008). Phosphatidylinositol 3-kinases belong to the lipid kinase family. They can phosphorylate inositol ring 3'-OH group in inositol phospholipids. Class Ia PI3Ks consist of a catalytic subunit and an adaptor/regulatory subunit. While class Ia PI3Ks are activated by receptors with protein kinase activity, class Ib PI3Ks are activated by

receptors coupled with G proteins. Upon activation by growth factor stimulation class Ia proteins catalyze the formation of phosphatidylinositol-3,4,5-trisphosphate (PI-3,4,5-P3), a secondary messenger molecule from phosphatidylinositol-4,5-bisphosphate (PI-4,5-P2). Phosphoinositide-dependent kinase-1 (PDK1) and protein kinase B (PKB/Akt) are recruited by PI-3,4,5-P3 to the membrane (Vara JAF 2004). PDK1 and PDK2 activate Akt by phosphorylation of threonine 308 and serine 473 (Anderson KE 2003). Akt is translocated to the nucleus, where many of its substrates are present (Meier R 1999).

Akt inactivates pro-apoptotic B-cell lymphoma 2 (Bcl-2) family member Bad, procaspase-9, which is an initiator caspase in the apoptosis and Forkhead family of transcription factors that induce the expression of pro-apoptotic factors (e.g. Fas ligand). In addition, Akt activates transcription factor cyclic AMP response element-binding protein (CREB), IκB kinase (IKK) - thereby inducing NF-κB transcriptional activity, which leads to the activation of transcription of different survival genes. P21 and P27 are also phosphorylated by Akt, resulting in the inhibition of their antiproliferative activity. Other targets of Akt include glycogen synthase kinase-3 (GSK3), insulin-receptor substrate-1 (IRS-1) and mammalian target of rapamycin (mTOR).

In recent years, alteration in the PI3K/Akt pathway have been found in a large number of human cancers either with the overexpression of cell surface receptors, or their constitutive activation, thereby the downstream signaling of this pathway being activated as a result (Blume-Jensen P 2001, Osaki M 2004). One of the studied examples is the tyrosine kinase receptor erbB2 (also known as HER2) is overexpressed in many cancers, including breast cancer. Based on the research of Zhou et al. erbB2-erbB3 dimers activate PI3K/Akt pathway in tumor cells (Blume-Jensen P 2001, Zhou BP 2000).

Gene mutations of PIK3CA (Samuels Y 2004), gene amplification of Akt2 (Bellacosa A 1995), overexpression of Akt3 mRNA (Nakatani K 1999) and overexpression of Akt isoforms was demonstrated in breast cancer (Vivanco I 2002). Mutation of PTEN, a PI-3,4,5-P3 phosphatase which negatively regulates the PI3K/Akt pathway has also been promoted in breast cancer (Osaki M 2004).

Uncontrolled activation of Akt can lead to cancer development (Osaki M 2004) and there is strong evidence that the activation of PI3K/Akt pathway is related to tumor cell resistance in chemotherapy and radiation therapy. Thus, inhibiting Akt activation has a potential therapeutic value (Vara JAF 2004).

There are several drugs targeting PI3K/Akt pathway related molecules focusing on either upstream targets like EGFR or HER-2/Neu, downstream targets like mTOR or focus on PI3K (Vara JAF 2004).

A naturally occurring bioflavonoid, quercetin was found to inhibit PI3K, however it also inhibits other kinases for example phosphatidylinositol 4-kinase and several tyrosine and serine/threonine kinases. Analogs of quercetin have been synthesized and evaluated for their ability to inhibit PI3K. LY294002 was found to selectively inhibit PI3K and it has a 2.7-fold greater potency than quercetin (Vlahos CJ 1993).

2.8 Targeting the mitochondria

Mitochondria have become novel targets for anti-cancer strategies, one of the main reasons is that mitochondrial metabolism is a key player in the development and progression of cancer as well as in metastasis (Dong L 2020). In the 1920s, Otto Warburg and colleagues observed the common features of cancer cells' altered metabolism: increased glucose uptake and fermentation of glucose to lactate, even in the presence of oxygen (Warburg O 1925, Liberti MV 2016). Warburg later postulated that cancer originates from irreversible injury to respiration followed by an increase in glycolysis to replace ATP loss due to defective oxidative phosphorylation (Warburg O 1956).

However, oxidative phosphorylation has been recently recognized to play an important role in oncogenesis. Recent studies demonstrated that the mitochondria of cancer cells can alternate between glycolysis and oxidative phosphorylation to meet the metabolic demands of the cell and to promote survival (Dong L 2020). The only tumor cells shown to exhibit mitochondrial dysfunction are those that have mutations in the citric acid cycle enzymes succinate dehydrogenase or fumarate hydratase (Weinberg F 2010).

Although, through aerobic glycolysis the rate of glucose metabolism is higher than by lactate production, the anaerobic processes occur 10-100 times faster (Liberti MV 2016), which gives an advantage when competing for shared and limited energy resources. By switching between aerobic and anaerobic glycolysis tumor cells adapt fast to the changes in the microenvironment (Pfeiffer T 2001).

Based on the above mentioned findings, targeting the mitochondria shows great promise to enhance the efficiency of anti-cancer drugs. Additionally, targeting the mitochondria could mitigate treatment resistance, another crucial factor of today's anti-cancer therapy.

Mitochondria-targeted nanocarriers and drugs conjugated to mitochondria-targeting ligands are the most common approaches (Battogtokh G 2018).

Targeting mitochondrial metabolism includes blocking the electron transport chain (ETC), citric acid cycle and oxidative phosphorylation (Dong L 2020). ETC inhibitors include metformin and tamoxifen. The anti-diabetic drug metformin has shown anti-cancer properties by inhibiting the mitochondrial respiratory complex I and mitochondrial ATP production (Weinberg SE 2015, Wheaton WW 2014), while tamoxifen suppresses mitochondrial complex I-dependent respiration (Jordan VC 1993).

Glutamine plays an important role in replenishing the citric acid cycle intermediates and thereby utilizing them for biosynthesis in cancer cells (Hensley CT 2013). Many cancers show addiction to glutamine. To inhibit its catabolism, specific glutaminase inhibitors were developed, such as tetrahydrobenzo derivative 968 (Wang JB 2010). Isocitrate dehydrogenase 1 and 2 catalyze the conversion of isocitrate to alpha-ketoglutarate. In multiple cancers, both enzymes have been found mutated, they can be potential targets for anti-cancer therapy (Weinberg SE 2015). Inhibitors of the enzymes include dichloroacetate and AGI-5198 (Golub D 2019, Chitneni SK 2018).

FV-429, a hexokinase inhibitor, induced apoptosis in cancer cells not only by inhibiting glycolysis, but by disrupting mitochondrial function. Hexokinase II (HKII) is overexpressed in cancer cells and can bind to the voltage-dependent anion channel (VDAC) on the mitochondrial outer membrane, thereby eliciting anti-apoptotic effects. Hexokinase II inhibition interferes with the HKII-VDAC interaction, which leads to mitochondria-mediated apoptosis (Dong L 2019).

A new perspective of antioxidant design was to transport them directly into the mitochondria, as more than 95 % of cellular ROS are derived from there. However, for conventional antioxidants it is difficult to enter mitochondria and reach the main parts of ROS sites (Wang JY 2020, Sheu SS 2005). To achieve mitochondrial targeting, antioxidants were linked to lipophilic cations (triphenylphosphonium, rhodamine 123) and peptides (mitochondria-penetrating peptide, mitochondria-targeting sequence peptide) (Wang JY 2020, Battogtokh G 2018).

2.9 Lipophilic cations as mitochondria-specific delivery molecules

The advantageous structure of triphenylphosphonium (TPP) has been freqently used in the design of mitochondria-targeted compounds. As TPP is a lipophilic cation, its delocalized positive charge enables the agent to easily permeate lipid bilayers. This is a serious advantage when compared to the transport of hydrophobic compounds, that need tissue-specific carriers. Depending on the mitochondrial membrane potential (−150 to −180 mV) lipophilic cations can achieve efficient uptake and accumulation several hundredfold within the mitochondria (Murphy MP 1997, Smith RA 2003). Selective targeting can be accomplished: cancer cells have higher mitochondrial membrane potential (ΔΨm) than non-cancer cells, also ΔΨm of cancer cells is higher compared to their own cytosol (Zielonka J 2017). After administration, more than 90% of the intracellular lipophilic cations were found to be located in the mitochondria (Smith RA 2003). After oral administration the uptake of TPP-based drugs by the mitochondria was fast and organ-selective; they accumulated within the heart, skeletal muscle, liver, and brain of mice (Smith RA 2003, Porteous CM 2021). By dose determination, it should be taken into consideration that lipophilic cations are toxic at high concentrations, because ATP synthesis is disrupted by excessive uptake of the compound by the mitochondria (Smith RA 2003).
A well-known TPP conjugated compound is Mito-carboxy proxyl (Mito-CP). This TPP conjugated superoxide dismutase mimetic was the first mitochondria-targeted nitroxide compound. It was used for studying the role of the mitochondrial superoxide in cancer cell proliferation (Dhanasekaran A 2005). While in various cancer cells, including breast cancer, the cytotoxic effect of Mito-CP was observed, it didn't markedly affect non-cancerous cells (Cheng G 2012, Boyle KA 2018). Recently, a novel component-derivative of Mito-CP, a pyrroline nitroxide attached dyphenylphosphine compound, hexadecyl (1-oxyl-2,2,5,5-tetramethyl-2,5-dihydro-1H-pyrrol-3-yl) diphenyl phosphonium bromide (HO-5114), was synthesized with promising cytotoxic effect (Isbera M 2021).

2.10 Triple-negative breast cancer and its possible mitochondrial targeting

Recently, the bioenergetics of cancer cells is receiving increased interest among researchers in the field (Schulze A 2012, Reda A 2019). Breast cancer cells have profound bioenergetic, histological, and genetic differences compared to normal cells (Reda A 2019). A recent study showed that inhibiting glycolysis in hormone-responsive breast cancer cells (MCF7) and triple-negative breast cancer cells (MDA-MB-231) had different outcome. The metabolic adaptations of TNBC cells to glycolytic inhibition surpassed that of MCF7 cells. Beside lower apoptotic

rate, greater respiratory capacity and less proton leak was also characteristic for MDA-MB-231 cells. As TNBC cells possess tightly coupled mitochondria, targeting only the glycolysis might not be an effective strategy. These results suggest that the mitochondrial aid-in-reserve must be selectively blocked to achieve greater cytotoxic effect (Reda A 2019).

It is well known that triple-negative breast cancer is associated with a poor prognosis and limited therapeutic options and because mitochondria play pivotal roles in early relapse and the metastatic spread of TNBC the development of novel therapeutic means is needed (Collignon J 2016).

3. OBJECTIVES

In this study, we investigated the response of different types of breast cancer cell lines to:

- a combination of conventional chemotherapeutic agent and synthetic lethality-based therapeutic compound supplemented with Akt inhibition to prevent undesired cytoprotective effects of the latter. We used the TNBC cell line MDA-MB-231 and estrogen and progesterone receptor-positive cell line MCF7, and treated these with the third-generation platinum compound oxaliplatin, the PARP inhibitor olaparib and the PI3K inhibitor LY294002. The triple combination of them is warranted to be examined in vitro to improve further the chemotherapeutic strategies. If in this experiment proper anti-cancer effects can be presented it will pave the way towards in vivo experiments, in order to develop new human chemotherapeutic protocols to improve oncological therapies.

- a novel component-derivative of Mito-CP, a pyrroline nitroxide attached dyphenylphosphine compound, HO-5114. Our goal was to investigate whether the mitochondrial effects of HO-5114 could participate in its cytotoxic and antiproliferative effects. In these experiments MDA-MB-231 and MCF7 cells were used. Based on the results of the study, in vivo research could be added to investigate the toxicity and anti-neoplastic effect of HO-5114 in vivo.

3. MATERIALS AND METHODS

3.1 Reagents

Olaparib(4-(3-{[4-(Cyclopropylcarbonyl)-1-piperazinyl]carbonyl}-4-fluorobenzyl)-1(2H)-phthalazinone) was purchased from MedChemExpress (Monmouth Junction, NJ, United States). It was dissolved in dimethyl sulfoxide (DMSO) before treatment and for each treatment a new solution was made.

Oxaliplatin([SP-4-2-(1R-trans)]-(1,2-Cyclohexanediamine-N,N′)[ethanedioata(2--)-O,O']platinum) was purchased from Accord Healthcare (Munich, Germany). Akt pathway inhibitor LY294002 (2-(Morpholin-4-yl)-8-phenyl-4H-1-benzopyran-4-one) was purchased from Selleckchem (Houston, Texas, USA). Hexadecyl (1-oxyl-2,2,5,5-tetramethyl-2,5-dihydro-1H-pyrrol-3-yl) diphenyl phosphonium bromide (HO-5114) was synthesized and purified by Prof. Tamás Kálai and Mostafa Isbera (Department of Organic and Pharmacological Chemistry, Medical School, University of Pécs, Hungary). All other reagents were of the highest purity commercially available. Chemical structures of the above-mentioned reagents can be seen on Figure 1. Structures were designed using Chemspace software (Chemspace US Inc, Monmouth Junction, New Jersey, USA).

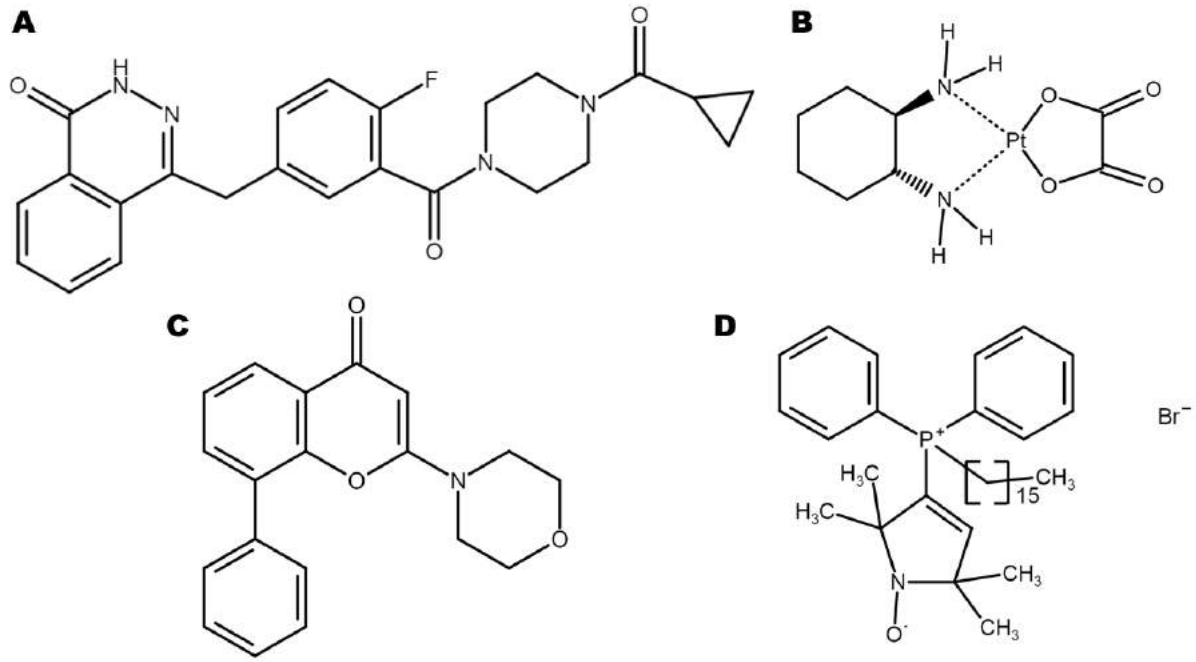

Figure 1. Chemical structure of olaparib (A), oxaliplatin (B), LY294002 (C) and HO-5114 (D)

3.2 Cell Cultures

MCF7 (ER+, PR+, HER2-) and MDA-MB-231 (TNBC) cell lines were purchased from American Type Culture Collection (Manassas, VA, USA). Cells were grown and maintained in a humidified incubator at 37 °C with 5 % CO_2. Estrogen and progesterone receptor-positive MCF7 cells were cultured in RPMI (Biosera, Nuaille, France) supplemented with 10 % fetal bovine serum (FBS). Triple-negative MDA-MB-231 cells were cultured in DMEM Low Glucose (Biosera, Nuaille, France) augmented with 10 % FBS (Thermo Fisher, Life Technologies, Milan, Italy).

3.3 Survival Assay

3-(4,5-dimethylthiazol-2-yl)-2,5-diphenyl tetrazolium bromide (MTT) assay was used to examine cell viability. The assay is dependent on the ability of viable cells to metabolise a water-soluble tetrazolium salt into a water-insoluble formazan product. This reaction is catalyzed by mitochondrial reductase enzyme (Twentyman PR, 1987). Formazan is then solubilized and the concentration determined by optical density at 570 nm. The result is a sensitive assay with excellent linearity up to $\sim 10^6$ cells per well (Kumar P, 2018).
Cells were seeded at a density of 3×10^3/well in 96-well cell culture plates for 24 h before treatment. After 72 h treatment using olaparib (2 μM), oxaliplatin (25 μM) and LY294002 (1 μM), and their combination, the medium was replaced containing 0.5 % MTT substrate (100 μL/well). After 2 h incubation at 37 °C the medium was discarded and DMSO was added (100 μL/well). Given the purple color of the soluble formazan product, absorbance was measured at 570 nm using the GloMax®-Multi Instrument (Promega, Madison, WI, United States).

3.4 SRB Viability Assay

The sulforhodamine B (SRB) assay can be used to measure drug-induced cytotoxicity. The principle of the assay is based on the ability of the protein dye sulforhodamine B to bind electrostatically and pH dependent on protein basic amino acid residues of trichloroacetic acid-fixed cells. Under mild acidic conditions it binds to and under mild basic conditions it can be extracted from cells and solubilized for measurement (Voigt W, 2005).
Cells were seeded at a density of an 8×10^3/well in 96-well cell culture plates 24 h before the treatment. After 24 h of treatment with 1, 2.5, 5, or 10 μM of HO-5114, 1 mM n-acetyl cysteine (NAC), a common ROS scavenger and their combination, the medium was discarded, and the

cells were washed with phosphate buffered saline (PBS; Biowest, Nuaille, France) and fixed in 100 µL of a cold 10 % trichloroacetic acid (TCA) solution (Sigma-Aldrich Co., Budapest, Hungary) for 30 min at 4 °C. After TCA was discarded, the cells were washed with a 1 % acetic acid solution (Sigma-Aldrich Co., Budapest, Hungary) and dried overnight at room temperature. The next day, 70 µL 0.1 % sulforhodamine B (SRB) (Sigma-Aldrich Co., Budapest, Hungary) in a 1 % acetic acid solution was added to the wells for 20 min at room temperature. The plates were washed 5 times with a 1 % acetic acid solution and dried for at least 2 h. Added to the cell was 200 µL of a 10 mM TRIS solution (Sigma-Aldrich Co., Budapest, Hungary) and the samples were incubated at room temperature on a plate shaker for 3 h. Absorbance was measured at 560 and 600 nm simultaneously using the GloMax®-Multi Instrument (Promega, Madison, WI, USA). OD600 was subtracted as the background from the OD560 values.

3.5 Apoptosis Assay using MUSE Cell Analyzer

Live, early apoptotic, late apoptotic and dead cells were quantified using the MUSE Annexin V and Dead Cell Kit (Luminex Corporation, Austin, Texas, United States). The experiment was carried out according to the manufacturer's instructions. Cells were cultured in 6-well plates (1.5×10^5/well) and treated with olaparib (2 µM), oxaliplatin (25 µM) and LY294002 (1 µM) and their combination for 72 h. After the treatment cells were collected and diluted in their medium to a concentration of 5×10^5/mL. Twenty minutes incubation in the dark at room temperature followed the addition of 100 µL Annexin V reagent. The calcium binding protein, Annexin V can bind to phosphatidylserine (PS), which is normally restricted to the inner leaflet of the plasma membrane and is, therefore, only exposed to the cell cytoplasm. During apoptosis PS becomes exposed on the outer leaflet of the plasma membrane and Annexin V can bind to it (Crowley LC, 2016). Annexin V-FITC positive cells were considered as apoptotic (early and late apoptotic) and were expressed as % of the total cell number examined. The MUSE Cell Analyzer device was used to assess the samples and 5000 single cell events were measured per sample.

3.6 Flow Cytometric Analysis of Cell Death

A flow cytometry analysis was applied to quantify the ratio of live, early apoptotic, and late apoptotic/dead cell populations. The cells were seeded into 6-well plates at a starting density of 10^5/well 24 h before they were treated with 1, 2.5, 5, or 10 µM of HO-5114 for 24 h. The FITC-

Annexin V Apoptosis Detection Kit with propidium iodide (PI) (BioLegend, San Diego, CA, USA) was used to label cells according to the manufacturer's instructions. While Annexin V binds phosphatidylserine, PI is a fluorochrome that binds and labels nucleic acids (Crowley LC, 2016, Riccardi C 2006). The samples were measured with a SONY SH800 Cell Sorter (SONY Biotechnology, San Jose, CA, USA). Debris and aggregates had been eliminated by gating, and at least 20000 single cell events were acquired per sample. The analysis was carried out with Cell Sorter Software (SONY Biotechnology, San Jose, CA, USA). Double negative (Annexin V−/PI−) cells were considered live. Annexin V positive (Annexin V+/PI−) and double positive (Annexin V+/PI+) cells were identified as early and late apoptotic, respectively. PI positive (Annexin V−/PI+) necrotic cells were not detected. They were likely eliminated during the washing steps prior to staining.

3.7 Measurement of reactive oxygen species generation

To measure reactive oxygen species (ROS) production, cells were plated (3×10^3/well) in wells of a 96-well plate, were cultured for 24 h and then they were treated for 72 h with olaparib (2 μM), oxaliplatin (25 μM) and LY294002 (1 μM), and their combination. The medium was replaced by Krebs-Henseleit solution containing 2 % FBS and 2 μM carboxy-H2DCFDA (Thermo scientific, Waltham, MA, United States). After 30 min incubation, ROS generation was measured using GloMax®-Multi Instrument (Promega, Madison, WI, United States) at respective excitation/emission wavelengths of 490/530 nm.

For the HO-5114 treatment, the cells were seeded at a starting density of 1.5×10^4/well into 96-well plates and were cultured for 24 h. The cells were treated with 1, 2.5, 5, 10, or 20 μM of HO-5114 in a Krebs-Henseleit solution supplemented with 10 % FBS and containing dihydrorhodamine 123 (Sigma-Aldrich Co., Budapest, Hungary). The assay is based on measuring the fluorescence of rhodamine 123 produced quantitatively from its non-fluorescent reduced form by the cellular ROS. ROS generation was monitored from 0 min until 4 h using the GloMax®-Multi Instrument (Promega, Madison, WI, USA) at respective excitation/emission wavelengths of 490/525 nm.

3.8 Cell Cycle Analysis

Cells were cultured in 6-well plates (1.5×10^5/well) 24 h before treatment, and were treated with olaparib (2 μM), oxaliplatin (25 μM) and LY294002 (1 μM), and their combination, for 72 h. To assess cell cycle, flow cytometry analysis was applied. In brief, cells were harvested,

washed with Dulbecco's phosphate-buffered saline (DPBS) (Biosera, Nuaille, France) and fixed with 70 % ethanol (Molar Chemicals Kft., Halasztelek, Hungary) at 4 °C overnight. After fixation, the cells were centrifuged and washed twice with DPBS. Aliquots of cells (0.5×10^6) were stained with 500 µl propidium iodide (PI) (Merck KGaA, Darmstadt, Germany)/RNAse A (Thermo scientific, Waltham, MA, United States) solution containing 0.02 mg/mL PI and 10 µg/mL RNAse A in PBS-0.1 % Triton-X 100 (Sigma, St. Louis, MO, United States). SONY SH800 Cell Sorter (SONY Biotechnology, San Jose, CA, United States) was used to measure fluorescent intensities. Debris and aggregates had been discriminated by gating, and at least 5000 single cell events were measured per sample. Data were analyzed and cell-cycle distributions were determined using ModFit LT (Verity software House, Topsham, ME, United States) software.

3.9 Measurement of Mitochondrial Bioenergetics

To analyze respiratory and glycolytic energy production, oxygen consumption rate (OCR) and extracellular acidification rate (ECAR) were measured simultaneously by a Seahorse XFp Extracellular Flux Analyzer (Agilent Technologies, Santa Clara, CA, USA). The cells were plated at a starting density of 1.5×10^4/well into Seahorse XFp Cell Culture Miniplates 24 h before treatment. The medium was replaced by the Seahorse XF Assay Media (pH 7.4) containing 10 mM glucose, 2 mM L-glutamine, and 1 mM pyruvate. After measuring the basal respiration for 18 min, HO-5114 was added to the medium at a final concentration of 1 or 2.5 µM and 1 mM NAC and the cells were further incubated for 4 h. In the final 75 min of incubation, recording of OCR and ECAR was resumed, and the following modulators were injected sequentially: oligomycin (1.5 µM final concentration), FCCP (1 µM final concentration), and rotenone and antimycin A (0.5 µM final concentration each). The OCR and ECAR data were normalized to total cellular protein, which was determined by the Micro BCA Protein Assay kit (Thermo Fisher Scientific, Waltham, MA, USA).

3.10 Measurement of Mitochondrial Membrane Potential

The cells were seeded to glass coverslips in 6-well plates at a starting density of 1.5×10^5 cells/well and were cultured for 24 h. They were treated with 1 and 2.5 µM HO-5114 for 1 or 2.5 h for the MCF7 or MDA-MB-231 lines, respectively. After treatment, the cells were washed in PBS and incubated for 15 min at 37 °C in a modified Krebs-Henseleit solution containing 100 ng/mL of the cationic carbocyanine dye JC-1 (5,5′,6,6′-tetrachloro-

1,1′,3,3′tetraethylbenzimidazolylcarbocyanine iodide). Following incubation, the cells were washed once with a modified Krebs-Henseleit solution and then visualized by a Nikon Eclipse Ti-U fluorescent microscope equipped with a Spot RT3 camera using a 20× objective lens and epifluorescence illumination. The same microscopic fields were imaged with a 490 nm bandpass excitation and >590 nm (red) or <546 nm (green) emission filters, consecutively. For quantifying red and green fluorescent intensities, their respective greyscale images were normalized to three randomly chosen spots of their backgrounds. Red and green fluorescent intensities were calculated as the percentage of their sum.

3.11 Colony Formation Assay

The cells were seeded at a starting density of 2×10^3/well into 6-well plates and were cultured for 24 h before they were exposed to 50, 75, 100, or 250 nM of HO-5114 for seven days. For olaparib, oxaliplatin and LY294002 treatment, cell density was 3×10^3/well at the seeding and cells were cultured for 24 h before treatment. After 14 days of treatment with 2 μM olaparib, 25 μM oxaliplatin and 1 μM LY294002, alone and in combination, the cells were washed with PBS and were stained with 0.1 % Coomassie Brilliant blue R 250 (Merck KGaA, Darmstadt, Germany) in 30 % methanol (Sigma-Aldrich Co., Budapest, Hungary) and 10 % acetic acid. The tissue culture plates were imaged using a GE Healthcare ImageScanner II (AP Hungary Co., Budapest, Hungary) set for 600 dpi. The colonies were quantified using ImageJ software.

3.12 Measurement of Invasive Growth

To monitor the effects of olaparib, oxaliplatin, LY294002 and HO-5114 on the growth of MCF7 and MDA-MB-231 cells, we used the xCELLigence system that allows for the real-time, quantitative analysis of adherent cells. The measurement method is based on the use of electronic microtiter plates (E-Plate®), in the xCELLigence Real-Time Cell Analysis (RTCA) device (ACEA Biosciences, San Diego, CA, USA). The instrument measures electron flow transmitted between gold microelectrodes fused to the bottom surface of a microtiter plate in the presence of an electrically conductive culturing medium. Adherent cells cultured in the plates change the impedance expressed as arbitrary units called the cell index, the magnitude of which is dependent on number, morphology, size, and attachment properties of the cells (Hamidi H 2017).

The instrument was placed in a humidified incubator at 37 °C and 5 % CO_2. Cells were seeded at the starting density of 1×10^3/well and were cultured for 24 h. Then, the cells were exposed

to 2 µM olaparib, 25 µM oxaliplatin and 1 µM LY294002, alone and in combination and 75, 100, and 250 nM HO-5114 for seven days in the E-Plate®, during which the impedance was measured each hour.

3.13 Statistical Analysis

The results are presented as the mean and the correlated standard error of the mean (SEM) of at least three independent experiments. The statistical differences between the groups were analyzed by a one-way ANOVA with the Tukey post-hoc test using OriginPro® software (Originlab Corp., Northampton, MA, USA). The differences among the groups were regarded as significant at $p < 0.05$.

4. RESULTS I - Olaparib, oxaliplatin, LY294002 and their combination treatment on MDA-MB-231 and MCF7 cells

4.1 Effect of olaparib, oxaliplatin and LY294002 on cell viability

To determine the effect of olaparib, oxaliplatin and LY294002 alone and in combination on the viability of MDA-MB-231 and MCF7 cells, MTT assay was performed. As shown in Figure 2A,C, the PARP inhibitor olaparib alone did not decrease viability significantly in either cell line. The viability of MDA-MB-231 reached more than 90 % and for the MCF7 cells this value was over 80 %. However, the platinum drug oxaliplatin reduced viability of the TNBC line MDA-MB-231 to approximately 60 % substantially and, more pronouncedly, the estrogen and progesterone receptor-positive non-TNBC line MCF7 where viable cell make up around 40 %. Although there are several articles implying synergy between PARP inhibitors and platinum compounds (Cseh AM 2019, Mann M 2019, Rottenberg S 2008) our results show that olaparib and oxaliplatin had neither a synergistic, nor an additive effect at the applied concentrations, since their combination caused about the same extent of cell death as oxaliplatin alone (Figure 2).

More than 95 % of MDA-MB-231 cells were viable after LY294002 treatment, indicating that the TNBC cells were resistant to the Akt pathway inhibitor (Figure 2B).

In contrast, LY294002 caused a significant amount of cell death (~50 %) in the MCF7 cell line (Figure 2D). While the cytotoxic effect of oxaliplatin was enhanced by LY294002 in both cell lines, this effect was not observed in the olaparib treatment. Furthermore, addition of the PARP inhibitor to the co-treatment of oxaliplatin and LY294002 didn't increase cell death in MDA-MB-231 and MCF7 (Figure 2B,D).

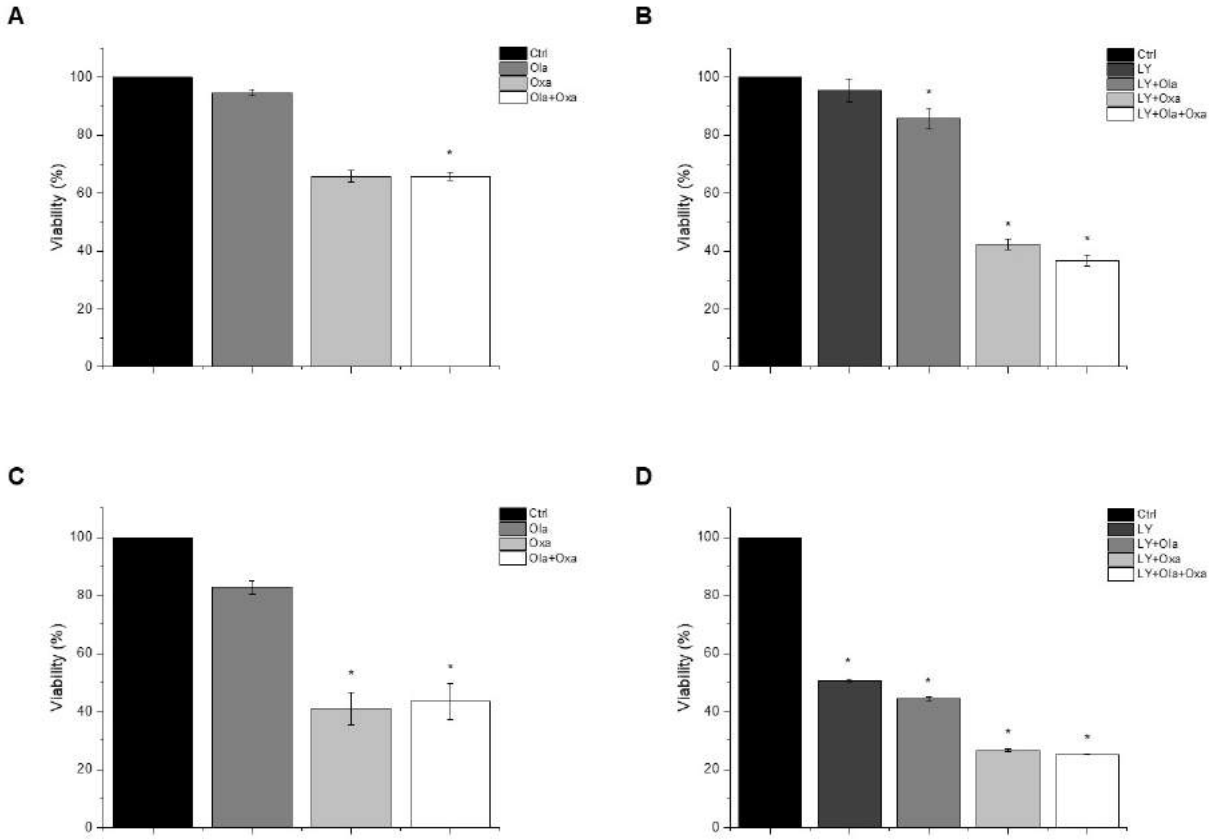

Figure 2. The effects of Ola, Oxa and LY on the viability of TNBC MDA-MB-231 (**A**,**B**) and non-TNBC MCF7 (**C**,**D**) cells were evaluated by MTT assay. Cells were treated with 2 μM olaparib, 25 μM oxaliplatin, 1 μM LY294002 alone and in combination for 72 h. Data are shown as mean ± SEM of at least three separate experiments. * $p < 0.05$ compared with the untreated cells. Ola—olaparib; Oxa—oxaliplatin; LY—LY294002; TNBC—triple-negative breast cancer; MTT-3-(4,5-dimethylthiazol-2-yl)-2,5-diphenyltetrazolium bromide.

4.2 Effect of olaparib, oxaliplatin and LY294002 on cell death processes

Flow cytometry was performed to examine which type of cell death olaparib, oxaliplatin and LY294002 elicited. Flow cytometric measurements were performed after double-staining the treated cells with fluorescently labelled Annexin V and propidium iodide, to demonstrate apoptosis and necrosis, respectively. We found that less than 5% of cell death caused by the compounds investigated was necrotic, and most of the dying cells were in their early apoptotic stage under the experimental conditions we used (Figure 3). The olaparib treatment did not generate apoptosis in the breast cancer cell lines, as live cell ratio of both cells was approximately 82 % (Figure 3A,C). Oxaliplatin significantly increased early apoptosis in both cell lines, late apoptosis also increased in MDA-MB-231 and MCF7 cells, significantly in the MCF7 cells (Figure 3A, C). LY294002 alone caused about the same level of apoptosis in both cell lines as olaparib did (Figure 3C,D). On the other hand, treatment of the cells with LY294002 together with olaparib, oxaliplatin or their combination did not significantly change

the distribution of cells among live, early, and late apoptotic populations in either of the cell lines (Figure 3C,D).

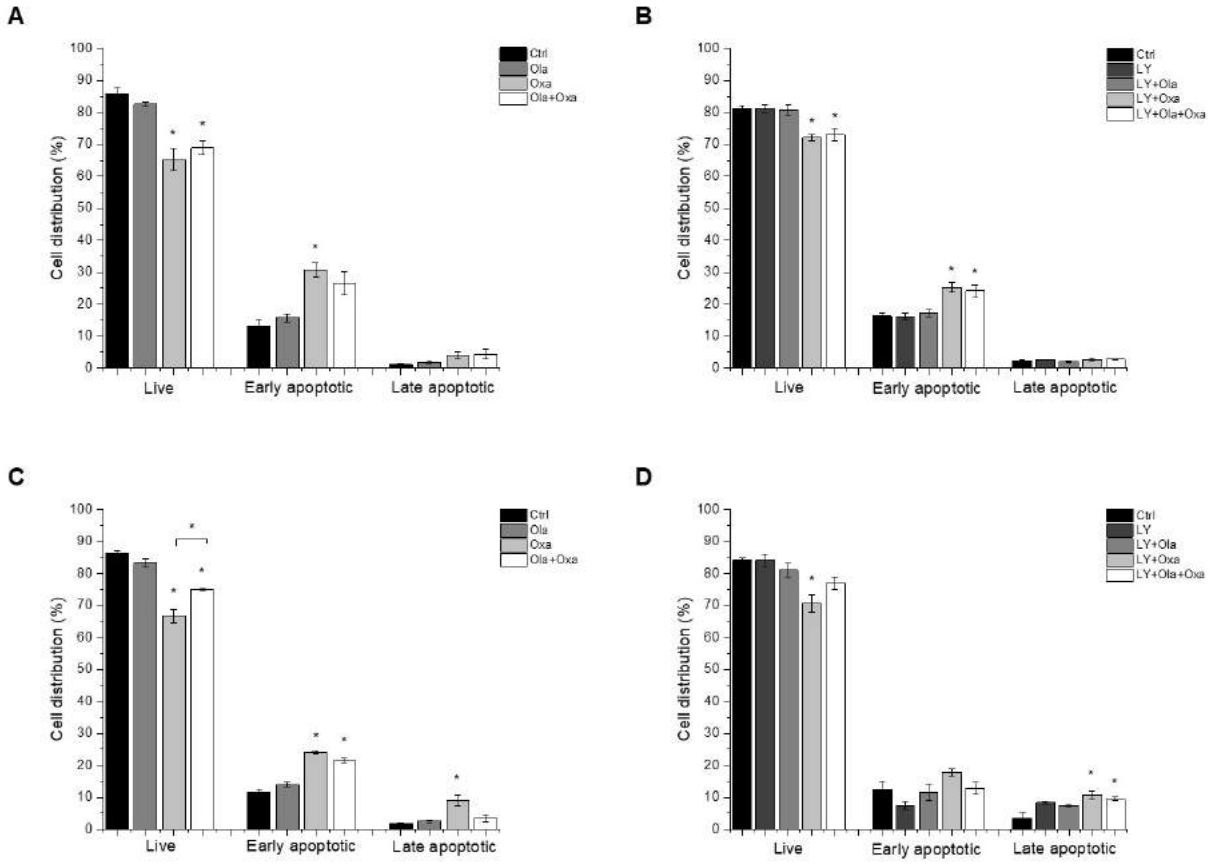

Figure 3. The effects of Ola, Oxa and LY on MDA-MB-231 (**A**,**B**) and MCF7 (**C**,**D**) cell apoptosis were detected by MUSE Cell Analyzer using MUSE Annexin V and Dead Cell Kit after 72 h treatment with 2 µM olaparib, 25 µM oxaliplatin, 1 µM LY294002 alone and in combination. Results are shown as mean ±SEM of at least three separate experiments. * $p < 0.05$ compared with the untreated cells. Ola—olaparib; Oxa—oxaliplatin; LY—LY294002.

4.3 Effect of olaparib, oxaliplatin and Akt pathway inhibitor on ROS production

The ROS generation capacity of olaparib, oxaliplatin and LY294002 was measured using a carboxy-H2DCFDA assay. ROS can oxidize the non-fluorescent dye yielding its fluorescent form, which intensity can be measured. Marked differences were found between MDA-MB-231 (Figure 4A,B) and MCF7 (Figure 4C,D) lines among the treatment groups. Olaparib increased ROS production in MCF7 cells, although the effect did not reach a statistically significant level (Figure 4C). In contrast, the drug did not induce any ROS production in MDA-MB-231 cells (Figure 4A). Oxaliplatin caused significant ROS production in the triple-negative breast cancer cells which was enhanced by olaparib co-treatment, although olaparib's enhancing effect did not reach a statistically significant level (Figure 4A). The Akt pathway inhibitor did not affect ROS production either alone or in any combination with olaparib and

oxaliplatin (Figure 4B). On the other hand, oxaliplatin did not affect ROS production of MCF7 cells and attenuated ROS production induced either by olaparib (Figure 4C), LY294002, or their combination (Figure 4D). However, these negative effects of oxaliplatin did not reach a statistically significant level. The Akt pathway inhibitor alone induced a similar level of ROS production in MCF7 cells as that caused by olaparib (Figure 4D).

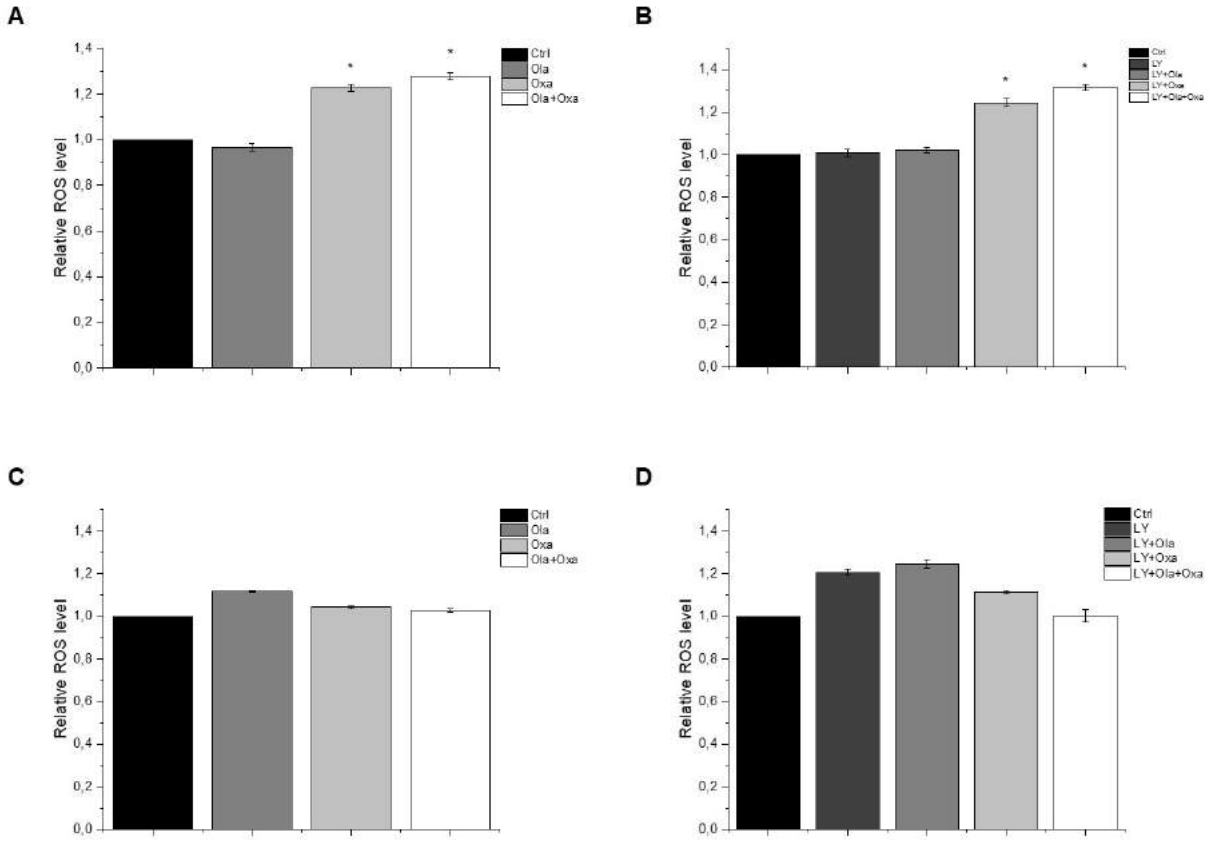

Figure 4. Effects of Ola, Oxa and LY on ROS production by MDA-MB-231 (**A**,**B**) and MCF7 (**C**,**D**) cells treated with 2 µM olaparib, 25 µM oxaliplatin and 1 µM LY294002. Results are shown as mean ±SEM of at least three separate experiments. *$p < 0.05$ compared with the untreated cells. Ola—olaparib; Oxa—oxaliplatin; LY—LY294002.

4.4 Effect of olaparib, oxaliplatin and Akt pathway inhibitor on the cell cycle

Flow cytometry was used to determine which cell cycle phase the cells had reached after treatment with different combinations of olaparib, oxaliplatin and LY294002. The distribution of control MDA-MB-231 cells among G1, S and G2/M phases was 55.57%, 22.8% and 21.63%, respectively, which was not affected by the PARP inhibitor olaparib (Figure 5A,C), the Akt pathway inhibitor LY294002, or their combination (Figure 5B,D). In contrast, oxaliplatin treatment arrested the cells in the S phase of their cycle (Figure 5C) which was not affected by olaparib co-treatment (Figure 5C). However, LY294002 co-treatment attenuated oxaliplatin's

arresting effect, which was further reduced when olaparib was included in the combination treatment (Figure 5D).

The cell cycle phase distribution of control MCF7 cells was slightly different from that of MDA-MB-231 cells. Approximately 51.26% of control cells were in G1; 28.64% in S and 20.1% were in G2/M phase (Figure 5E,G). As with the MDA-MB-231 line, oxaliplatin arrested MCF7 cells in the S phase of their cycle (Figure 5G) and olaparib co-treatment did not have any further effect on it (Figure 5G). However, the PARP inhibitor increased the number of G2/M phase cells at the expense of S phase, although this effect did not reach a statistically significant level (Figure 5G). Additionally, LY294002 significantly enhanced the number of G1-phase cells at the expense of S and G2/M phase cells. This effect was not affected by olaparib co-treatment but was significantly counteracted by oxaliplatin (Figure 5H).

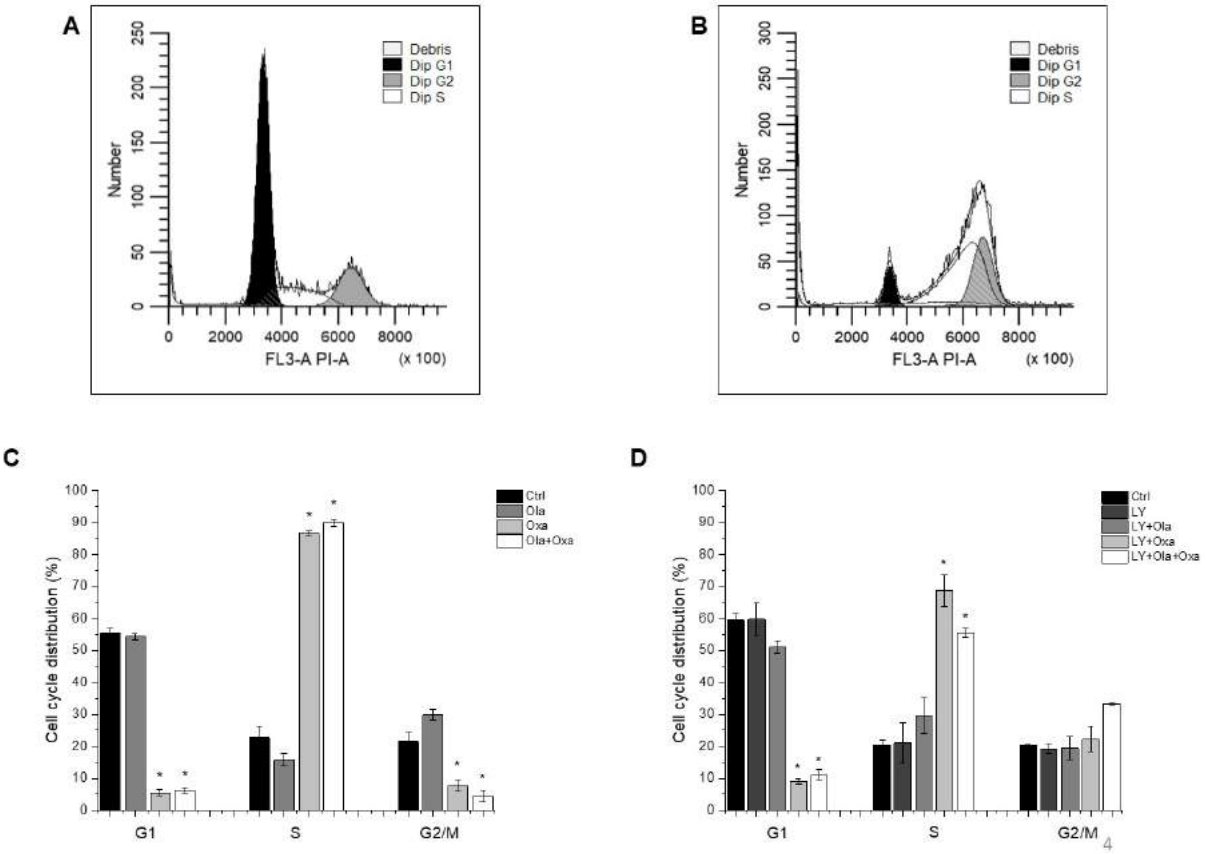

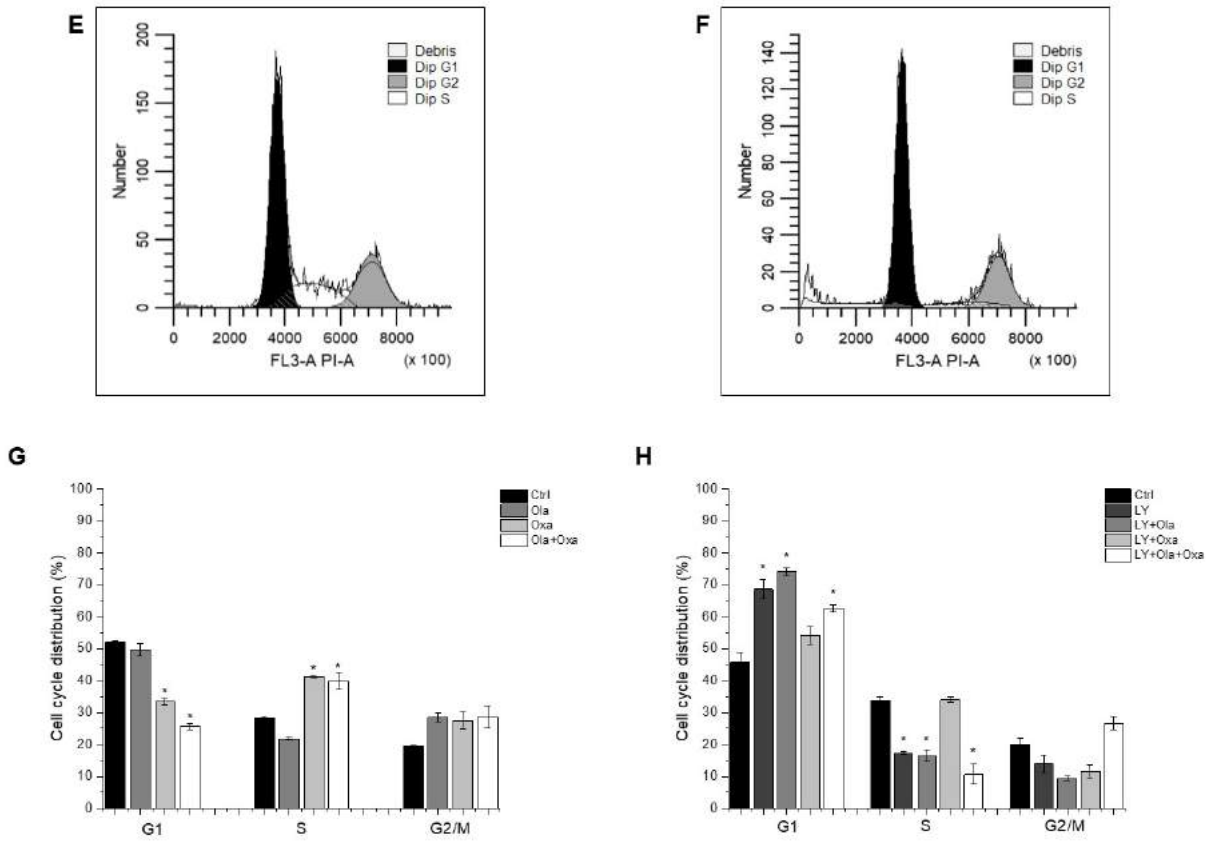

Figure 5. Flow cytometry analysis of MDA-MB-231 (**A**–**D**) and MCF7 (**E**–**H**) cell-cycle distribution. Cells were cultured and treated for 72 h with 2 μM olaparib, 25 μM oxaliplatin and 1 μM LY294002 alone and in combination. The cell-cycle distribution was determined with propidium iodide staining. The histograms show cell-cycle phases of control cells (**A**,**E**) and cells treated with combination of olaparib, oxaliplatin and LY294002 (**B**,**F**). The bar charts represent effect of single and combined treatment on cell cycle phase distribution (**C**,**D**,**G**,**H**). Results are expressed as mean ±SEM of at least three separate experiments. * $p < 0.05$ compared with the untreated cells.

4.5 Effect of olaparib, oxaliplatin and Akt pathway inhibitor on colony formation

Colony formation assay was performed to assess cellular proliferation capacity. Olaparib and oxaliplatin significantly decreased colony numbers of both cell lines, although the non-TNBC line MCF7 was more sensitive to the cytostatic drugs than the TNBC line MDA-MB-231 (Figure 6A,C). Furthermore, oxaliplatin attenuated colony formation to a much greater extent than olaparib did (Figure 6A,C). A combination of olaparib and oxaliplatin caused a similar decrease in colony formation as oxaliplatin did alone (Figure 6A,C), indicating a lack of synergy, even additivity, between the two substances. LY294002 alone decreased colony formation to about the same extent as olaparib did in MDA-MB-231 cells (Figure 6A,B). In case of MCF7 cells LY294002 caused an even greater decrease in colony numbers compared to olaparib treatment (Figure 6C,D). The PARP inhibitor and to a greater extent, oxaliplatin both augmented the Akt pathway inhibitor's effect on colony formation (Figure 6B,D). Again,

the combination of olaparib and oxaliplatin had about the same effect as the latter alone (Figure 6B,D).

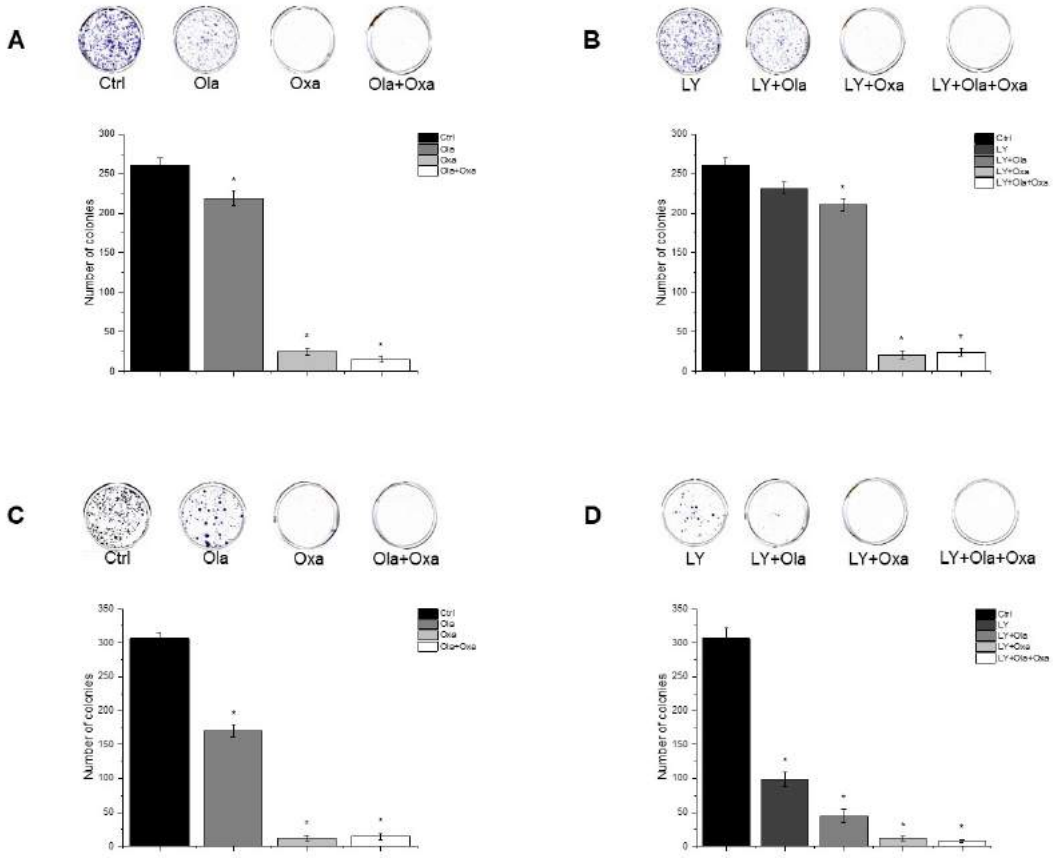

Figure 6. Effects of Ola, Oxa and LY on colony formation by MDA-MB-231 (**A**,**B**) and MCF7 (**C**,**D**) cells. Cells were seeded in six-well plates and after one day treated with 2 μM olaparib, 25 μM oxaliplatin, 1 μM LY294002 alone and in combination. Cells were treated for 14 days before being stained with Coomassie Blue. Results are shown as mean ± SEM of at least three separate experiments. * $p < 0.05$. Ola—olaparib; Oxa—oxaliplatin; LY—LY294002

4.6 Effect of olaparib and oxaliplatin on invasive growth

Invasive growth of the cell lines was assessed by the xCelligence Real-Time Cell Analysis (RTCA) system. As with the colony formation experiments, olaparib and, to a much greater extent, oxaliplatin decreased invasive growth in both cell lines (Figure 7). Again, MCF7 line was more sensitive to the PARP inhibitor and to the cytostatic drugs than MDA-MB-231, and combination of the two drugs had about the same effect as oxaliplatin alone had (Figure 7).

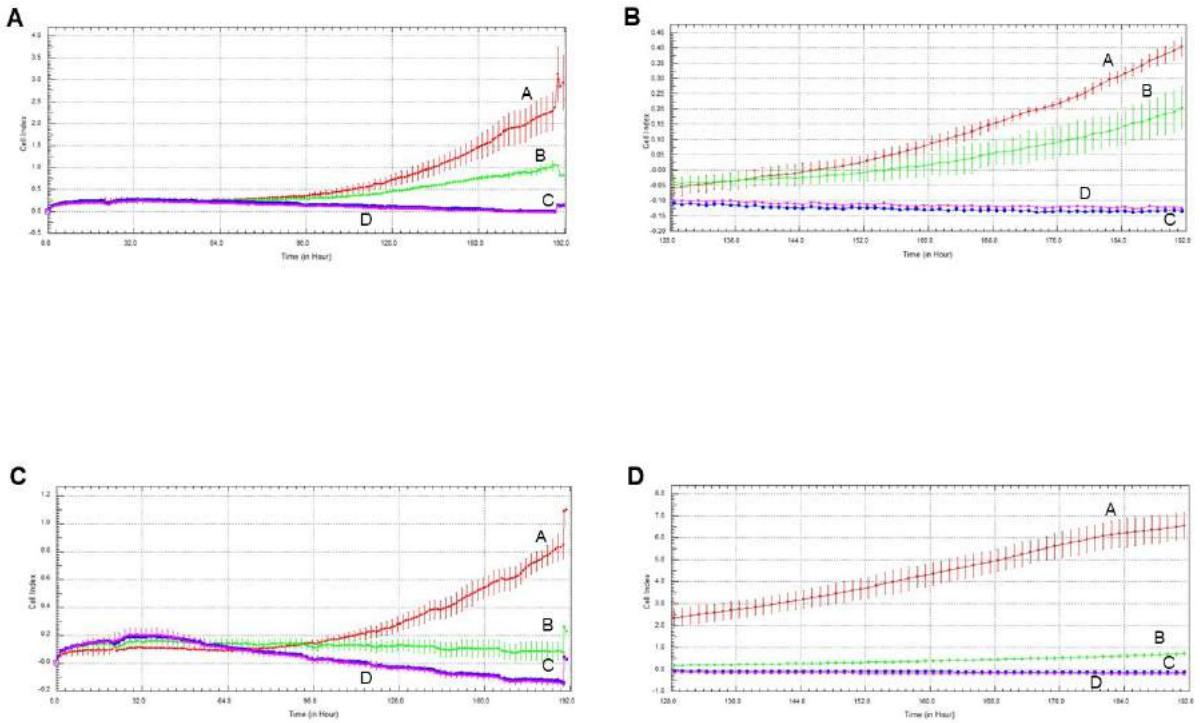

Figure 7. Effect of olaparib and oxaliplatin on invasive growth of MDA-MB-231 (**A**) and MCF7 (**B**) cells treated with 2 µM olaparib and 25 µM oxaliplatin. Line A—control, Line B—2 µM olaparib treatment, Line C—25 µM oxaliplatin treatment, Line D—combination treatment.

4.7 Effect of olaparib, oxaliplatin and Akt pathway inhibitor on invasive growth

The Akt pathway inhibitor decreased invasive growth, and its effect on MCF7 cells was more pronounced than on MDA-MB-231 cells (Figure 8). Both olaparib and oxaliplatin treatment augmented LY294002′s effect, decreasing invasive growth to the detection limit (Figure 8).

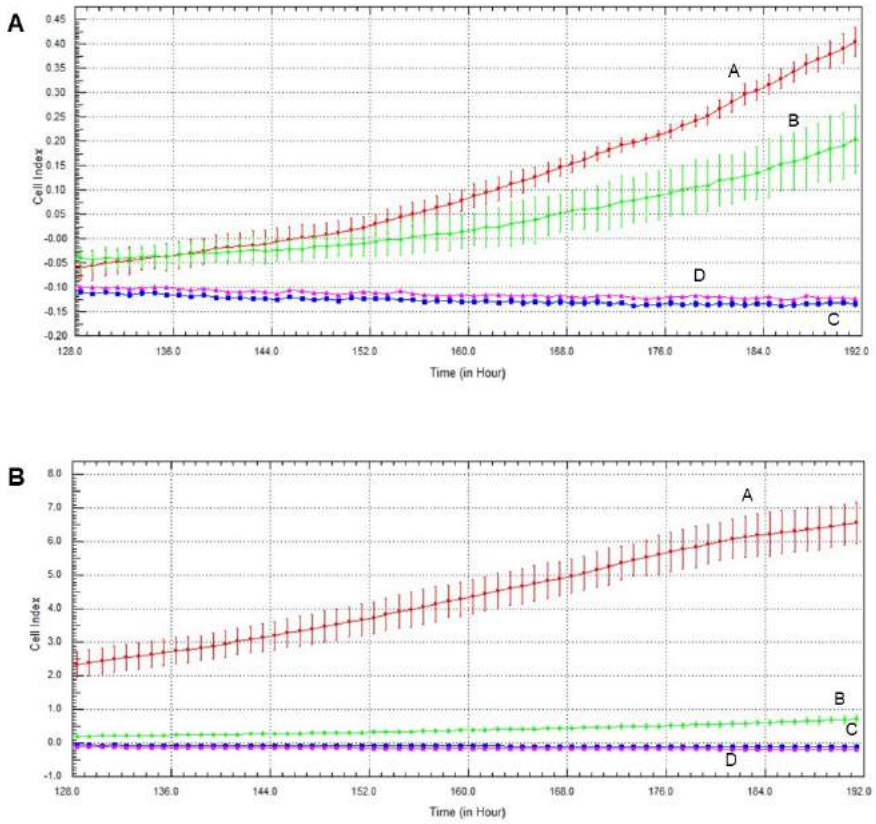

Figure 8. Effects of olaparib, oxaliplatin and LY294002 on invasive growth of MDA-MB-231 (**A**) and MCF7 (**B**) cells treated with 2 µM olaparib, 25 µM oxaliplatin and 1 µM LY294002. Line A—control, Line B—1 µM LY294002 treatment, Line C—2 µM olaparib and 25 µM oxaliplatin, Line D—combination treatment of 1 µM LY294002, 2 µM olaparib and 25 µM oxaliplatin.

5. DISCUSSION AND CONCLUSION I

Several studies have reported the synergistic effect of PARP inhibitors and chemotherapeutic platinum agents in various tumors. Olaparib and platinum compound carboplatin have been found to have modest activity in patients with sporadic TNBC (Lee JM 2017). Combination of PARP inhibitor PJ34 and anti-neoplastic agent cisplatin has been found to have cytotoxic synergy in non-small-cell lung-cancer line A549 (Michels J 2013). Furthermore, PJ34 enhanced the proliferation suppressive effect of cisplatin in liver-cancer cell line HepG2 (Huang SH 2008). The importance of the PI3K/Akt pathway in therapy resistance has been highlighted, demonstrating that its activation results in decreased sensitivity to chemotherapeutic agents (Komeili-Movahhed T 2015). Furthermore, PI3K/Akt pathway inhibitors have been known to cause more favorable outcomes when co-administered with usual anti-cancer drugs (Imai Y 2012). To provide experimental support for the rationale of combination therapy in TNBC, Zhao et al. investigated various combinations of olaparib, carboplatin and buparlisib, a pan-PI3K inhibitor in two human TNBC lines and a HR+ breast-cancer line (Zhao H 2018). By using a calculation (Chou C 2010) based on the median-effect equation, they found a synergistic cytostatic effect of the combination therapy in TNBC lines but not in the HR+ line (Zhao H 2018). We approached the question of synergy from a practical point of view. Instead of determining dose-response effects, we used single, therapeutically relevant concentrations of each drug, and applied these individually and in all possible combinations in experiments on viability, type of cell death, ROS production, cell-cycle phase, colony formation and invasive growth.

We found that 72 h of olaparib treatment decreased viability of MCF7 cells to a much greater extent than that of MDA-MB-231 cells (Figure 2). Elevated PARP-1 expressions have been reported in a wide range of human cancers including breast cancer, and an especially high PARP-1 expression has been found in TNBC which can explain our results (Cseh AM 2019). Furthermore, in complete agreement with our data, other studies have found the cytotoxic effect of oxaliplatin to be higher in MCF7 than in TNBC cells (Movahhed-Komeili T 2015). Several studies have reported the synergistic cytostatic effect of PARP inhibitors and platinum agents (Lee JM 2017, Michels J 2015, Huang SH 2008), and one study reported synergism in combined therapy comprising olaparib, carboplatin and the PI3K inhibitor buparlisib in TNBC lines but not in a HR+ breast-cancer line (Zhao H 2018). In contrast, under our experimental conditions, olaparib did not enhance the cytotoxic properties of oxaliplatin (Figure 2), and we could not detect synergism, nor even an additive effect between these two drugs. The PI3K inhibitor

LY294002 decreased viability of the TNBC but not the HR+ line when combined with olaparib, oxaliplatin or both. However, these effects did not reach a statistically significant level (Figure 2). These data compellingly indicate that, at therapeutically relevant concentrations, cytotoxicity of the platinum compound dominated that of the PARP inhibitor and the PI3K inhibitor. At lower platinum compound and higher concentrations of PARP and PI3K a synergistic effect likely appears and a regression-based model could indicate an overall synergy that may explain the conflict between our results (Figure 2) and the findings of others (Lee JM 2017, Michels J 2015, Huang SH 2008, Zhao H 2018). Additionally, platinum compounds induce ROS production (Stankovic JSK 2020) and PARP inhibitors are known to protect against oxidative stress (Cseh AM 2019), which could explain the absence of synergy between the PARP inhibitor and the platinum agent that we observed. Accordingly, blocking the PI3K/Akt pathway by the PI3K inhibitor LY294002 increased the cytotoxicity of olaparib and oxaliplatin co-treatment, although the effect did not reach a statistically significant level (Figure 2).

We found that olaparib and oxaliplatin killed MDA-MB-231 and MCF7 cells predominantly by apoptosis (Figure 3). The apoptosis resistance of the two cell lines is different. MDA-MB-231 line has high levels of mutant p53 (Hui L 2006), whereas MCF7 line has wild-type p53 (Robinson BW 2001). Additionally, TNBC cells have 10-fold greater phospholipase D (PLD) activity than MCF7 cells. Mutant p53 and elevated PLD activity play a significant role in the survival of cancer cells and can contribute to the suppression of apoptosis (Hui L 2006). Nevertheless, the effect of the various treatments on distribution among live, early and late-apoptotic populations was similar in both cell lines (Figure 3). In this respect it is worth noting that the washing steps before and after the staining procedure remove most non-adherent cells, and the flow cytometry method used to determine the type of cell death analyses stained cells only, regardless of the original cell number and their sensitivity to the various treatments.

Among other mechanisms, ROS-mediated processes play a prominent role in remodelling cancer phenotypes resistant to apoptosis which acquire enhanced metastatic properties (Godet I 2019). In solid tumors, hypoxia and the resulting hypoxia-inducible factor (HIF)-1α mediated metabolic plasticity play a pivotal role in malignant transformation (Schito L 2016). However, in cell culturing conditions, uniform oxygen partial pressure and practically inexhaustible extracellular fuel supply obscure these processes. Accordingly, we studied ROS production which reflects metabolic plasticity (Ward PS 2012) and is compatible with cell culturing conditions. Increased ROS production by the platinum compounds (Stankovic JSK 2020) could induce DNA breaks that may accumulate when PARP is inhibited leading to cell death. Such a

mechanism could account for the observed synergism between platinum compounds and PARP inhibitors (Lee JM 2017, Michels J 2015, Huang SH 2008). In complete agreement with the literature, we found that oxaliplatin- but not olaparib or the Akt pathway inhibitor LY294002-induced ROS formation in the TNBC MDA-MB-231 line and LY294002, but olaparib did not augment oxaliplatin's effect (Figure 4). On the other hand, the treatments alone or in combination failed to induce significant ROS production in the non-TNBC MCF7 line (Figure 4). However, increased vulnerability of MCF7 cells to the treatments resulted in a death rate, compared to that of MDA-MB-231 cells (Figure 2), leaving fewer surviving cells to produce ROS. Furthermore, MCF7 cells could produce less ROS as they represent an earlier stage of metabolic transformation than the TNBC MDA-MB-231 cell line does (Reda A 2019). Combination of these and possibly other factors could account for the observed difference between the cell lines.

Centrosome amplification occurring in the S phase of the cell cycle, is known to be associated with malignant transformation in various tissue types. Centrosome amplification is regarded as a marker for aggressiveness, even with invasive breast and prostate cancers (Ogden A 2013). Accordingly, we expected to find that the MDA-MB-231line had a higher percentage of cells in the S phase of their cycle than the MCF7 cells. However, we observed the opposite trend in the two cell lines (Figure 5C vs. Figure 5G) indicates that other factors, probably synchronization of cell cycles due to passages during culturing (Golubev A 2012) dominated centrosome amplification in determining the distribution of cell-cycle phases in these two breast cancer cell lines. In both cell lines, although to a different extent, oxaliplatin arrested most of the cells in their S phase, and this was not affected by olaparib co-treatment (Figure 5C,G). These data are consistent with the DNA crosslinking effect of the platinum compound, which prevents cells from crossing the G2 checkpoint.

The TNBC cell line MDA-MB-231 represents a more aggressive, apoptosis- and therapy-resistant phenotype than the non-TNBC MCF7 line does. As measures of this aggressiveness, we assessed colony formation (Figure 6) and invasive growth (Figure 7 and Figure 8). These data were completely consistent with the results for viability (Figure 1), with the literature and with the aforementioned view about aggressiveness of the two cell lines. They provide two additional experimental evidence for the lack of synergy between olaparib and oxaliplatin (Figure 6, Figure 7 and Figure 8). Furthermore, they indicate (Figure 6B,D) that Akt pathway inhibition could be advantageous in combined therapy with PARP inhibitors, as it blocks their Akt-mediated cytoprotective effects (Gallyas F Jr 2020).

In conclusion, we provided experimental evidence for the lack of synergy between olaparib, a PARP inhibitor widely used in cancer therapy, and oxaliplatin, a third-generation platinum compound. These results are in conflict with the findings of others (Lee JM 2017, Michels J 2015, Huang SH 2008, Zhao H 2018), probably because, at therapeutically realistic concentrations, the cytostatic effect of the platinum compound dominates that of the PARP inhibitor. We have also demonstrated the advantage of using an Akt pathway inhibitor to augment the cytostatic properties of the platinum compound and/or to prevent the cytoprotective effects of PARP inhibition. Furthermore, we have shown the therapy resistance of the TNBC line MDA-MB-231 over the estrogen- and progesterone receptor-positive line MCF7, although we failed to advance our understanding of differences in sensitivity to chemotherapy among different types of breast cancers.

6. RESULTS II - Treatment of MDA-MB-231 and MCF7 cells with novel mitochondria-targeted pyrroline nitroxide HO-5114

6.1 Effect of HO-5114 on cell viability

To assess its anti-neoplastic potential, TNBC MDA-MB-231 and HR+BC MCF7 cells were treated with 1, 2.5, 5 or 10 µM HO-5114 for 24 and 48 h and then determined their viability using the sulforhodamine B (SRB) assay. The SRB assay measures protein content that is considered to be more proportional to the cell count than metabolic activity, which can under- or over-estimate the cell count if the studied substance inhibits or uncouples mitochondrial oxidative phosphorylation (Vichai V 2006). HO-5114 decreased viability in both breast cancer lines in a concentration- and time-dependent manner (Figure 9) and significant differences could be observed between 24 and 48 h treatment in both cell lines except in 10 µM treatment, where viability was below 10 % after 24 h. In agreement with the view that TNBC is more chemotherapy-resistant than HR+BC, the MDA-MB-231 cells were more resistant against HO-5114 treatment than the MCF7 cells (Figure 9).

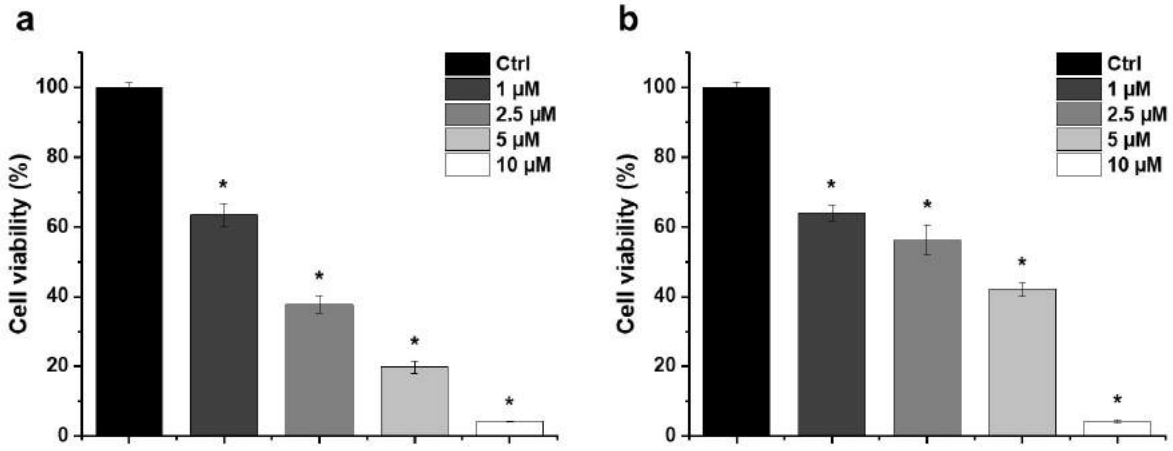

Figure 9. Effect of HO-5114 on the viability of human breast cancer lines. MCF7 (**a**) and MDA-MB-231 (**b**) cells were treated with 1, 2.5, 5 or 10 µM HO-5114 for 24 or 48 h, and then the viability was determined by the SRB assay. Data are shown as mean ± standard error of the mean (SEM) of at least three independent experiments running in three parallels each. * $p < 0.05$ compared to the cells treated for 24 h.

6.2 Determination of the type of HO-5114-induced cell death

The type of HO-5114-induced cell death was determined using flow cytometry. The cells were treated exactly as for the viability measurement for 24 h, and then they were double-stained with fluorescein isothiocyanate (FITC) conjugated Annexin V and propidium iodide (PI). The

latter enters the cell if the plasma membrane is disrupted, binds to the double-stranded DNA, and becomes intensely fluorescent, indicating necrosis. The former binds to phosphatidylserine, a marker of apoptosis when it is on the plasma membrane's outer layer. Double positivity indicates late apoptotic/dead cells. In MCF7 cells, HO-5114 treatment increased the ratio of early—and to a much higher extent—late apoptotic/dead cells on the expense of live cells in a concentration-dependent manner in the whole concentration range tested (Figure 10a,c). In contrast, <5 μM concentrations of HO-5114 did not have a significant effect on the MDA-MB-231 cells; however, 10 μM of HO-5114 had a pronounced effect. It lowered the live cell ratio to 25% while increasing the ratio of early and late apoptotic/dead cells to 10% and 65%, respectively (Figure 10b,d).

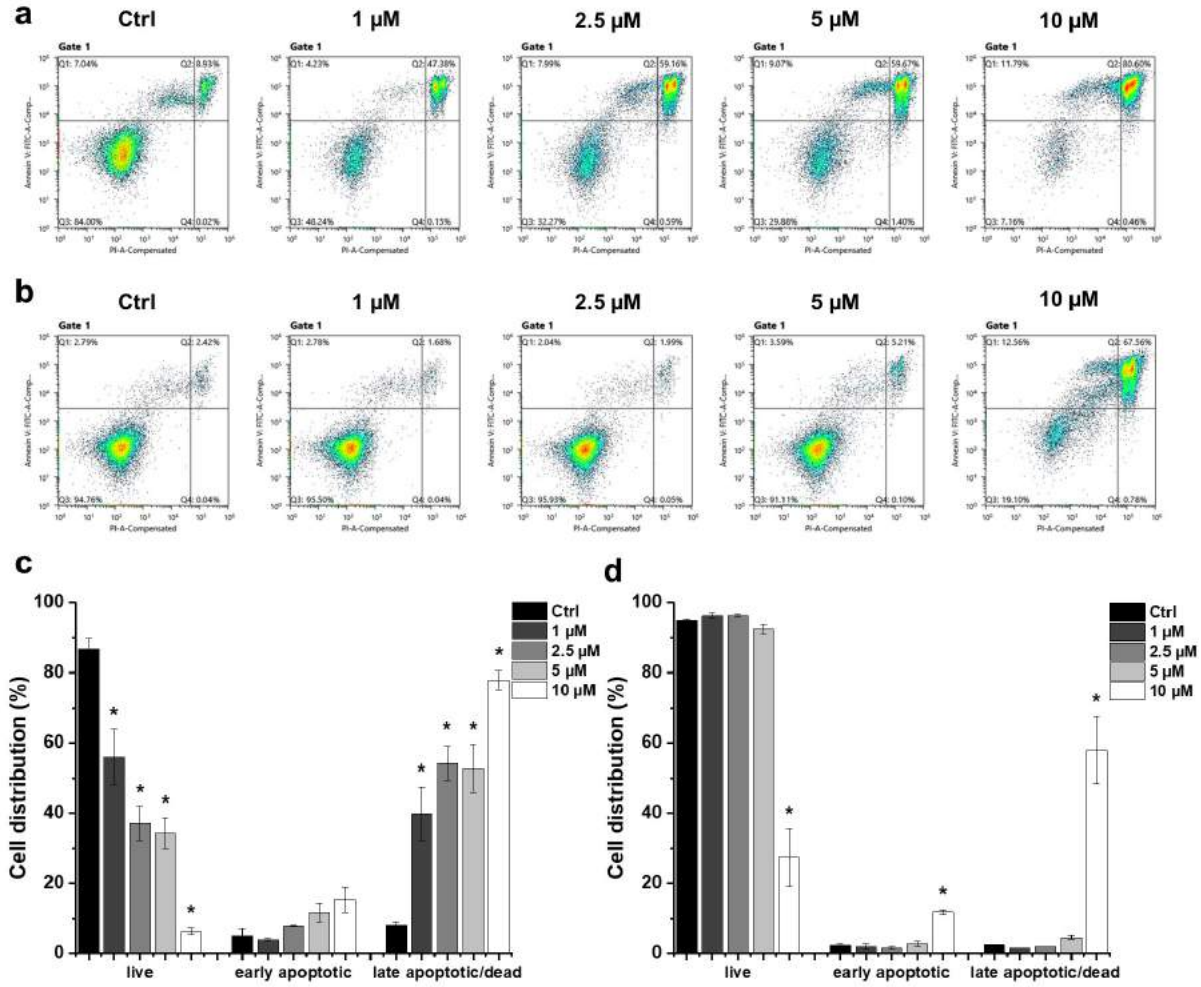

Figure 10. Effect of HO-5114 on the apoptosis of human breast cancer lines. MCF7 (**a**,**c**) and MDA-MB-231 (**b**,**d**) cells were treated with 1, 2.5, 5 or 10 μM HO-5114 for 24 h, and then the cells were double-stained with FITC-Annexin V and PI and were exposed to a flow cytometry analysis. Dot plots (**a**,**b**) show the distribution of early apoptotic, late apoptotic, and live cells (Q1, Q2 and Q3 quadrants, respectively). Bar charts (**c**,**d**) represent the results of at least three independent experiments. The results are shown as mean ± SEM. * $p < 0.05$ compared to the untreated cells.

6.3 Effect of HO-5114 on reactive oxygen species generation

In many cases, anti-neoplastic agents induce ROS production in cancer cells (Ghoneum A 2020). Accordingly, we studied HO-5114-induced ROS production in human breast cancer lines using the dihydrorhodamine 123 assay after 4 h treatment. At a 10 μM concentration, which lowered the viability of both human cancer lines to less than 10% of that of the untreated control, HO-5114 caused ROS production to the extent of about 1.7 and 2 times of the untreated control in the TNBC and HR+BC lines, respectively (Figure 11). Treatment with lower concentrations of HO-5114 that still induced a massive decrease in the viability of both cell lines caused no or only slight cellular ROS production (Figure 11), suggesting that the induction of oxidative stress was unlikely involved among the mechanisms of HO-5114′s cytotoxicity.

Increasing HO-5114′s concentration to 20 µM elevated ROS production proportionally in both cell lines (Figure 11), indicating that ROS production was likely far from the saturation level under these conditions.

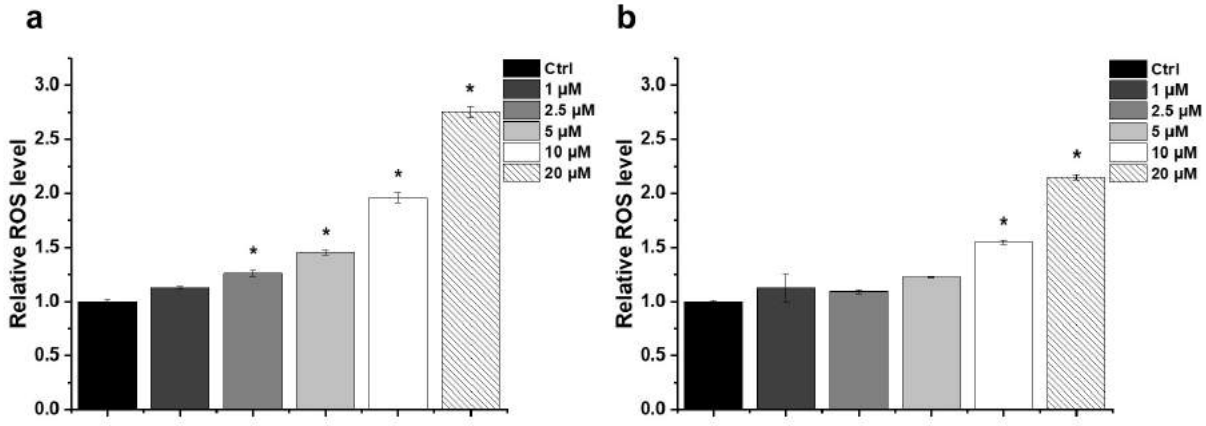

Figure 11. Effect of HO-5114 on cellular ROS production in human breast cancer lines. MCF7 (**a**) and MDA-MB-231 (**b**) cells were treated with 1, 2.5, 5, 10 or 20 µM HO-5114 for 4 h, and then ROS accumulation was assessed by the quantitative formation of fluorescent rhodamine 123 oxidized by the ROS from its non-fluorescent reduced precursor. The results are shown as mean ± SEM of at least three independent experiments. * $p < 0.05$ compared to the untreated cells.

To investigate the role of oxidative stress induction in the anti-neoplastic effect of HO-5114, we studied how an antioxidant affects HO-5114′s cytotoxicity in BC cells. To this end, we treated the MCF7 and MDA-MB-231 cells with 1, 2.5, 5 or 10 µM HO-5114 for 24 h in the presence or absence of 1 mM N-acetylcysteine (NAC) and then measured the viability using the SRB assay. We could not observe any effect of NAC on HO-5114′s cytotoxicity in the case of the HR+BC line MCF-7 (Figure 12a). In contrast, in the TNBC line MDA-MB-231, NAC significantly increased the viability of the control cells as well as the cells treated with up to 5 µM HO-5114; however, at a 10 µM HO-5114 concentration, there was no difference in viability between cells treated in the presence and absence of NAC (Figure 12b).

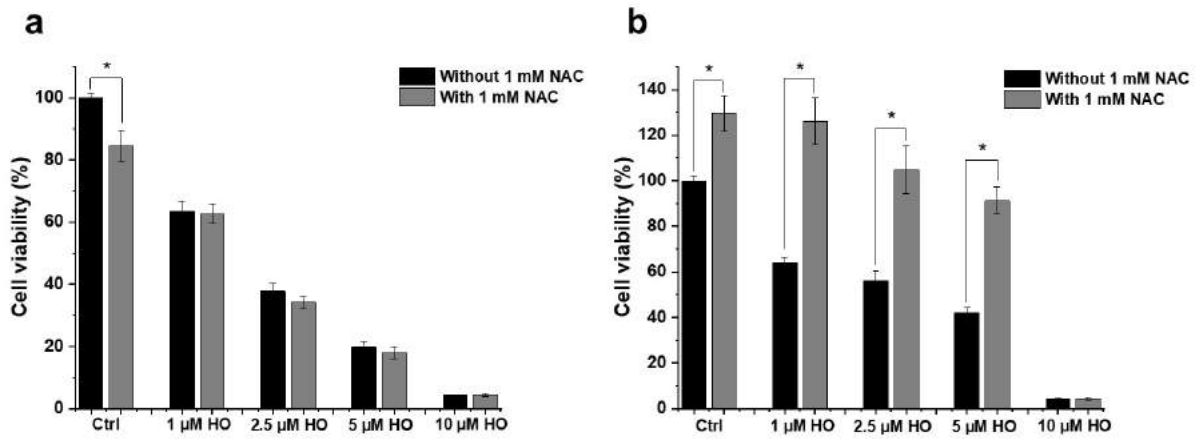

Figure 12. Effect of NAC on HO-5114′s cytotoxicity in human breast cancer lines. MCF7 (**a**) and MDA-MB-231 (**b**) cells were treated with 1, 2.5, 5 or 10 μM HO-5114 for 24 h in the absence or presence of 1 mM NAC, and then the viability was determined using the SRB assay. Data are shown as mean ± SEM of at least three independent experiments running in three parallels each. * $p < 0.05$ compared to the cells untreated with NAC.

6.4 Effect of HO-5114 on ΔΨm

HO-5114 is targeted to the mitochondria due to its diphenyl phosphonium component. Therefore, we studied whether it affects ΔΨm by measuring the JC-1 fluorescence. Based on its cationic properties, JC-1 is taken up by the mitochondria in a ΔΨm-dependent manner. In healthy mitochondria, it forms red fluorescent J-aggregates. Mitochondrial damage results in decreased ΔΨm, leading to a lower accumulation of JC-1 in the form of green fluorescent monomers, while the fluorescence disappears when the ΔΨm dissipates completely. After merely a 1 h treatment, HO-5114 at the concentration of 1 μM caused a significant drop in the ΔΨm of MCF7 cells, while increasing the drug's concentration to 2.5 μM resulted in a massive ΔΨm loss indicated by the almost complete disappearance of the red fluorescence of JC-1 (Figure 13a,c). The MDA-MB-231 line was more resistant to HO-5114; the same concentrations triggered basically the same changes in the ΔΨm that were observed for the MCF7 cells, but it necessitated 2.5 h of treatment rather than 1 h only (Figure 13b,d).

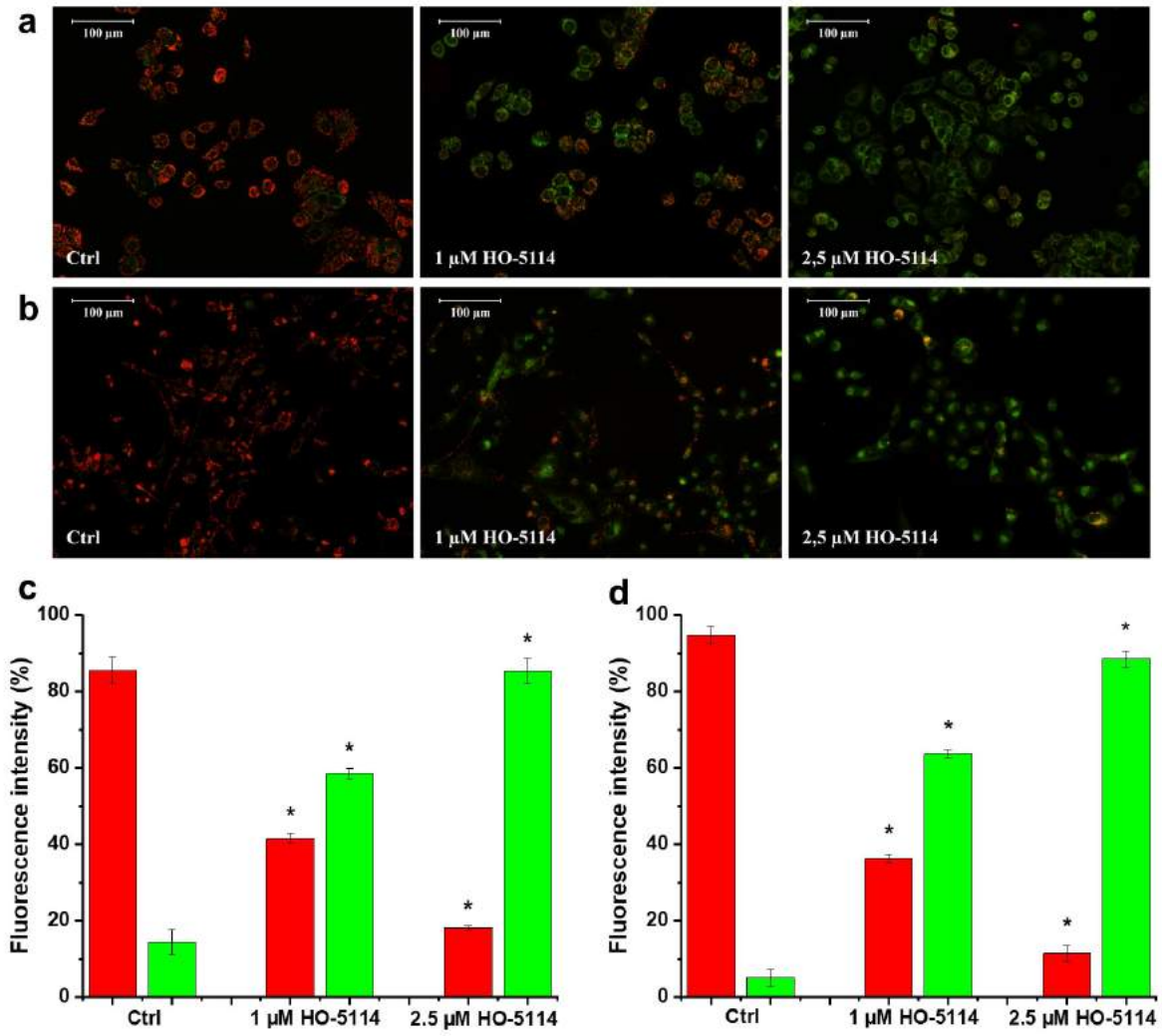

Figure 13. Effect of HO-5114 on the viability of human breast cancer lines. MCF7 (**a**,**c**) and MDA-MB-231 (**b**,**d**) cells were treated with 1 or 2.5 µM HO-5114 for 1 (**a**,**c**) or 2.5 (**b**,**d**) h, and then $\Delta\Psi_m$ was assessed by fluorescence microscopy after loading the cells with the lipophilic, cationic fluorescent dye, JC-1. Red and green fluorescence indicates normal and depolarized $\Delta\Psi_m$, respectively. Representative merged images of the same field acquired from the microscope's red and green channels separately are presented (**a**,**b**). Quantitative assessment of $\Delta\Psi_m$, (**c**,**d**) expressed as the % of fluorescence intensity, means ± SEM of three independent experiments. Quantitative comparisons are true within the same color only. Red and green bars denote red and green fluorescence, respectively. * $p < 0.05$ compared to the untreated cells.

6.5 Effect of HO-5114 on mitochondrial energy production

Due to the increasing importance of energy metabolism among the pathomechanisms of cancer (Dong L 2019), we studied the effect of HO-5114 on the mitochondrial energy production of MDA-MB-231 and MCF7 lines using the Seahorse XFp Cell Mito Stress Test Kit. The device simultaneously measures the real-time cellular oxygen consumption rate (OCR) and extracellular acidification rate (ECAR), indicators of mitochondrial respiration and aerobic glycolysis, respectively. The cells were treated with 1 or 2.5 µM HO-5114 for 4 h, while OCR and ECAR were monitored during the last 75 min of treatment. Basal respiration was recorded

for 15 min (Figure 14a; 1), and then the FoF1 ATPase inhibitor oligomycin was administered to assess ATP production (Figure 14a; 4). After another 20 min of recording, mitochondrial electron transport and ATP synthesis were uncoupled from each other by adding carbonyl cyanide 4-(trifluoromethoxy) phenylhydrazone (FCCP) to determine maximal respiration (Figure 14a; 3). After an additional further 20 min of recording, mitochondrial respiration was blocked by adding rotenone and antimycin A, inhibitors of Complex I and III of the mitochondrial respiratory chain, to determine proton leak and non-mitochondrial oxygen consumption (Figure 14a; 2 and 5).

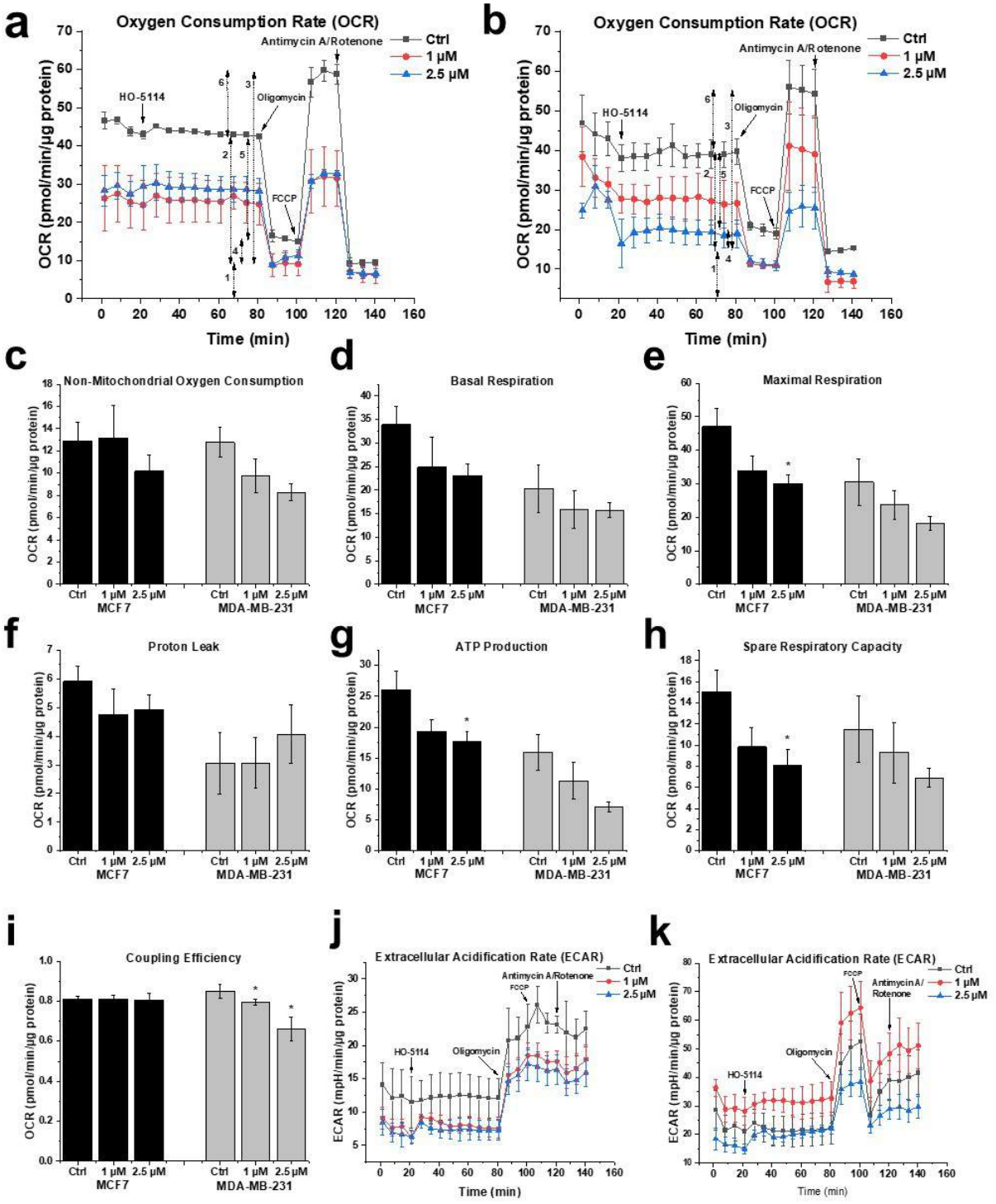

Figure 14. Effect of HO-5114 on the energy metabolism of human breast cancer lines. The cells were treated with 1 or 2.5 μM HO-5114 for 4 h, while OCR and ECAR were monitored during the last 75 min of treatment. The F_oF_1 ATP synthase inhibitor oligomycin (o), the uncoupler FCCP, and the respiratory inhibitors rotenone and antimycin A (R+AmA) were added at the bold arrows. (**a**) OCR recordings in the MCF7 line. The double-headed arrows with numbers next to them indicate: (1) basal respiration, (2) proton leak, (3) maximal respiration, (4) ATP production, (5) non-mitochondrial oxygen consumption, and (6) spare respiratory capacity. (**b**) OCR recordings in the MDA-MB-231 line. (**c**–**i**) Parameters derived from (**a**,**b**); for explanation, see the text and (**a**). (**c**) Non-mitochondrial oxygen consumption. (**d**) Basal respiration. (**e**) Maximal respiration. (**f**) Proton leak. (**g**) Mitochondrial ATP production. (**h**) Spare respiratory capacity. (**i**) Coupling efficiency. (**j**) ECAR recordings in the MCF7 line. (**k**) ECAR recordings in the MDA-MB-231 line. OCR and ECAR data were normalized to mg protein content and presented as means ± standard deviation (SD) of three independent experiments running in two parallels. * $p < 0.05$ compared to the untreated cells.

From the recorded raw data (Figure 14a,b), the Seahorse instrument generated multiple parameters of cellular energy metabolism (Figure 14c–i) that were all diminished by HO-5114 treatment except the proton leak, which was not affected in either cell line (Figure 14f). Furthermore, coupling efficiency that indicates how tightly respiration is coupled to ATP synthesis was not affected in the MCF7 line but was decreased in the MDA-MB-231 line (Figure 14i). The parameters of cellular energy metabolism associated with mitochondrial oxygen consumption, such as basal respiration, maximal respiration, and ATP production, were lower in the TNBC cells than in the HR+BC cells. Furthermore, 1 and 2.5 μM HO-5114 decreased these parameters to about the same extent for the latter cell line, while it affected them in a concentration-dependent manner for the former (Figure 14d,e,g). Administration of the ATP synthase inhibitor oligomycin diminished OCR, which was accompanied by an elevation in ECAR in both cell lines (Figure 14j,k). HO-5114 at a concentration of 1 and 2.5 μM reduced ECAR to about the same extent in the MCF7 line, while it increased and decreased ECAR compared to the untreated control at 1 and 2.5 μM, respectively (Figure 14j,k).

Similar to the viability studies, we investigated the effect of NAC on the energy metabolism of untreated and HO-5114-treated BC cells. To this end, we included 1 mM NAC in a set of HO-5114-treated cells throughout the experiment. In the presence of NAC, the effect of HO-5114 on all parameters of cellular energy metabolism except the proton leak was reversed, in a higher extent for the MDA-MB-231 line than for the MCF7 line (Figure 15). In the MCF7 cells, HO-5114 decreased the proton leak that was further decreased in the presence of NAC. In contrast, HO-5114 increased the proton leak of the MDA-MB-231 cells that was further increased in the presence of NAC (Figure 15f).

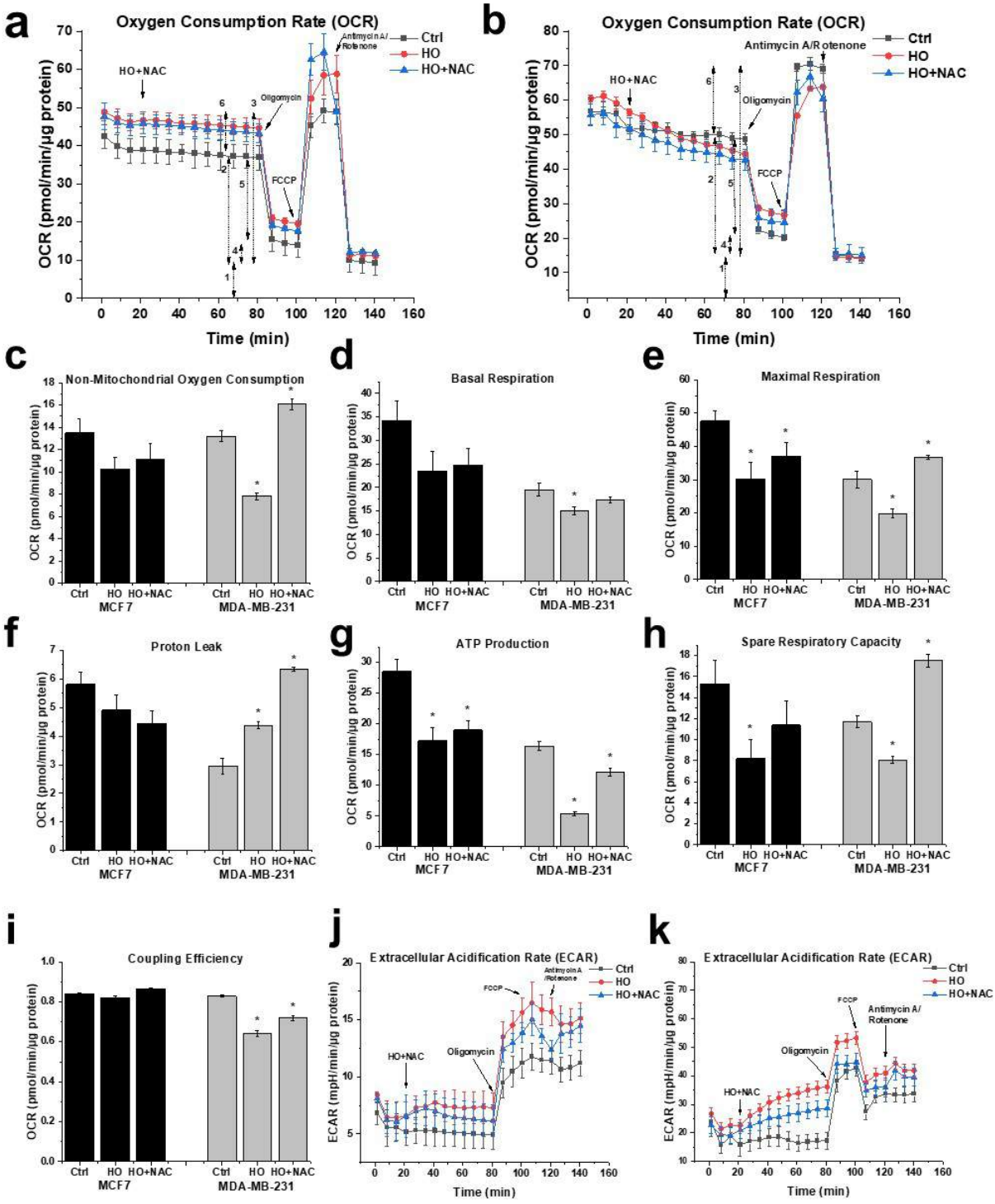

Figure 15. Effect of HO-5114 and NAC on the energy metabolism of human breast cancer lines. The cells were treated with 2.5 µM HO-5114 in the presence (blue line) and absence (red line) of 1 mM NAC for 4 h, while OCR and ECAR were monitored during the last 75 min of treatment. The F_oF_1 ATP synthase inhibitor oligomycin (o), the uncoupler FCCP, and the respiratory inhibitors rotenone and antimycin A (R + AmA) were added at the bold arrows. (**a**) OCR recordings in the MCF7 line. The double-headed arrows with numbers next to them indicate: (1) basal respiration, (2) proton leak, (3) maximal respiration, (4) ATP production, (5) non-mitochondrial oxygen consumption, and (6) spare respiratory capacity. (**b**) OCR recordings in the MDA-MB-231 line. (**c**–**i**) Parameters derived from (**a**,**b**); for explanation, see the text and (**a**). (**c**) Non-mitochondrial oxygen consumption. (**d**) Basal respiration. (**e**) Maximal respiration. (**f**) Proton leak. (**g**) Mitochondrial ATP production. (**h**) Spare respiratory capacity. (**i**) Coupling efficiency. (**j**) ECAR recordings in the MCF7 line. (**k**) ECAR recordings in the MDA-MB-231 line. OCR and ECAR data were normalized to mg protein content and presented as means ± SD of three independent experiments running in two parallels. * $p < 0.05$ compared to the untreated cells.

6.6 Effect of HO-5114 on colony formation

A colony formation assay was performed to assess the proliferation capacity of MCF7 and MDA-MB-231 cells treated with different concentrations of HO-5114. The cells were cultured in the presence of 50, 75, 100 or 250 nM of HO-5114 for seven days, and then the colonies were stained and counted. The drug effectively reduced colony formation in a concentration-dependent manner in both cell lines (Figure 16). Interestingly, the TNBC line was more sensitive to the treatment than the HR+BC line; 250 nM HO-5114 completely eradicated the MDA-MB-231 cells, while it allowed the survival of about 10 colonies of MCF7 cells (Figure 16).

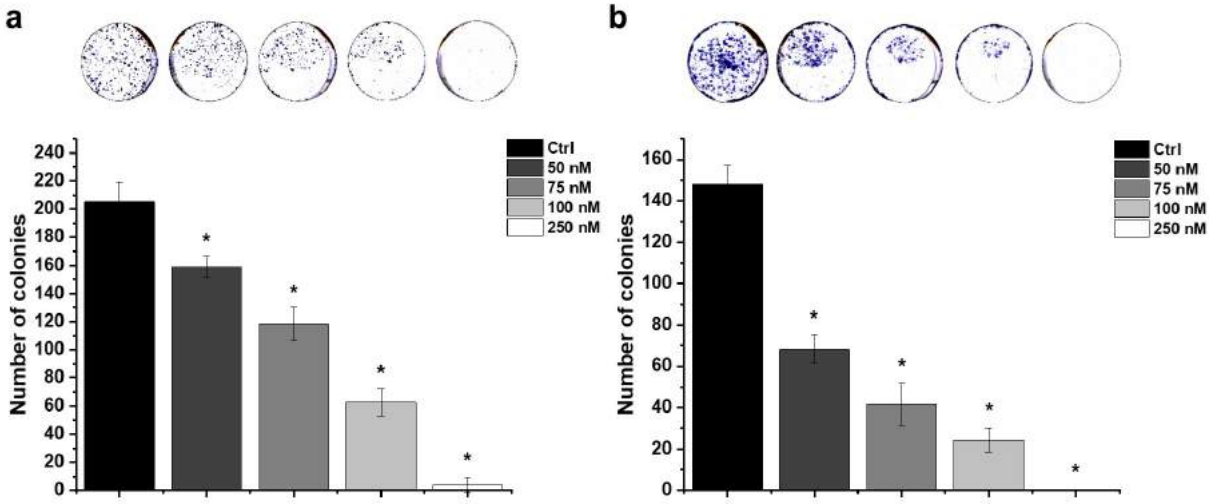

Figure 16. Effect of HO-5114 on the colony formation of human breast cancer lines. MCF7 (**a**) and MDA-MB-231 (**b**) cells were cultured in the presence of 0, 50, 75, 100 or 250 nM of HO-5114 for seven days and then were stained with Coomassie Blue, and the colonies were counted. The results are shown as mean ± SEM of at least three independent experiments. * $p < 0.05$ compared to the untreated cells.

6.7 Effect of HO-5114 on invasive growth

Cell proliferation, migration, and invasion are important in understanding tumor progression and metastasis formation (Dowling CM 2014). We used the xCELLigence Real-Time Cell Analysis method to assess the effect of HO-5114 on the invasive growth characteristics of MCF7 and MDA-MB-231 cells. The instrument measures electron flow transmitted between gold microelectrodes fused to the bottom surface of a microtiter plate in the presence of an electrically conductive culturing medium. Adherent cells cultured in the plates change the impedance expressed as arbitrary units called the cell index, the magnitude of which is dependent on number, morphology, size, and attachment properties of the cells. The cells were cultured in the presence of 75, 100 or 250 nM of HO-5114 for seven days, while the cell index

was monitored in real-time. The drug effectively reduced the cell index in a concentration-dependent manner in both cell lines (Figure 17). At the highest concentration (250 nM), HO-5114 decreased invasive growth close to the detection limit in both cell lines. Similar to the colony formation experiments, the TNBC line was more sensitive to the treatment than the HR+BC line (Figure 17).

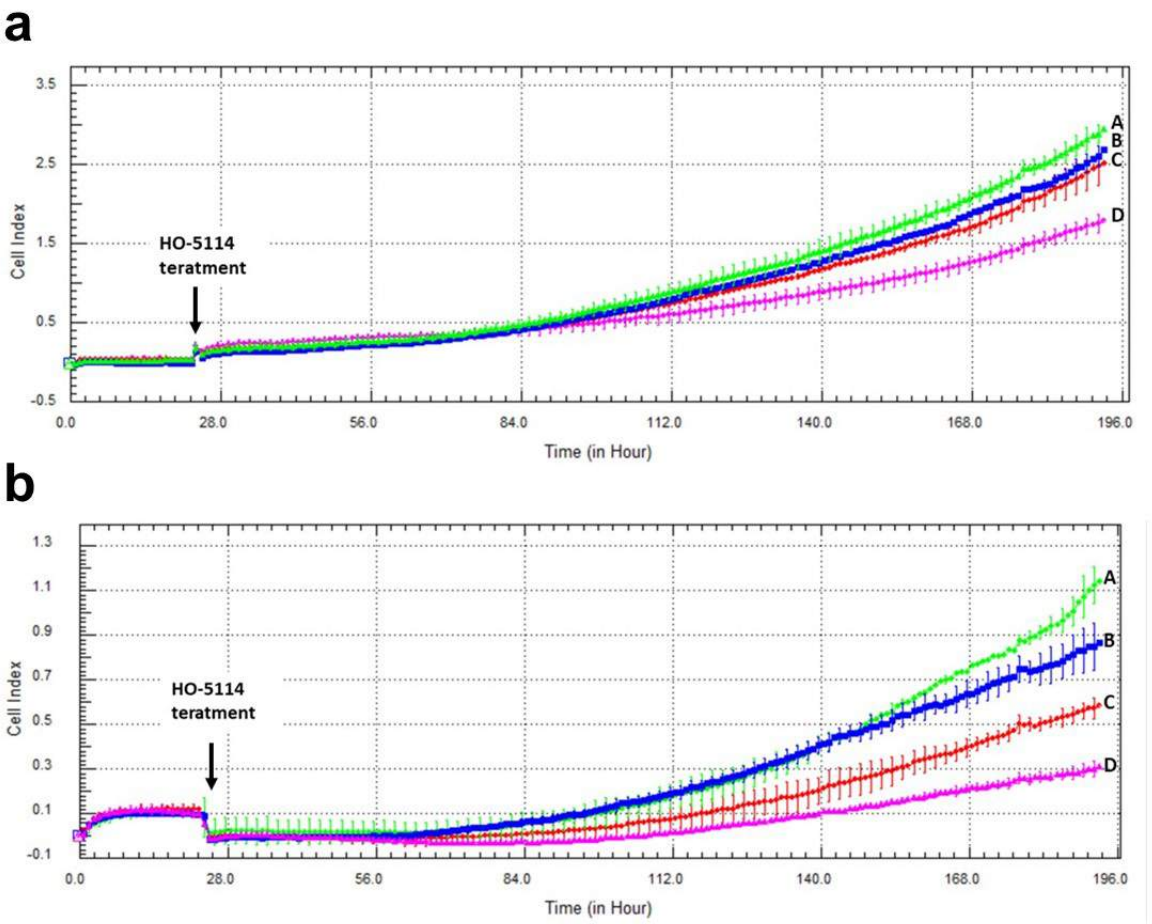

Figure 17. Effect of HO-5114 on the invasive growth of human breast cancer lines. MCF7 (**a**) and MDA-MB-231 (**b**) cells were cultured in the presence of 0 (line A), 75 (line B), 100 (line C), or 250 (line D) nM of HO-5114 for seven days, while the cell index was monitored in real-time. The results are shown as mean ± SEM of at least three independent experiments. * $p < 0.05$ compared to the untreated cells.

7. DISCUSSION AND CONCLUSION II

TNBC is considered to have a poorer prognosis and a more limited targeted therapy repertoire than the HR+ subtype (Masoud V 2017). Additionally, the energy metabolism of the two breast cancer subtypes differs profoundly, which is indicated by the opposite effect of mitochondrial rescue on glycolytically inhibited HR+BC and TNBC cells; it is negative for the former and positive for the latter (Reda A 2019). Accordingly, mitochondria-targeted compounds that compromise mitochondrial energy production may prove effective in the therapy of TNBC (Cheng G 2012). Mito-CP was reported to deplete the cellular ATP level, to inhibit mitochondrial oxygen consumption, to affect mitochondrial morphology, and to dissipate ΔΨm (Boyle KA 2018). As a component-derivative of Mito-CP (Isbera M 2021), HO-5114 was expected to have similar mitochondrial effects. The drug exceeded these expectations because 10 μM of HO-5114 suppressed viability to about the same extent as 50 μM Mito-CP during a 24 h exposure (Isbera M 2021). In complete agreement with these previous results, in the present study, we found that even 1 μM of HO-5114 decreased the viability of both human breast cancer lines by more than 35%, while it almost completely suppressed it at a 10 μM concentration (Figure 9). At a longer exposure time (48 h), the drug's anti-proliferative effect became more pronounced in both the HR+ and the TNBC lines (Figure 9).

Mitochondria affect cancer cell survival through at least three major mechanisms: energy production, the intrinsic apoptotic pathway, and ROS generation (Guerra F 2017). These three pathways are interrelated because apoptosis is an energy-dependent process, while energy shortage and the resulting decrease in ΔΨm leads to the release of pro-apoptotic intermembrane proteins, such as cytochrome c, an apoptosis-inducing factor, and endonuclease G (Burke PJ 2017). ROS damages the mitochondrial electron-transport chain and thus the ATP production, while the compromised electron-transport chain produces more ROS (Weinberg F 2010). ROS activates apoptosis via damaging macromolecules and interfering with the pro-apoptotic signaling pathways (Redza-Dutordoir M 2016). This explains why a substantial induction of apoptosis after a 24 h exposure to 10 μM of HO-5114 in the TNBC line was observed, while lower concentrations of the drug were ineffective in this respect (Figure 10b). In contrast, and in full agreement with the widely accepted view that TNBC is more apoptosis-resistant than HR+BC (Collignon J 2016), even 1 μM of HO-5114 induced massive apoptosis in the MCF7 line (Figure 10a).

ROS participates in mediating cancer phenotype remodeling that manifests in apoptosis resistance and increased metastatic properties (Godet I 2019). The chronic hypoxia prevalent

in solid tumors results in the constant activation of the HIF1α transcription factor that induces a malignant transformation associated metabolic remodeling (Schito L 2016); however, we found a very similar extent of HO-5114-induced ROS formation in the MCF7 and MDA-MB-231 lines (Figure 11), although the latter represents a higher stage of metabolic transformation than the former (Godet I 2019). The moderate increase in ROS accumulation in response to an increased HO-5114 concentration to 20 μM (Figure 11) also indicated that ROS production in the BC lines was insensitive to HO-5114 treatment, contrary to the expectation. The difference in conditions between solid tumors and the cell culture, where uniform oxygen and fuel supply is provided, may account for the discrepancy between the expected and observed ROS production. Elevated ROS production is considered to be necessary for survival and growth of TNBC cells in vitro (Sarmiento-Salinas FL 2019), therefore, antioxidants are expected to hinder their survival (Kwon Y 2021). However, we found that the antioxidant NAC increased the viability of control MDA-MB-231, while it did not affect MCF7 cells, indicating a higher ROS level that impeded proliferation in the former (Figure 12). The viability promoting effect of NAC overcompensated for the cytotoxic effect of HO-5114 at the concentration of up to 5 μM, but at 10 μM, it failed to do so (Figure 12b). The absence of NAC's effect on HO-5114′s cytotoxicity in the HR+BC line (Figure 12a) indicated not only a reduced chronic oxidative stress in it compared to the TNBC line but also suggested differences in metabolic reprogramming between the two BC cell lines (Martínez-Reyes I 2021).

The driving force for ATP synthesis is provided by ΔΨm; however, it has additional essential roles, such as transporting nuclearly encoded mitochondrial proteins (Neupert W 2007), transporting K^+, Ca^{2+}, and Mg^{2+} (Zorova LD 2018), generating ROS (Korshunov SS 1997), mitochondrial quality control (Srinivasan S 2017), and the regulation of pro-apoptotic intermembrane protein release (Green DR 1998, Tait SW 2013, Fatokun AA 2014). Cell survival essentially relies on the maintenance of ΔΨm. Accordingly, in ischemic situations, the F_oF_1 ATPase can operate in reverse mode and consume ATP to maintain ΔΨm to rescue the cell. The ATP is supplied by the substrate-level phosphorylation of non-glucose substrates under these conditions; however, considering the amount of the available non-glucose substrate pool, this survival attempt is often futile (Baxter P 2014, Chinopoulos C 2018, Chinopoulos 2020). In solid tumors, the cancer cells must adapt their metabolism to the chronic hypoxia and partially ischemic situation (Weinberg SE 2015, Ashley N 2009). In contrast to ROS induction, we observed a very sensitive response of ΔΨm loss to HO-5114 treatment. Even 1 μM of the drug induced significant changes in ΔΨm during as short a treatment as 1 h for the MCF7 line and 2.5 h for the MDA-MB-231 line (Figure 13).

Cancer cells face a double challenge in producing enough energy and a sufficient metabolic intermediate for proliferation in a predominantly hypoxic and partially ischemic environment (Bennett NK 2020). Mostly, they rely on glycolysis rather than mitochondrial oxidative phosphorylation, even if sufficient oxygen is available for the latter (Warburg O 1956). Accordingly, increased glucose uptake is a characteristic feature of tumors that is used to identify them by ^{18}F-deoxyglucose positron emission tomography (Gatenby RA 2004, Kroemer G 2008) for diagnostic purposes. On the other hand, the most malignant cancer types, such as metastatic tumor cells, therapy-resistant tumor cells, and cancer stem cells, rely on mitochondrial ATP synthesis (LeBleu VS 2014, Lin CS 2018). The survival, proliferation, and metastasis of these cells depend on the oxidative phosphorylation and form the basis of their therapy resistance (Hirpara J 2019, Zhang G 2016). Accordingly, for the most malignant cancer types, oxidative phosphorylation is an emerging therapeutic target (Ashton TM 2018), and drugs significantly affecting tumor cell metabolism may have therapeutic value (Weinberg SE 2015). Considering its effects on energy metabolism in human breast cancer lines, HO-5114 fulfills this criterion. At a 1 and 2.5 μM concentration, it significantly diminished all OCR-related parameters in both cell lines except coupling efficiency (Figure 14). HO-5114 at a 2.5 μM concentration reduced ATP production that could contribute to the drug's anti-metastatic property. In complete agreement with its effect on the viability of BC lines, NAC counteracted the inhibitory effect of HO-5114 on the various parameters of cellular energy metabolism except the proton leak (Figure 15). These data support the conclusion that HO-5114 affects the energy metabolism of the BC lines. The proton leak can indicate damage to the mitochondrial respiratory chain or regulation of mitochondrial ATP synthesis via uncoupling proteins (UCPs) (Baffy G 2017). Indeed, the role of UCP2 in regulating the balance between substrate-level and oxidative phosphorylation has recently been reported (Vozza A 2014). We found that both BC lines increased ECAR, i.e., substrate-level phosphorylation when oxidative ATP production was blocked by oligomycin (Figure 14 and Figure 15). ECAR in the MDA-MB-231 line even returned to its initial rate when the oxidative phosphorylation was uncoupled by FCCP (Figure 14 and Figure 15), demonstrating that the balance between the two ATP producing machinery is more responsive in the TN than in the HR+BC cells.

The hormone receptor status determines the cell proliferation, differentiation, and cancer progression properties of breast cancers (Karamanou K 2020). Accordingly, the MDA-MB-231 line represents a more aggressive, apoptosis- and therapy-resistant phenotype than the HR+ MCF7 line. The results of the aforementioned experiments that involved 1–24 h exposure to HO-5114 were in line with this view; however, in the colony formation (Figure 16) and invasive

growth (Figure 17) experiments, where the cells were exposed to a 50–250 nM concentration of the drug for seven days, MDA-MB-231 proved to be more sensitive to the treatment than the MCF7 line. The reason for this difference in sensitivity to HO-5114 treatment between short- and long-term exposure is not clear based on the experiments.

In conclusion, all data acquired in this study indicated that HO-5114 had a robust anti-neoplastic effect on cultured BC cells. Furthermore, resistance to HO-5114 treatment did not differ markedly between the HR+ and TNBC lines. The latter even seemed to be more sensitive to the drug in models involving long-term treatment; however, in vitro cell culture effects translate poorly to human therapy. Accordingly, to establish the therapeutic potentiality of HO-5114, follow up experiments have to be performed in animal models for determining its in vivo toxicity and anti-neoplastic effectiveness.

8. SUMMARY

Breast cancer is a major cause of death among women worldwide. Therapeutic options have broadened in the last decades, however there is a subtype of breast cancer which doesn't have targeted therapy. Triple-negative breast cancer is an aggressive phenotype with poorer prognosis.

In the first part of the study olaparib, oxaliplatin and PI3K inhibitors and their combination were examined. Olaparib is a frequently used PARP inhibitor for patients with BRCA mutations while oxaliplatin is a third generation platinum agent. Previous studies showed synergy of PARP inhibitors with platinum compounds, giving us the idea to investigate their effects on the two cell lines. In this study estrogen receptor-positive and progesterone receptor-positive MCF7 cells and triple-negative MDA-MB-231 cells were used to investigate their response to a new combination of drugs and to a novel Mito-CP derivative. The combination of these two compounds were augmented by PI3K inhibitor LY294002 to enhance the cytotoxic effect of oxaliplatin and to prevent the cytoprotective effect of olaparib. However our findings show a lack of synergy between them.

Therefore, in the second part of the study the novel Mito-CP derivative, HO-5114 was under investigation. There is a growing interest in targeting the mitochondria, as they are recognized targets for treating aggressive, metastatic and chemoresistant tumors. Mito-CP showed cytotoxic properties in various cancer cells, including breast cancer. Our study confirmed a significant anti-neoplastic effect of HO-5114 in both cell lines, interestingly the TNBC cell line was more sensitive to long-term treatment than the HR+ cell line.

9. REFERENCES

Allemani C, Weir HK, Carreira H, Harewood R, Spika D, Wang XS, Bannon F, Ahn JV, Johnson CJ, Bonaventure A, Marcos-Gragera R, Stiller C, Azevedo e Silva G, Chen WQ, Ogunbiyi OJ, Rachet B, Soeberg MJ, You H, Matsuda T, Bielska-Lasota M, Storm H, Tucker TC, Coleman MP; CONCORD Working Group. Global surveillance of cancer survival 1995-2009: analysis of individual data for 25,676,887 patients from 279 population-based registries in 67 countries (CONCORD-2). Lancet. 2015 Mar 14;385(9972):977-1010

Anderson KE, Jackson SP. Class I phosphoinositide 3-kinases. Int J Biochem Cell Biol. 2003 Jul;35(7):1028-33

Ashley N, Poulton J. Mitochondrial DNA is a direct target of anti-cancer anthracycline drugs. Biochem Biophys Res Commun. 2009 Jan 16;378(3):450-5

Ashton TM, McKenna WG, Kunz-Schughart LA, Higgins GS. Oxidative Phosphorylation as an Emerging Target in Cancer Therapy. Clin Cancer Res. 2018 Jun 1;24(11):2482-2490

Azamjah N, Soltan-Zadeh Y, Zayeri F. Global Trend of Breast Cancer Mortality Rate: A 25-Year Study. Asian Pac J Cancer Prev. 2019;20(7):2015-2020

Baffy G. Mitochondrial uncoupling in cancer cells: Liabilities and opportunities. Biochim Biophys Acta Bioenerg. 2017 Aug;1858(8):655-664

Battogtokh G, Cho YY, Lee JY, Lee HS, Kang HC. Mitochondrial-Targeting Anti-cancer Agent Conjugates and Nanocarrier Systems for Cancer Treatment. Front Pharmacol. 2018 Aug 17;9:922

Baxter P, Chen Y, Xu Y, Swanson RA. Mitochondrial dysfunction induced by nuclear poly(ADP-ribose) polymerase-1: a treatable cause of cell death in stroke. Transl Stroke Res. 2014 Feb;5(1):136-44

Bellacosa A, de Feo D, Godwin AK, Bell DW, Cheng JQ, Altomare DA, Wan M, Dubeau L, Scambia G, Masciullo V, Ferrandina G, Benedetti Panici P, Mancuso S, Neri G, Testa JR. Molecular alterations of the AKT2 oncogene in ovarian and breast carcinomas. Int J Cancer. 1995 Aug 22;64(4):280-5

Bennett NK, Nguyen MK, Darch MA, Nakaoka HJ, Cousineau D, Ten Hoeve J, Graeber TG, Schuelke M, Maltepe E, Kampmann M, Mendelsohn BA, Nakamura JL, Nakamura K. Defining the ATPome reveals cross-optimization of metabolic pathways. Nat Commun. 2020 Aug 28;11(1):4319

Blume-Jensen P, Hunter T. Oncogenic kinase signalling. Nature. 2001 May 17;411(6835):355-65

Boyle KA, Van Wickle J, Hill RB, Marchese A, Kalyanaraman B, Dwinell MB. Mitochondria-targeted drugs stimulate mitophagy and abrogate colon cancer cell proliferation. J Biol Chem. 2018 Sep 21;293(38):14891-14904

Budán F, Varjas T, Nowrasteh G, Varga Z, Boncz I, Cseh J, Prantner I, Antal T, Pázsit E, Gobel G, Bauer M, Gracza T, Perjési P, Ember I, Gyöngyi Z. Early modification of c-myc, Ha-ras and p53 expressions by N-methyl-N-nitrosourea. In Vivo. 2008 Nov-Dec;22(6):793-7

Budán F, Varjas T, Nowrasteh G, Prantner I, Varga Z, Ember A, Cseh J, Gombos K, Pázsit E, Gobel G, Bauer M, Gracza T, Arany I, Perjési P, Ember I, Kiss I. Early modification of c-myc, Ha-ras and p53 expressions by chemical carcinogens (DMBA, MNU). In Vivo. 2009 Jul-Aug;23(4):591-8

Buonomo OC, Caredda E, Portarena I, Vanni G, Orlandi A, Bagni C, Petrella G, Palombi L, Orsaria P. New insights into the metastatic behavior after breast cancer surgery, according to well-established clinicopathological variables and molecular subtypes. PLoS One. 2017 Sep 18;12(9):e0184680

Burke PJ. Mitochondria, Bioenergetics and Apoptosis in Cancer. Trends Cancer. 2017 Dec;3(12):857-870

Chen GG, Zeng Q, Tse GM. Estrogen and its receptors in cancer. Med Res Rev. 2008 Nov;28(6):954-74

Cheng G, Zielonka J, Dranka BP, McAllister D, Mackinnon AC Jr, Joseph J, Kalyanaraman B. Mitochondria-targeted drugs synergize with 2-deoxyglucose to trigger breast cancer cell death. Cancer Res. 2012 May 15;72(10):2634-44

Chinopoulos C, Seyfried TN. Mitochondrial Substrate-Level Phosphorylation as Energy Source for Glioblastoma: Review and Hypothesis. ASN Neuro. 2018 Jan-Dec;10:1759091418818261

Chinopoulos C. Acute sources of mitochondrial NAD+ during respiratory chain dysfunction. Exp Neurol. 2020 May;327:113218

Chitneni SK, Reitman ZJ, Spicehandler R, Gooden DM, Yan H, Zalutsky MR. Synthesis and evaluation of radiolabeled AGI-5198 analogues as candidate radiotracers for imaging mutant IDH1 expression in tumors. Bioorg Med Chem Lett. 2018;28(4):694-699

Chou TC. Drug combination studies and their synergy quantification using the Chou-Talalay method. Cancer Res. 2010 Jan 15;70(2):440-6

Collignon J, Lousberg L, Schroeder H, Jerusalem G. Triple-negative breast cancer: treatment challenges and solutions. Breast Cancer (Dove Med Press). 2016 May 20;8:93-107

Collins P, Webb C. Estrogen hits the surface. Nat Med. 1999 Oct;5(10):1130-1

Cseh AM, Fabian Z, Quintana-Cabrera R, Szabo A, Eros K, Soriano ME, Gallyas F, Scorrano L, Sumegi B. PARP Inhibitor PJ34 Protects Mitochondria and Induces DNA-Damage Mediated Apoptosis in Combination With Cisplatin or Temozolomide in B16F10 Melanoma Cells. Front Physiol. 2019 May 7;10:538

de Gramont A, Figer A, Seymour M, Homerin M, Hmissi A, Cassidy J, Boni C, Cortes-Funes H, Cervantes A, Freyer G, Papamichael D, Le Bail N, Louvet C, Hendler D, de Braud F, Wilson C, Morvan F, Bonetti A. Leucovorin and fluorouracil with or without oxaliplatin as first-line treatment in advanced colorectal cancer. J Clin Oncol. 2000 Aug;18(16):2938-47

Dasari S, Tchounwou PB. Cisplatin in cancer therapy: molecular mechanisms of action. Eur J Pharmacol. 2014 Oct 5;740:364-78

Dhanasekaran A, Kotamraju S, Karunakaran C, Kalivendi SV, Thomas S, Joseph J, Kalyanaraman B. Mitochondria superoxide dismutase mimetic inhibits peroxide-induced oxidative damage and apoptosis: role of mitochondrial superoxide. Free Radic Biol Med. 2005 Sep 1;39(5):567-83

Dong L, Gopalan V, Holland O, Neuzil J. Mitocans Revisited: Mitochondrial Targeting as Efficient Anti-Cancer Therapy. Int J Mol Sci. 2020 Oct 26;21(21):7941

Dong L, Neuzil J. Targeting mitochondria as an anti-cancer strategy. Cancer Commun (Lond). 2019 Oct 25;39(1):63

Dowling CM, Herranz Ors C, Kiely PA. Using real-time impedance-based assays to monitor the effects of fibroblast-derived media on the adhesion, proliferation, migration and invasion of colon cancer cells. Biosci Rep. 2014 Jul 29;34(4):e00126

Drew Y. The development of PARP inhibitors in ovarian cancer: from bench to bedside. Br J Cancer. 2015;113 Suppl 1(Suppl 1):S3-S9

Durkacz BW, Omidiji O, Gray DA, Shall S. (ADP-ribose)n participates in DNA excision repair. Nature. 1980 Feb 7;283(5747):593-6

Eliyahu D, Goldfinger N, Pinhasi-Kimhi O, Shaulsky G, Skurnik Y, Arai N, Rotter V, Oren M. Meth A fibrosarcoma cells express two transforming mutant p53 species. Oncogene. 1988 Sep;3(3):313-21

Eliyahu D, Raz A, Gruss P, Givol D, Oren M. Participation of p53 cellular tumour antigen in transformation of normal embryonic cells. Nature. 1984 Dec 13-19;312(5995):646-9

Estaquier J, Vallette F, Vayssiere JL, Mignotte B. The mitochondrial pathways of apoptosis. Adv Exp Med Biol. 2012;942:157-83

Fatokun AA, Dawson VL, Dawson TM. Parthanatos: mitochondrial-linked mechanisms and therapeutic opportunities. Br J Pharmacol. 2014 Apr;171(8):2000-16

Fearon ER, Hamilton SR, Vogelstein B. Clonal analysis of human colorectal tumors. Science. 1987 Oct 9;238(4824):193-7

Fearon ER, Vogelstein B. A genetic model for colorectal tumorigenesis. Cell. 1990 Jun 1;61(5):759-67

Gallyas F Jr, Sumegi B. Mitochondrial Protection by PARP Inhibition. Int J Mol Sci. 2020 Apr 16;21(8):2767

Gatenby RA, Gillies RJ. Why do cancers have high aerobic glycolysis? Nat Rev Cancer. 2004 Nov;4(11):891-9

Ghoneum A, Abdulfattah AY, Warren BO, Shu J, Said N. Redox Homeostasis and Metabolism in Cancer: A Complex Mechanism and Potential Targeted Therapeutics. Int J Mol Sci. 2020 Apr 28;21(9):3100

Godet I, Shin YJ, Ju JA, Ye IC, Wang G, Gilkes DM. Fate-mapping post-hypoxic tumor cells reveals a ROS-resistant phenotype that promotes metastasis. Nat Commun. 2019 Oct 24;10(1):4862

Golub D, Iyengar N, Dogra S, Wong T, Bready D, Tang K, Modrek AS, Placantonakis DG. Mutant Isocitrate Dehydrogenase Inhibitors as Targeted Cancer Therapeutics. Front Oncol. 2019 May 17;9:417

Golubev A. Transition probability in cell proliferation, stochasticity in cell differentiation, and the restriction point of the cell cycle in one package. Prog Biophys Mol Biol. 2012 Sep;110(1):87-96

GLOBOCAN 2020 Hungary pdf downloaded 30th August 2021
https://gco.iarc.fr/today/data/factsheets/populations/348-hungary-fact-sheets.pdf

Gonzalez H, Hagerling C, Werb Z. Roles of the immune system in cancer: from tumor initiation to metastatic progression. Genes Dev. 2018;32(19-20):1267-1284

Grandage VL, Gale RE, Linch DC, Khwaja A. PI3-kinase/Akt is constitutively active in primary acute myeloid leukaemia cells and regulates survival and chemoresistance via NF-kappaB, Mapkinase and p53 pathways. Leukemia. 2005 Apr;19(4):586-94

Greaves M, Maley CC. Clonal evolution in cancer. Nature. 2012 Jan 18;481(7381):306-13

Green DR, Reed JC. Mitochondria and apoptosis. Science. 1998 Aug 28;281(5381):1309-12

Guerra F, Arbini AA, Moro L. Mitochondria and cancer chemoresistance. Biochim Biophys Acta Bioenerg. 2017 Aug;1858(8):686-699

Hamidi H, Lilja J, Ivaska J. Using xCELLigence RTCA Instrument to Measure Cell Adhesion. Bio Protoc. 2017;7(24):e2646.

Hammond ME, Hayes DF, Dowsett M, Allred DC, Hagerty KL, Badve S, Fitzgibbons PL, Francis G, Goldstein NS, Hayes M, Hicks DG, Lester S, Love R, Mangu PB, McShane L, Miller K, Osborne CK, Paik S, Perlmutter J, Rhodes A, Sasano H, Schwartz JN, Sweep FC, Taube S, Torlakovic EE, Valenstein P, Viale G, Visscher D, Wheeler T, Williams RB, Wittliff JL, Wolff AC. American Society of Clinical Oncology/College Of American Pathologists guideline recommendations for immunohistochemical testing of estrogen and progesterone receptors in breast cancer. J Clin Oncol. 2010 Jun 1;28(16):2784-95

Harbeck N, Penault-Llorca F, Cortes J, Gnant M, Houssami N, Poortmans P, Ruddy K, Tsang J, Cardoso F. Breast cancer. Nat Rev Dis Primers. 2019 Sep 23;5(1):66.

Hensley CT, Wasti AT, DeBerardinis RJ. Glutamine and cancer: cell biology, physiology, and clinical opportunities. J Clin Invest. 2013 Sep;123(9):3678-84

Herskowitz I. Functional inactivation of genes by dominant negative mutations. Nature. 1987 Sep 17-23;329(6136):219-22

Hinds P, Finlay C, Levine AJ. Mutation is required to activate the p53 gene for cooperation with the ras oncogene and transformation. J Virol. 1989 Feb;63(2):739-46

Hirpara J, Eu JQ, Tan JKM, Wong AL, Clement MV, Kong LR, Ohi N, Tsunoda T, Qu J, Goh BC, Pervaiz S. Metabolic reprogramming of oncogene-addicted cancer cells to OXPHOS as a mechanism of drug resistance. Redox Biol. 2019 Jul;25:101076

Ho GY, Woodward N, Coward JI. Cisplatin versus carboplatin: comparative review of therapeutic management in solid malignancies. Crit Rev Oncol Hematol. 2016 Jun;102:37-4

Huang SH, Xiong M, Chen XP, Xiao ZY, Zhao YF, Huang ZY. PJ34, an inhibitor of PARP-1, suppresses cell growth and enhances the suppressive effects of cisplatin in liver cancer cells. Oncol Rep. 2008 Sep;20(3):567-72

Hui L, Zheng Y, Yan Y, Bargonetti J, Foster DA. Mutant p53 in MDA-MB-231 breast cancer cells is stabilized by elevated phospholipase D activity and contributes to survival signals generated by phospholipase D. Oncogene. 2006 Nov 23;25(55):7305-10

Imai Y, Yoshimori M, Fukuda K, Yamagishi H, Ueda Y. The PI3K/Akt inhibitor LY294002 reverses BCRP-mediated drug resistance without affecting BCRP translocation. Oncol Rep. 2012 Jun;27(6):1703-9

Isbera M, Bognár B, Gallyas F, Bényei A, Jekő J, Kálai T. Syntheses and Study of a Pyrroline Nitroxide Condensed Phospholene Oxide and a Pyrroline Nitroxide Attached Diphenylphosphine. Molecules. 2021 Jul 19;26(14):4366

Jamieson ER, Lippard SJ. Structure, Recognition, and Processing of Cisplatin-DNA Adducts. Chem Rev. 1999 Sep 8;99(9):2467-98

Jenkins JR, Rudge K, Redmond S, Wade-Evans A. Cloning and expression analysis of full length mouse cDNA sequences encoding the transformation associated protein p53. Nucleic Acids Res. 1984 Jul 25;12(14):5609-26

Jordan VC. Fourteenth Gaddum Memorial Lecture. A current view of tamoxifen for the treatment and prevention of breast cancer. Br J Pharmacol. 1993 Oct;110(2):507-17

Joshi H, Press MF. Molecular oncology of breast cancer. In: Bland KI, Copeland EM, Klimberg VS, Gradishar WJ, eds. The Breast. Philadelphia, PA: Elsevier;2018:22

Karamanou K, Franchi M, Vynios D, Brézillon S. Epithelial-to-mesenchymal transition and invadopodia markers in breast cancer: Lumican a key regulator. Semin Cancer Biol. 2020 May;62:125-133

Komeili-Movahhed T, Fouladdel S, Barzegar E, Atashpour S, Hossein Ghahremani M, Nasser Ostad S, Madjd Z, Azizi E. PI3K/Akt inhibition and down-regulation of BCRP re-sensitize MCF7 breast cancer cell line to mitoxantrone chemotherapy. Iran J Basic Med Sci. 2015 May;18(5):472-7

Korshunov SS, Skulachev VP, Starkov AA. High protonic potential actuates a mechanism of production of reactive oxygen species in mitochondria. FEBS Lett. 1997 Oct 13;416(1):15-8

Kraiss S, Quaiser A, Oren M, Montenarh M. Oligomerization of oncoprotein p53. J Virol. 1988 Dec;62(12):4737-44. doi: 10.1128/JVI.62.12.4737-4744.1988

Kroemer G, Pouyssegur J. Tumor cell metabolism: cancer's Achilles' heel. Cancer Cell. 2008 Jun;13(6):472-8

Kumar P, Nagarajan A, Uchil PD. Analysis of Cell Viability by the MTT Assay. Cold Spring Harb Protoc. 2018 Jun 1;2018(6)

Kwon Y. Possible Beneficial Effects of N-Acetylcysteine for Treatment of Triple-Negative Breast Cancer. Antioxidants (Basel). 2021 Jan 24;10(2):169

LeBleu VS, O'Connell JT, Gonzalez Herrera KN, Wikman H, Pantel K, Haigis MC, de Carvalho FM, Damascena A, Domingos Chinen LT, Rocha RM, Asara JM, Kalluri R. PGC-1α mediates mitochondrial biogenesis and oxidative phosphorylation in cancer cells to promote metastasis. Nat Cell Biol. 2014 Oct;16(10):992-1003

Lee JM, Hays JL, Chiou VL, Annunziata CM, Swisher EM, Harrell MI, Yu M, Gordon N, Sissung TM, Ji J, Figg WD, Minasian L, Lipkowitz S, Wood BJ, Doroshow J, Kohn EC. Phase I/Ib study of olaparib and carboplatin in women with triple negative breast cancer. Oncotarget. 2017 Mar 25;8(45):79175-79187

Liberti MV, Locasale JW. The Warburg Effect: How Does it Benefit Cancer Cells? Trends Biochem Sci. 2016 Mar;41(3):211-218

Lin CS, Liu LT, Ou LH, Pan SC, Lin CI, Wei YH. Role of mitochondrial function in the invasiveness of human colon cancer cells. Oncol Rep. 2018 Jan;39(1):316-330

Loibl S, Poortmans P, Morrow M, Denkert C, Curigliano G. Breast cancer. Lancet. 2021 May 8;397(10286):1750-1769

Maajani K, Jalali A, Alipour S, Khodadost M, Tohidinik HR, Yazdani K. The Global and Regional Survival Rate of Women With Breast Cancer: A Systematic Review and Meta-analysis. Clin Breast Cancer. 2019 Jun;19(3):165-177

Mann M, Kumar S, Sharma A, Chauhan SS, Bhatla N, Kumar S, Bakhshi S, Gupta R, Kumar L. PARP-1 inhibitor modulate β-catenin signaling to enhance cisplatin sensitivity in cancer cervix. Oncotarget. 2019 Jul 2;10(42):4262-4275

Martínez-Reyes I, Chandel NS. Cancer metabolism: looking forward. Nat Rev Cancer. 2021 Oct;21(10):669-680

Masoud V, Pagès G. Targeted therapies in breast cancer: New challenges to fight against resistance. World J Clin Oncol. 2017 Apr 10;8(2):120-134

Maughan KL, Lutterbie MA, Ham PS. Treatment of breast cancer. Am Fam Physician. 2010 Jun 1;81(11):1339-46

Meier R, Hemmings BA. Regulation of protein kinase B. J Recept Signal Transduct Res. 1999 Jan-Jul;19(1-4):121-8

Michels J, Vitale I, Senovilla L, Enot DP, Garcia P, Lissa D, Olaussen KA, Brenner C, Soria JC, Castedo M, Kroemer G. Synergistic interaction between cisplatin and PARP inhibitors in non-small cell lung cancer. Cell Cycle. 2013 Mar 15;12(6):877-83

Morales J, Li L, Fattah FJ, Dong Y, Bey EA, Patel M, Gao J, Boothman DA. Review of poly (ADP-ribose) polymerase (PARP) mechanisms of action and rationale for targeting in cancer and other diseases. Crit Rev Eukaryot Gene Expr. 2014;24(1):15-28

Murphy MP. Selective targeting of bioactive compounds to mitochondria. Trends Biotechnol. 1997 Aug;15(8):326-30

Nakatani K, Thompson DA, Barthel A, Sakaue H, Liu W, Weigel RJ, Roth RA. Up-regulation of Akt3 in estrogen receptor-deficient breast cancers and androgen-independent prostate cancer lines. J Biol Chem. 1999 Jul 30;274(31):21528-32

Neupert W, Herrmann JM. Translocation of proteins into mitochondria. Annu Rev Biochem. 2007;76:723-49

Ogden A, Rida PC, Aneja R. Heading off with the herd: how cancer cells might maneuver supernumerary centrosomes for directional migration. Cancer Metastasis Rev. 2013 Jun;32(1-2):269-87

Osaki M, Oshimura M, Ito H. PI3K-Akt pathway: its functions and alterations in human cancer. Apoptosis. 2004 Nov;9(6):667-76

Parada LF, Land H, Weinberg RA, Wolf D, Rotter V. Cooperation between gene encoding p53 tumour antigen and ras in cellular transformation. Nature. 1984 Dec 13-19;312(5995):649-51

Pfeiffer T, Schuster S, Bonhoeffer S. Cooperation and competition in the evolution of ATP-producing pathways. Science. 2001 Apr 20;292(5516):504-7

Ponder BA, Wilkinson MM. Direct examination of the clonality of carcinogen-induced colonic epithelial dysplasia in chimeric mice. J Natl Cancer Inst. 1986 Oct;77(4):967-76

Porteous CM, Logan A, Evans C, Ledgerwood EC, Menon DK, Aigbirhio F, Smith RA, Murphy MP. Rapid uptake of lipophilic triphenylphosphonium cations by mitochondria in vivo following intravenous injection: implications for mitochondria-specific therapies and probes. Biochim Biophys Acta. 2010 Sep;1800(9):1009-17

Purnell MR, Whish WJ. Novel inhibitors of poly(ADP-ribose) synthetase. Biochem J. 1980 Mar 1;185(3):775-7

Reda A, Refaat A, Abd-Rabou AA, Mahmoud AM, Adel M, Sabet S, Ali SS. Role of mitochondria in rescuing glycolytically inhibited subpopulation of triple negative but not hormone-responsive breast cancer cells. Sci Rep. 2019 Sep 24;9(1):13748

Redza-Dutordoir M, Averill-Bates DA. Activation of apoptosis signalling pathways by reactive oxygen species. Biochim Biophys Acta. 2016 Dec;1863(12):2977-2992

Riccardi C, Nicoletti I. Analysis of apoptosis by propidium iodide staining and flow cytometry. Nat Protoc. 2006;1(3):1458-61

Riddell IA. Cisplatin and Oxaliplatin: Our Current Understanding of Their Actions. Met Ions Life Sci. 2018 Feb 5;18

Robinson BW, Shewach DS. Radiosensitization by gemcitabine in p53 wild-type and mutant MCF-7 breast carcinoma cell lines. Clin Cancer Res. 2001 Aug;7(8):2581-9

Rosenberg B, Vancamp L, Krigas T. Inhibition of cell division in Escherichia coli by electrolysis products from a platinum electrode. Nature. 1965 Feb 13;205:698-9

Rottenberg S, Jaspers JE, Kersbergen A, van der Burg E, Nygren AO, Zander SA, Derksen PW, de Bruin M, Zevenhoven J, Lau A, Boulter R, Cranston A, O'Connor MJ, Martin NM, Borst P, Jonkers J. High sensitivity of BRCA1-deficient mammary tumors to the PARP inhibitor AZD2281 alone and in combination with platinum drugs. Proc Natl Acad Sci U S A. 2008 Nov 4;105(44):17079-84

Samuels Y, Wang Z, Bardelli A, Silliman N, Ptak J, Szabo S, Yan H, Gazdar A, Powell SM, Riggins GJ, Willson JK, Markowitz S, Kinzler KW, Vogelstein B, Velculescu VE. High frequency of mutations of the PIK3CA gene in human cancers. Science. 2004 Apr 23;304(5670):554

Sarmiento-Salinas FL, Delgado-Magallón A, Montes-Alvarado JB, Ramírez-Ramírez D, Flores-Alonso JC, Cortés-Hernández P, Reyes-Leyva J, Herrera-Camacho I, Anaya-Ruiz M, Pelayo R, Millán-Pérez-Peña L, Maycotte P. Breast Cancer Subtypes Present a Differential Production of Reactive Oxygen Species (ROS) and Susceptibility to Antioxidant Treatment. Front Oncol. 2019 Jun 7;9:480

Schito L, Semenza GL. Hypoxia-Inducible Factors: Master Regulators of Cancer Progression. Trends Cancer. 2016 Dec;2(12):758-770

Scott RE, Wille JJ Jr, Wier ML. Mechanisms for the initiation and promotion of carcinogenesis: a review and a new concept. Mayo Clin Proc. 1984 Feb;59(2):107-17

Sheu SS, Nauduri D, Anders MW. Targeting antioxidants to mitochondria: a new therapeutic direction. Biochim Biophys Acta. 2006 Feb;1762(2):256-65

Siegel RL, Miller KD, Jemal A. Cancer statistics, 2020. CA Cancer J Clin. 2020 Jan;70(1):7-30

Slamon DJ, Clark GM, Wong SG, Levin WJ, Ullrich A, McGuire WL. Human breast cancer: correlation of relapse and survival with amplification of the HER-2/neu oncogene. Science. 1987 Jan 9;235(4785):177-82

Smith RA, Porteous CM, Gane AM, Murphy MP. Delivery of bioactive molecules to mitochondria in vivo. Proc Natl Acad Sci U S A. 2003 Apr 29;100(9):5407-12

Srinivasan S, Guha M, Kashina A, Avadhani NG. Mitochondrial dysfunction and mitochondrial dynamics-The cancer connection. Biochim Biophys Acta Bioenerg. 2017 Aug;1858(8):602-614

Stankovic JSK, Selakovic D, Mihailovic V, Rosic G. Antioxidant Supplementation in the Treatment of Neurotoxicity Induced by Platinum-Based Chemotherapeutics-A Review. Int J Mol Sci. 2020 Oct 20;21(20):7753

Sung, H, Ferlay, J, Siegel, RL, Laversanne, M, Soerjomataram, I, Jemal, A, Bray, F. Global cancer statistics 2020: GLOBOCAN estimates of incidence and mortality worldwide for 36 cancers in 185 countries. CA Cancer J Clin. 2021: 71: 209- 249

Tait SW, Green DR. Mitochondrial regulation of cell death. Cold Spring Harb Perspect Biol. 2013 Sep 1;5(9):a008706

Todd RC, Lippard SJ. Inhibition of transcription by platinum antitumor compounds. Metallomics. 2009;1(4):280-91

Torre LA, Siegel RL, Ward EM, Jemal A. Global Cancer Incidence and Mortality Rates and Trends--An Update. Cancer Epidemiol Biomarkers Prev. 2016 Jan;25(1):16-27

Turk AA, Wisinski KB. PARP inhibitors in breast cancer: Bringing synthetic lethality to the bedside. Cancer. 2018 Jun 15;124(12):2498-2506

Twentyman PR, Luscombe M. A study of some variables in a tetrazolium dye (MTT) based assay for cell growth and chemosensitivity. Br J Cancer. 1987 Sep;56(3):279-85

Vichai V, Kirtikara K. Sulforhodamine B colorimetric assay for cytotoxicity screening. Nat Protoc. 2006;1(3):1112-6

Vivanco I, Sawyers CL. The phosphatidylinositol 3-Kinase AKT pathway in human cancer. Nat Rev Cancer. 2002 Jul;2(7):489-50

Vlahos CJ, Matter WF, Hui KY, Brown RF. A specific inhibitor of phosphatidylinositol 3-kinase, 2-(4-morpholinyl)-8-phenyl-4H-1-benzopyran-4-one (LY294002). J Biol Chem. 1994 Feb 18;269(7):5241-8

Vogelstein B, Fearon ER, Hamilton SR, Kern SE, Preisinger AC, Leppert M, Nakamura Y, White R, Smits AM, Bos JL. Genetic alterations during colorectal-tumor development. N Engl J Med. 1988 Sep 1;319(9):525-32

Voigt W. Sulforhodamine B assay and chemosensitivity. Methods Mol Med. 2005;110:39-48
Crowley LC, Marfell BJ, Scott AP, Waterhouse NJ. Quantitation of Apoptosis and Necrosis by Annexin V Binding, Propidium Iodide Uptake, and Flow Cytometry. Cold Spring Harb Protoc. 2016 Nov 1;2016(11)

Vozza A, Parisi G, De Leonardis F, Lasorsa FM, Castegna A, Amorese D, Marmo R, Calcagnile VM, Palmieri L, Ricquier D, Paradies E, Scarcia P, Palmieri F, Bouillaud F, Fiermonte G. UCP2 transports C4 metabolites out of mitochondria, regulating glucose and glutamine oxidation. Proc Natl Acad Sci U S A. 2014 Jan 21;111(3):960-5

Vuong D, Simpson PT, Green B, Cummings MC, Lakhani SR. Molecular classification of breast cancer. Virchows Arch. 2014 Jul;465(1):1-14

Waks AG, Winer EP. Breast Cancer Treatment: A Review. JAMA. 2019 Jan 22;321(3):288-300

Wang JB, Erickson JW, Fuji R, Ramachandran S, Gao P, Dinavahi R, Wilson KF, Ambrosio AL, Dias SM, Dang CV, Cerione RA. Targeting mitochondrial glutaminase activity inhibits oncogenic transformation. Cancer Cell. 2010 Sep 14;18(3):207-19

Wang JY, Li JQ, Xiao YM, Fu B, Qin ZH. Triphenylphosphonium (TPP)-Based Antioxidants: A New Perspective on Antioxidant Design. ChemMedChem. 2020 Mar 5;15(5):404-410

Warburg O. On respiratory impairment in cancer cells. Science. 1956 Aug 10;124(3215):269-70

Warburg O. On the origin of cancer cells. Science. 1956 Feb 24;123(3191):309-14

Warburg O. The metabolism of carcinoma cells. The Journal of Cancer Research. 1925;9(1):148–163

Ward PS, Thompson CB. Metabolic reprogramming: a cancer hallmark even warburg did not anticipate. Cancer Cell. 2012 Mar 20;21(3):297-308

Weinberg, F.; Hamanaka, R.; Wheaton, W.W.; Weinberg, S.; Joseph, J.; Lopez, M.; Kalyanaraman, B.; Mutlu, G.M.; Budinger, G.R.; Chandel, N.S. Mitochondrial metabolism and ROS generation are essential for Kras-mediated tumorigenicity. Proc. Natl. Acad. Sci. USA 2010, 107, 8788–8793

Weinberg SE, Chandel NS. Targeting mitochondria metabolism for cancer therapy. Nat Chem Biol. 2015 Jan;11(1):9-15

Wheate NJ, Walker S, Craig GE, Oun R. The status of platinum anti-cancer drugs in the clinic and in clinical trials. Dalton Trans. 2010 Sep 21;39(35):8113-27

Wheaton WW, Weinberg SE, Hamanaka RB, Soberanes S, Sullivan LB, Anso E, Glasauer A, Dufour E, Mutlu GM, Budigner GS, Chandel NS. Metformin inhibits mitochondrial complex I of cancer cells to reduce tumorigenesis. Elife. 2014 May 13;3:e02242

Yao H, He G, Yan S, Chen C, Song L, Rosol TJ, Deng X. Triple-negative breast cancer: is there a treatment on the horizon? Oncotarget. 2017 Jan 3;8(1):1913-1924

Yuan, T., Cantley, L. PI3K pathway alterations in cancer: variations on a theme. Oncogene 27, 5497–5510 (2008)

Zhang G, Frederick DT, Wu L, Wei Z, Krepler C, Srinivasan S, Chae YC, Xu X, Choi H, Dimwamwa E, Ope O, Shannan B, Basu D, Zhang D, Guha M, Xiao M, Randell S, Sproesser K, Xu W, Liu J, Karakousis GC, Schuchter LM, Gangadhar TC, Amaravadi RK, Gu M, Xu C, Ghosh A, Xu W, Tian T, Zhang J, Zha S, Liu Q, Brafford P, Weeraratna A, Davies MA, Wargo JA, Avadhani NG, Lu Y, Mills GB, Altieri DC, Flaherty KT, Herlyn M. Targeting mitochondrial biogenesis to overcome drug resistance to MAPK inhibitors. J Clin Invest. 2016 May 2;126(5):1834-56

Zhao H, Yang Q, Hu Y, Zhang J. Antitumor effects and mechanisms of olaparib in combination with carboplatin and BKM120 on human triple-negative breast cancer cells. Oncol Rep. 2018 Dec;40(6):3223-3234

Zhou BP, Hu MC, Miller SA, Yu Z, Xia W, Lin SY, Hung MC. HER-2/neu blocks tumor necrosis factor-induced apoptosis via the Akt/NF-kappaB pathway. J Biol Chem. 2000 Mar 17;275(11):8027-31

Zielonka J, Joseph J, Sikora A, Hardy M, Ouari O, Vasquez-Vivar J, Cheng G, Lopez M, Kalyanaraman B. Mitochondria-Targeted Triphenylphosphonium-Based Compounds: Syntheses, Mechanisms of Action, and Therapeutic and Diagnostic Applications. Chem Rev. 2017 Aug 9;117(15):10043-10120

Zorova LD, Popkov VA, Plotnikov EY, Silachev DN, Pevzner IB, Jankauskas SS, Babenko VA, Zorov SD, Balakireva AV, Juhaszova M, Sollott SJ, Zorov DB. Mitochondrial membrane potential. Anal Biochem. 2018 Jul 1;552:50-59

PUBLICATIONS OF THE AUTHOR

Andreidesz K, Koszegi B, Kovacs D, Bagone Vantus V, Gallyas F, Kovacs K. Effect of Oxaliplatin, Olaparib and LY294002 in Combination on Triple-Negative Breast Cancer Cells. Int J Mol Sci. 2021 Feb 19;22(4):2056

IF: 5.924

Andreidesz K, Szabo A, Kovacs D, Koszegi B, Bagone Vantus V, Vamos E, Isbera M, Kalai T, Bognar Z, Kovacs K, Gallyas F Jr. Cytostatic Effect of a Novel Mitochondria-Targeted Pyrroline Nitroxide in Human Breast Cancer Lines. Int J Mol Sci. 2021 Aug 20;22(16):9016

IF: 5.924

SCIENTIFIC ACTIVITIES

Presentations on international conferences

Kitti Andreidesz, Krisztina Kovács: *Investigating the effects of a PARP inhibitor (HO3089) on monocrotaline-induced pulmonary hypertension in rat lung tissue*. Medical Conference for PhD Students and Experts of Clinical Sciences, Pécs, 27th October 2018

Kitti Andreidesz, Krisztina Kovács: *The effect of a PARP inhibitor, Olaparib in combination with Oxaliplatin treatment on breast cancer cell lines* XII. International and XIX. National Interdisciplinary Grastyán Conference, Pécs, April 4-5 2019

Kitti Andreidesz, Krisztina Kovács, Balázs Sümegi, Ferenc Gallyas: *Investigating the effects of a PARP inhibitor (HO3089) on monocrotaline-induced pulmonary hypertension in rat lung tissue.* Interdiszciplináris Doktorandusz Konferencia, Pécs, 24-25 May 2019

Kitti Andreidesz, Krisztina Kovács: *Investigating the modifications of signaling pathways in monocrotaline-induced pulmonary hypertension in rat lung tissue by PARP inhibitor HO-3089.* International Student Congress, Graz, Austria, 30th May – 1st June 2019

Kitti Andreidesz, Krisztina Kovács: *The effects of olaparib and oxaliplatin on breast cancer cell lines.* Medical Conference for PhD Students and Experts of Clinical Sciences, Pécs, 9th November 2019

Krisztina Kovacs, Kitti Andreidesz, Dominika Kovacs, Balazs Koszegi, Viola Bagone Vantus, Antal Tapodi, Balazs Veres, Ferenc Gallyas: *New therapeutic approaches in the treatment of triple-negative breast cancer.* 17th International Conference on Cancer and Cancer Therapy, Webinar, 12th November 2021

Poster presentation on international conference

Kitti Andreidesz, Krisztina Kovács, Balázs Sümegi, Ferenc Gallyas: *Investigating the effects of a PARP inhibitor HO-3089 on signaling pathways in monocrotaline-induced pulmonary hypertension in rat lung tissue.* Hungarian Molecular Life Science Conference, Eger, 29-31 May 2019

Poster presentation on national conference

Andreidesz Kitti, Kovács Krisztina, Sümegi Balázs, ifj. Gallyas Ferenc: *A PARP inhibitor HO-3089 hatása jelátviteli útvonalakra pulmonáris hipertóniában.* 49th Membrane Transport Conference, Sümeg, 14-17 May 2019

ACKNOWLEDGEMENTS

There are many people whom I would like to thank for their contributions. I would first like to express my gratitude to my supervisor Dr. Krisztina Kovács for giving me the opportunity to achieve my PhD. I wish to thank her for her patience, guidance and continuous support throughout the years.

I wish to express my gratitude to Prof. Ferenc Gallyas, the head of the Department of Biochemistry and Medical Chemistry for his support.

The completion of this work could not have been possible without the help of Dr. Ferenc Budán. Thank you for motivating me all the time!

I wish to thank my co-authors and my colleagues in the Department of Biochemistry and Medical Chemistry for their help.

Last but not the least, I would like to thank my best friend Csanád Rédei and my family for their love, encouragement and never ending support.

‘God doesn’t give you what you want… He creates the opportunity to do so.’

International Journal of
Molecular Sciences

MDPI

Article

Effect of Oxaliplatin, Olaparib and LY294002 in Combination on Triple-Negative Breast Cancer Cells

Kitti Andreidesz [1], Balazs Koszegi [1], Dominika Kovacs [1], Viola Bagone Vantus [1], Ferenc Gallyas [1,2,3] and Krisztina Kovacs [1,*]

[1] Department of Biochemistry and Medical Chemistry, University of Pécs Medical School, 7624 Pécs, Hungary; andreidesz.kitti@pte.hu (K.A.); balazs.koszegi@aok.pte.hu (B.K.); dominika.kovacs@aok.pte.hu (D.K.); viola.vantus@aok.pte.hu (V.B.V.); ferenc.gallyas@aok.pte.hu (F.G.)
[2] Szentagothai Research Centre, University of Pécs, 7624 Pécs, Hungary
[3] Nuclear-Mitochondrial Interactions Research Group, Hungarian Academy of Sciences, 1052 Budapest, Hungary
* Correspondence: krisztina.kovacs@aok.pte.hu; Tel.: +36-72-536-276; Fax: +36-72-535-277

Abstract: Triple-negative breast cancer (TNBC) has a poor prognosis as the therapy has several limitations, most importantly, treatment resistance. In this study we examined the different responses of triple-negative breast cancer line MDA-MB-231 and hormone receptor-positive breast cancer line MCF7 to a combined treatment including olaparib, a poly-(ADP ribose) polymerase (PARP) inhibitor, oxaliplatin, a third-generation platinum compound and LY294002, an Akt pathway inhibitor. We applied the drugs in a single, therapeutically relevant concentration individually and in all possible combinations, and we assessed the viability, type of cell death, reactive oxygen species production, cell-cycle phases, colony formation and invasive growth. In agreement with the literature, the MDA-MB-231 cells were more treatment resistant than the MCF7 cells. However, and in contrast with the findings of others, we detected no synergistic effect between olaparib and oxaliplatin, and we found that the Akt pathway inhibitor augmented the cytostatic properties of the platinum compound and/or prevented the cytoprotective effects of PARP inhibition. Our results suggest that, at therapeutically relevant concentrations, the cytotoxicity of the platinum compound dominated over that of the PARP inhibitor and the PI3K inhibitor, even though a regression-based model could have indicated an overall synergy at lower and/or higher concentrations.

Keywords: olaparib; oxaliplatin; Akt pathway inhibitor; TNBC; MCF7

Citation: Andreidesz, K.; Koszegi, B.; Kovacs, D.; Bagone Vantus, V.; Gallyas, F.; Kovacs, K. Effect of Oxaliplatin, Olaparib and LY294002 in Combination on Triple-Negative Breast Cancer Cells. *Int. J. Mol. Sci.* **2021**, *22*, 2056. https://doi.org/10.3390/ijms22042056

Academic Editor: Antonella Zannetti
Received: 31 January 2021
Accepted: 17 February 2021
Published: 19 February 2021

1. Introduction

In terms of incidence, breast cancer is the leading cancer type among women [1]. It is a heterogenous and hormone-dependent disease [2]; approximately 65–75% of cases are hormone receptor-positive (HR+; estrogen receptor-positive or progesterone receptor-positive) [3], while 15–20% are human epidermal growth-factor receptor 2 (HER2)- positive [4]. The triple-negative subtype (TNBC) represents 15% of all cases [5]. For HR+ and/or HER2+ breast cancers, targeted therapies are available. These include biological and/or hormonal therapy, in which the overexpressed or overactivated molecules are blocked specifically; in the case of HER2+ breast cancer, Herceptin is a widely used monoclonal antibody which binds to HER2, blocking its downstream signalling; in hormone receptor-positive breast cancer, tamoxifen is a regularly used selective estrogen receptor modulator of anti-oestrogenic effects [6]. In contrast, the treatment protocol for TNBC is mainly limited to chemotherapy. Besides the limited therapy options, recurrent tumor resistance and poor prognoses are emerging challenges [7] in TNBC.

The agents used in chemotherapy are rather non-selective as it has been demonstrated by platinum-based substances, which have been in clinical use for decades [8]. Their cytotoxicity is based on the formation of platinum-DNA adducts, leading to double-strand

DNA breaks and eventually cell death [8,9]. Cisplatin and carboplatin are widely used platinum-based agents in the treatment of non-small-cell lung cancer, and breast, ovarian and testicular cancer [10]. One major limiting factor in their therapeutic use is the possibility that the cancer cells develop intrinsic or acquired resistance to the treatment [8,11]. Oxaliplatin is a third-generation platinum compound. One of its benefits is decreased mutagenic activity compared to cisplatin and carboplatin, and it is often effective in cisplatin-resistant tumors [8,9]. It has been approved by the FDA for treatment of colorectal cancer [12], and it has the potential to replace other platinum compounds in therapy for other types of cancer including TNBC.

The nuclear Poly(ADP-ribose) polymerase (PARP) enzymes found in all nucleated cells are a family of enzymes involved mainly in DNA repair, namely in base excision and nucleotide excision repair. PARP-1 catalyses transfer of ADP-ribose of NAD^+ to a wide range of proteins. It binds to specific DNA sequences, and by self-ADP-ribosylation, it recruits repair machinery to the site of DNA damage [13]. PARP inhibition is cytotoxic in germline mutated BRCA1 and BRCA2 ovarian and breast cancer [14]. Olaparib is the most widely used PARP inhibitor in clinical therapy nowadays. It has been approved for the treatment of BRCA 1/2 mutated ovarian and metastatic breast cancer [15].

The PI3K/Akt/mTOR pathway play an important role in carcinogenesis and apoptosis resistance, promoting tumor growth and proliferation, and the activation of phosphatidylinositol 3-kinase (PI3K) has been associated with endocrine resistance, a major problem in the treatment of breast cancer [16–18]. Recently, based on the outcome of the phase III SOLAR-1 clinical trial (NCT02437318), the Food and Drug Administration approved (in combination with fulvestrant, an estrogen receptor antagonist) the PI3K p110α-isoform-specific inhibitor, alpelisib for use in the treatment of HR+/HER2- metastatic breast cancer. However, combination of isoform-specific PI3K inhibitors with immune checkpoint-, receptor- or enzyme inhibitors, including PARP inhibitors, could extend their therapeutic use to HER2+ or triple-negative breast cancers [19].

Combination chemotherapy was introduced more than 40 years ago [20]. Many DNA adduct-forming metallodrugs, in combination with other drugs of different molecular action, such as inhibition of protein synthesis or DNA repair mechanisms, can increase their therapeutic efficacy over monotherapy and can overcome chemotherapy resistance [21]. Several preclinical studies found a synergistic effect between platinum drugs and PARP inhibitors. However, experimental design, data acquisition and interpretation of preclinical and especially clinical studies are prone to errors and pitfalls which undermine certainty of this synergy [22]. Even the protective effect of PARP inhibitors against oxidative stress may impede this synergy, since oxidative stress contributes to the therapeutic effect of platinum drugs [23].

Accordingly, the present study aimed to investigate the response of TNBC line MDA-MB-231 versus HR+ breast cancer line MCF7 in a combined treatment comprising oxaliplatin, olaparib and LY294002 treatment.

2. Results

2.1. Effect of Olaparib, Oxaliplatin and Akt Pathway Inhibitor on Cell Viability

An MTT assay was performed to determine the effect of olaparib, oxaliplatin and LY294002 alone and in combination on MDA-MB-231 and MCF7 cells. As shown in Figure 1A,C, olaparib alone did not decrease viability significantly in either cell line. However, oxaliplatin reduced viability of the TNBC line MDA-MB-231 substantially and, more pronouncedly, the estrogen and progesterone receptor-positive non-TNBC line MCF7. Our results show that olaparib and oxaliplatin had neither a synergistic, nor an additive effect at the applied concentrations, since their combination caused about the same extent of cell death as oxaliplatin alone (Figure 1). The MDA-MB-231 cells were resistant to treatment with the Akt pathway inhibitor LY294002 (Figure 1B). In contrast, LY294002 caused about the same extent of cell death in the MCF7 cell line as oxaliplatin did (Figure 1D). Furthermore, LY294002 enhanced the effect of oxaliplatin but not that of olaparib on both

MDA-MB-231 and MCF7 cells. Additionally olaparib did not add to the effect of LY294002 and oxaliplatin (Figure 1B,D).

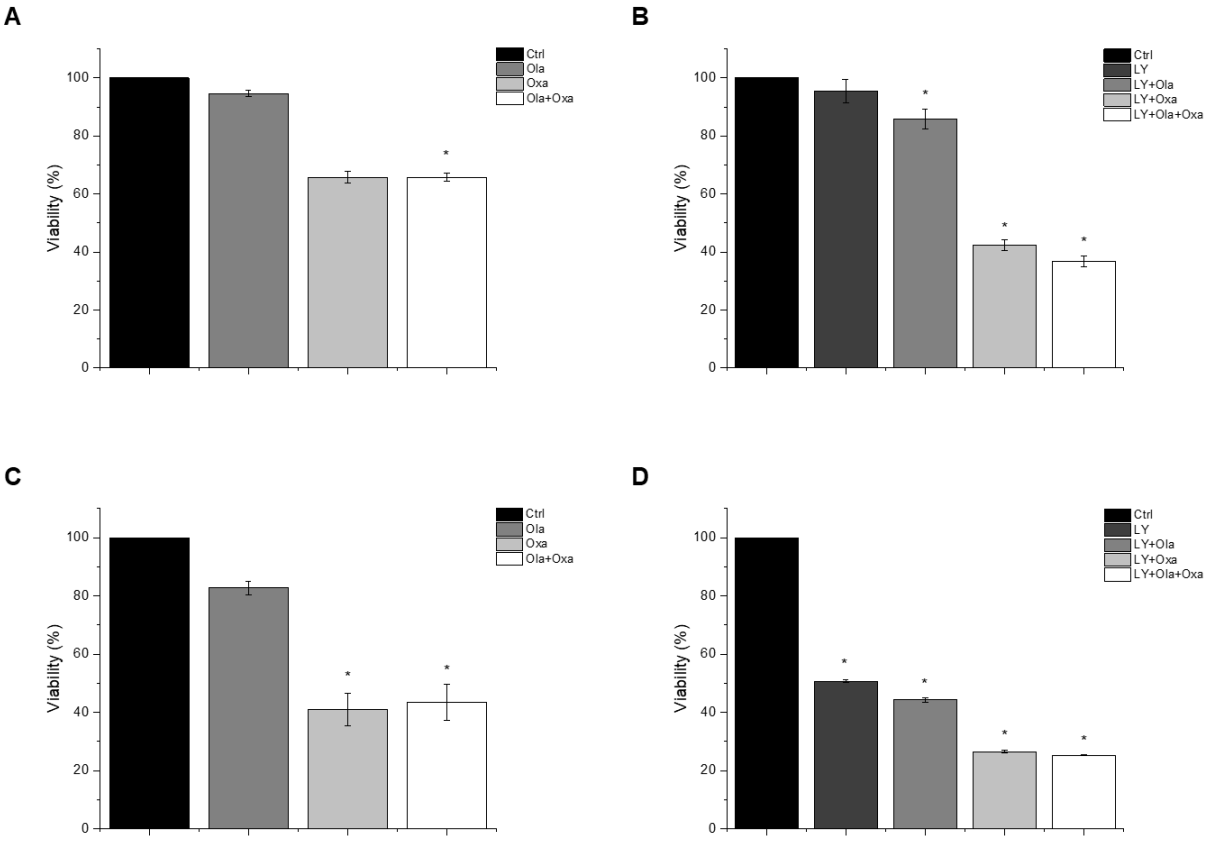

Figure 1. The effects of Ola, Oxa and LY on the viability of TNBC MDA-MB-231 (**A**,**B**) and non-TNBC MCF7 (**C**,**D**) cells were evaluated by MTT assay. Cells were treated with 2 μM olaparib, 25 μM oxaliplatin, 1 μM LY294002 alone and in combination for 72 h. Data are shown as mean ± SEM of at least three separate experiments. * $p < 0.05$ compared with the untreated cells. Ola—olaparib; Oxa—oxaliplatin; LY—LY294002; TNBC—triple-negative breast cancer; MTT-3-(4,5-dimethylthiazol-2-yl)-2,5-diphenyltetrazolium bromide.

2.2. Effect of Olaparib, Oxaliplatin and Akt Pathway Inhibitor on Cell Death Processes

We investigated which type of cell death LY294002, olaparib and oxaliplatin elicited by flow cytometry after double-staining the treated cells with fluorescently labelled Annexin V and propidium iodide, to demonstrate apoptosis and necrosis, respectively. We found that less than 5% of cell death caused by the compounds investigated was necrotic, and most of the dying cells were in their early apoptotic stage under the experimental conditions we used (Figure 2). Olaparib did not induce apoptosis in MDA-MB-231 and MCF7 cells, while oxaliplatin increased early and late apoptosis in both cell lines (Figure 2). The Akt pathway inhibitor LY294002 alone caused about the same level of apoptosis in both cell lines as oxaliplatin did (Figure 2C,D). On the other hand, treatment of the cells with LY294002 together with olaparib, oxaliplatin or their combination did not significantly change the distribution of cells among live, early, and late apoptotic populations in either of the cell lines (Figure 2C,D).

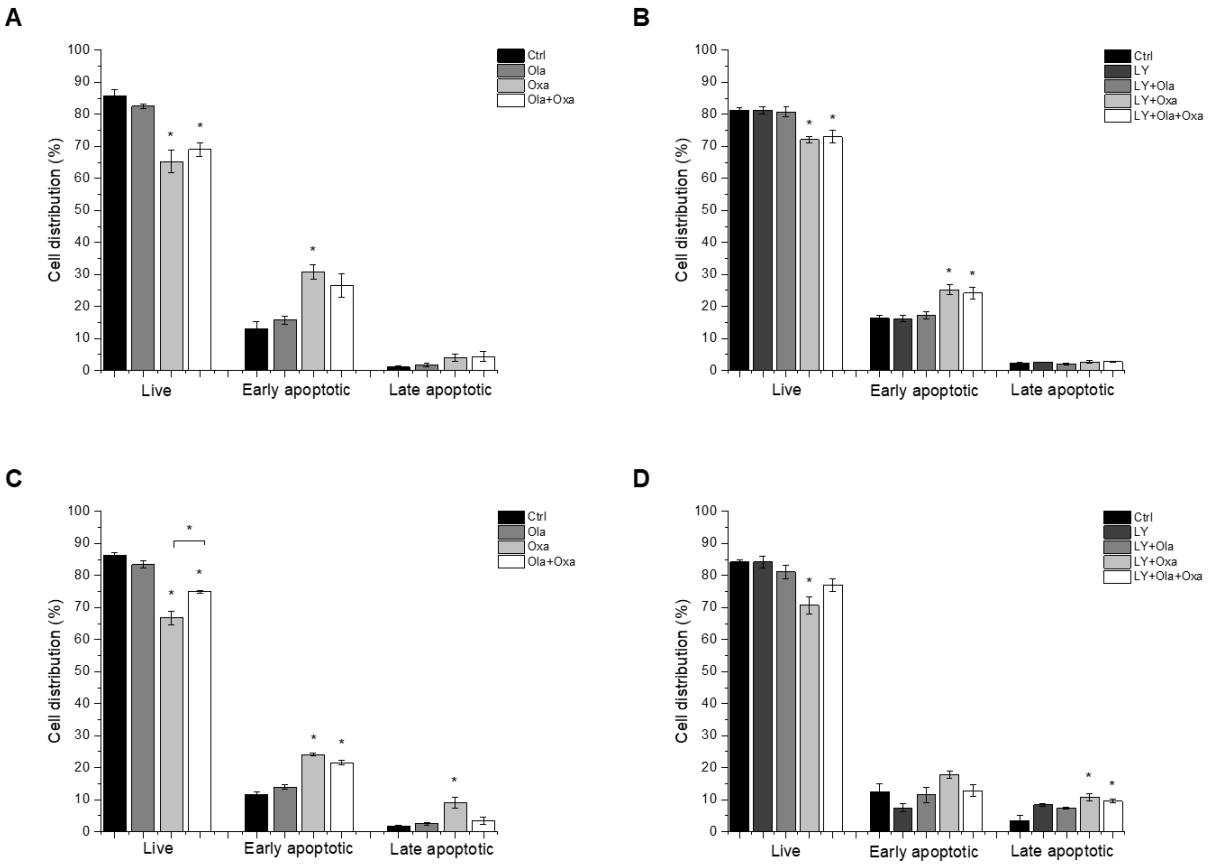

Figure 2. The effects of Ola, Oxa and LY on MDA-MB-231 (**A**,**B**) and MCF7 (**C**,**D**) cell apoptosis were detected by MUSE Cell Analyzer using MUSE Annexin V and Dead Cell Kit after 72 h treatment with 2 μM olaparib, 25 μM oxaliplatin, 1 μM LY294002 alone and in combination. Results are shown as mean ±SEM of at least three separate experiments. * $p < 0.05$ compared with the untreated cells. Ola—olaparib; Oxa—oxaliplatin; LY—LY294002.

2.3. Effect of Olaparib, Oxaliplatin and Akt Pathway Inhibitor on ROS Production

The reactive oxygen species (ROS) production capacity of olaparib, oxaliplatin and Akt pathway inhibitor LY294002 was measured using a carboxy-H2DCFDA assay. This assay measures fluorescence intensity of H2DCFDA, a fluorescent redox dye oxidized by the ROS from its non-fluorescent reduced form. We found marked differences between MDA-MB-231 (Figure 3A,B) and MCF7 (Figure 3C,D) lines among the treatment groups. The PARP inhibitor increased ROS production in MCF7 cells, although the effect did not reach a statistically significt level (Figure 3C). In contrast, the drug did not induce any ROS production in MDA-MB-231 cells (Figure 3A). Oxaliplatin caused significant ROS production in the triple-negative breast cancer cells which was enhanced by olaparib co-treatment, although olaparib's enhancing effect did not reach a statistically significt level (Figure 3A). The Akt pathway inhibitor did not affect ROS production either alone or in any combination with olaparib and oxaliplatin (Figure 3B). On the other hand, oxaliplatin did not affect ROS production of MCF7 cells and attenuated ROS production induced either by olaparib (Figure 3C), LY294002, or their combination (Figure 3D). However, these negative effects of oxaliplatin did not reach a statistically significant level. The Akt pathway inhibitor alone induced a similar level of ROS production in MCF7 cells as that caused by olaparib (Figure 3D).

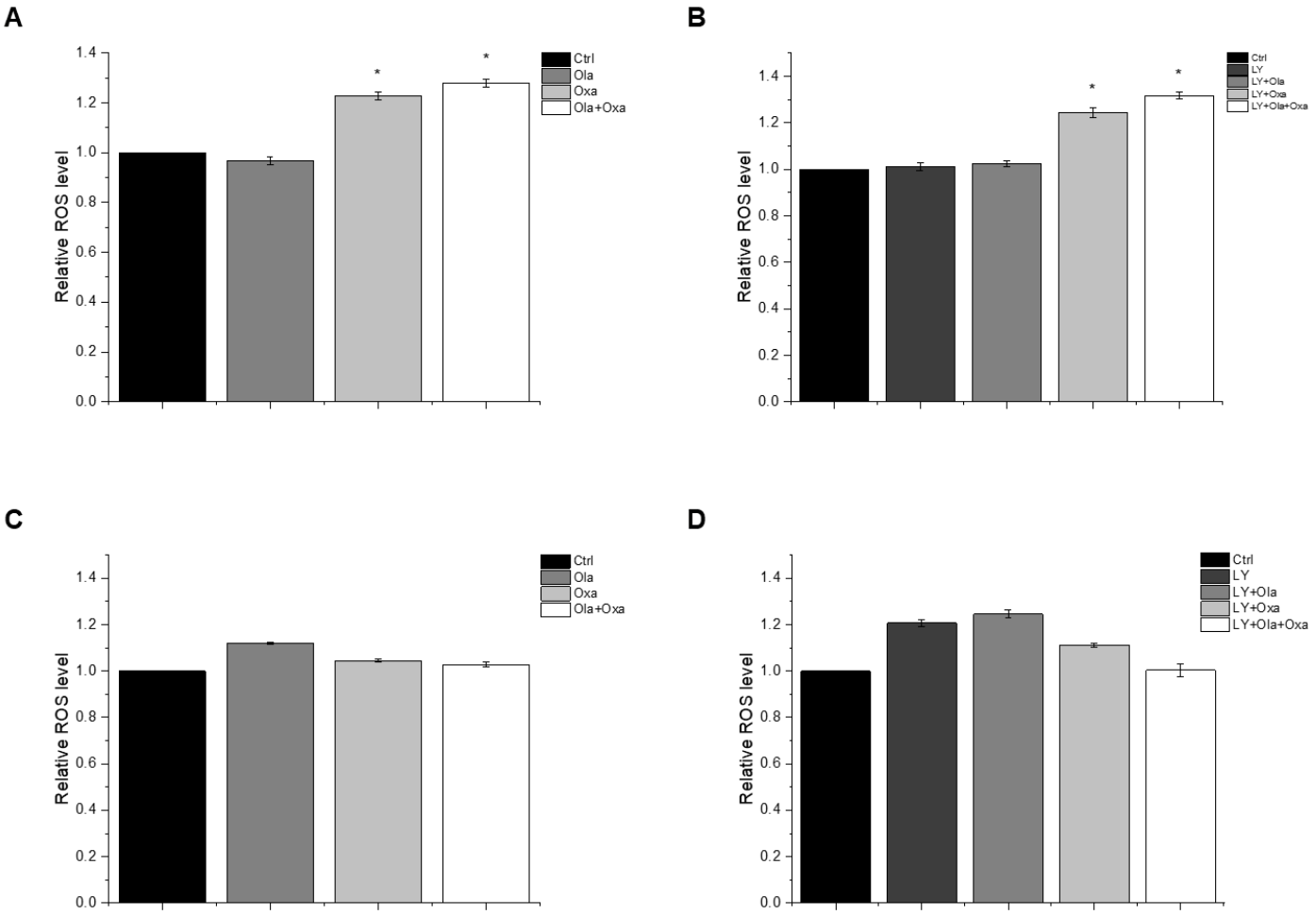

Figure 3. Effects of Ola, Oxa and LY on ROS production by MDA-MB-231 (**A**,**B**) and MCF7 (**C**,**D**) cells treated with 2 μM olaparib, 25 μM oxaliplatin and 1 μM LY294002. Results are shown as mean ±SEM of at least three separate experiments. * $p < 0.05$ compared with the untreated cells. Ola—olaparib; Oxa—oxaliplatin; LY—LY294002.

2.4. Effect of Olaparib, Oxaliplatin and Akt Pathway Inhibitor on the Cell Cycle

Flow cytometry was used to determine which cell cycle phase the cells had reached after treatment with different combinations of olaparib, oxaliplatin and LY294002. The distribution of control MDA-MB-231 cells among G1, S and G2/M phases was 55.57%, 22.8% and 21.63%, respectively, which was not affected by the PARP inhibitor olaparib (Figure 4A,C), the Akt pathway inhibitor LY294002, or their combination (Figure 4B,D). In contrast, oxaliplatin treatment arrested the cells in the S phase of their cycle (Figure 4C) which was not affected by olaparib co-treatment (Figure 4C). However, LY294002 co-treatment attenuated oxaliplatin's arresting effect, which was further reduced when olaparib was included in the combination treatment (Figure 4D).

The cell cycle phase distribution of control MCF7 cells was slightly different from that of MDA-MB-231 cells. Approximately 51.26% of control cells were in G1; 28.64% in S and 20.1% were in G2/M phase (Figure 4E,G). As with the MDA-MB-231 line, oxaliplatin arrested MCF7 cells in the S phase of their cycle (Figure 4G) and olaparib co-treatment did not have any further effect on it (Figure 4G). However, the PARP inhibitor increased the number of G2/M phase cells at the expense of S phase, although this effect did not reach a statistically significant level (Figure 4G). Additionally, LY294002 significantly enhanced the number of G1-phase cells at the expense of S and G2/M phase cells. This effect was not affected by olaparib co-treatment but was significantly counteracted by oxaliplatin (Figure 4H).

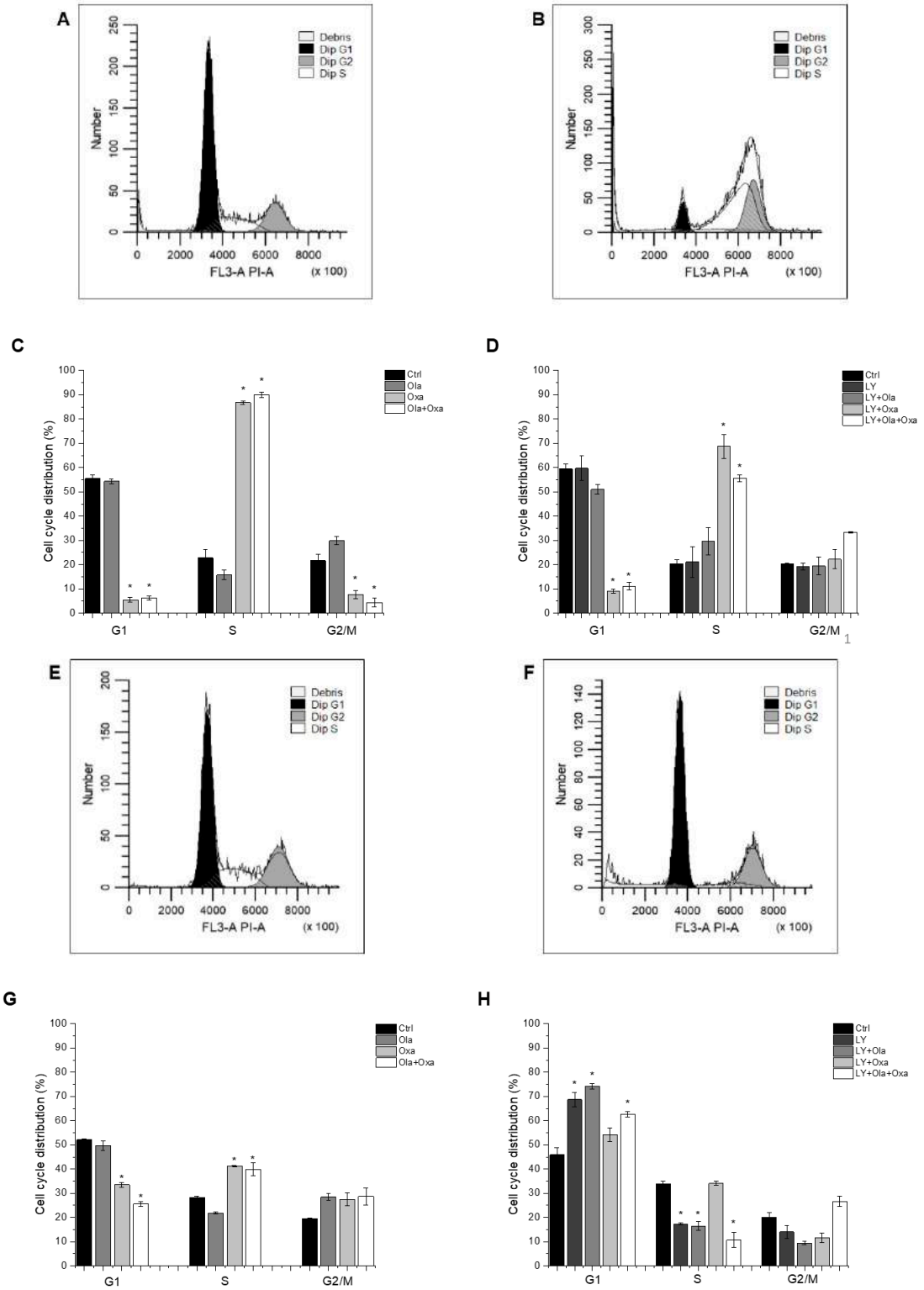

Figure 4. Flow cytometry analysis of MDA-MB-231 (**A**–**D**) and MCF7 (**E**–**H**) cell-cycle distribution. Cells were cultured and treated for 72 h with 2 μM olaparib, 25 μM oxaliplatin and 1 μM LY294002 alone and in combination. The cell-cycle distribution was determined with propidium iodide staining. The histograms show cell-cycle phases of control cells (**A**,**E**) and cells treated with combination of olaparib, oxaliplatin and LY294002 (**B**,**F**). The bar charts represent effect of single and combined treatment on cell cycle phase distribution (**C**,**D**,**G**,**H**). Results are expressed as mean ±SEM of at least three separate experiments. * $p < 0.05$ compared with the untreated cells.

2.5. Effect of Olaparib, Oxaliplatin and Akt Pathway Inhibitor on Colony Formation

To assess cellular proliferation capacity, a colony formation assay was performed. Olaparib and oxaliplatin significantly decreased colony numbers of both cell lines, although the non-TNBC line MCF7 was more sensitive to the cytostatic drugs than the TNBC line MDA-MB-231 (Figure 5A,C). Furthermore, oxaliplatin attenuated colony formation to a much greater extent than olaparib did (Figure 5A,C). A combination of olaparib and oxaliplatin caused a similar decrease in colony formationt as oxaliplatin did alone (Figure 5A,C), indicating a lack of synergy, even additivity, between the two substances. LY294002 alone decreased colony formation to about the same extent as olaparib did (Figure 5B,D). The PARP inhibitor andto a greater extent, oxaliplatin both augmented the Akt pathway inhibitor's effect on colony formation (Figure 5B,D). Again, combination of olaparib and oxaliplatin had about the same effect as the latter alone (Figure 5B,D).

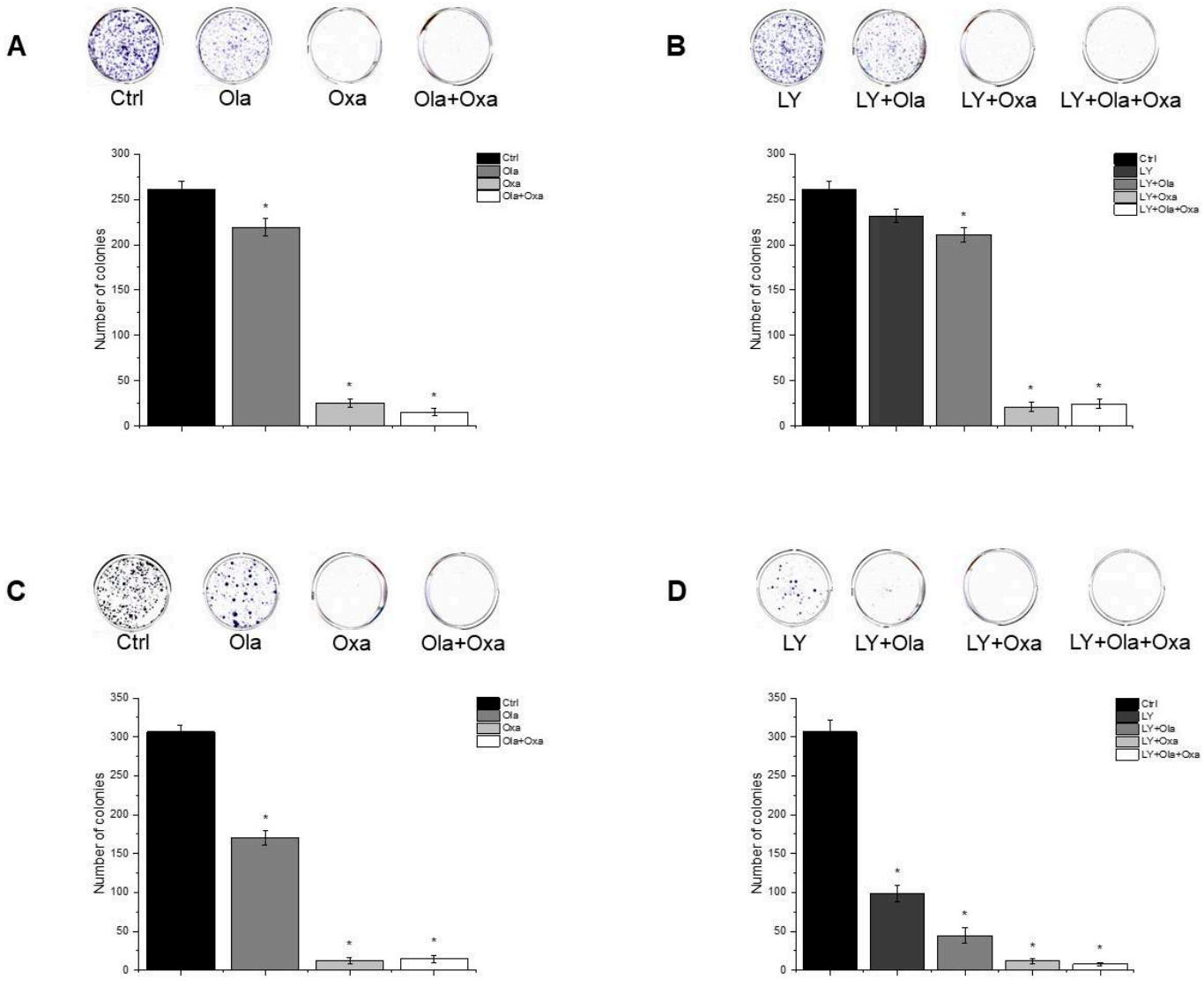

Figure 5. Effects of Ola, Oxa and LY on colony formation by MDA-MB-231 (**A**,**B**) and MCF7 (**C**,**D**) cells. Cells were seeded in six-well plates and after one day treated with 2 μM olaparib, 25 μM oxaliplatin, 1 μM LY294002 alone and in combination. Cells were treated for 14 days before being stained with Coomassie Blue. Results are shown as mean ± SEM of at least three separate experiments. * $p < 0.05$. Ola—olaparib; Oxa—oxaliplatin; LY—LY294002.

2.6. Effect of Olaparib and Oxaliplatin on Invasive Growth

Invasive growth of the cell lines was assessed the xCelligence Real-Time Cell Analysis (RTCA) system. As with the colony formation experiments, olaparib and, to a much greater extent oxaliplatin decreased invasive growth in both cell lines (Figure 6). Again, MCF7 line was more sensitive to the cytostatic drugs than MDA-MB-231, and combination of the two drugs had about the same effect as oxaliplatin alone had (Figure 6).

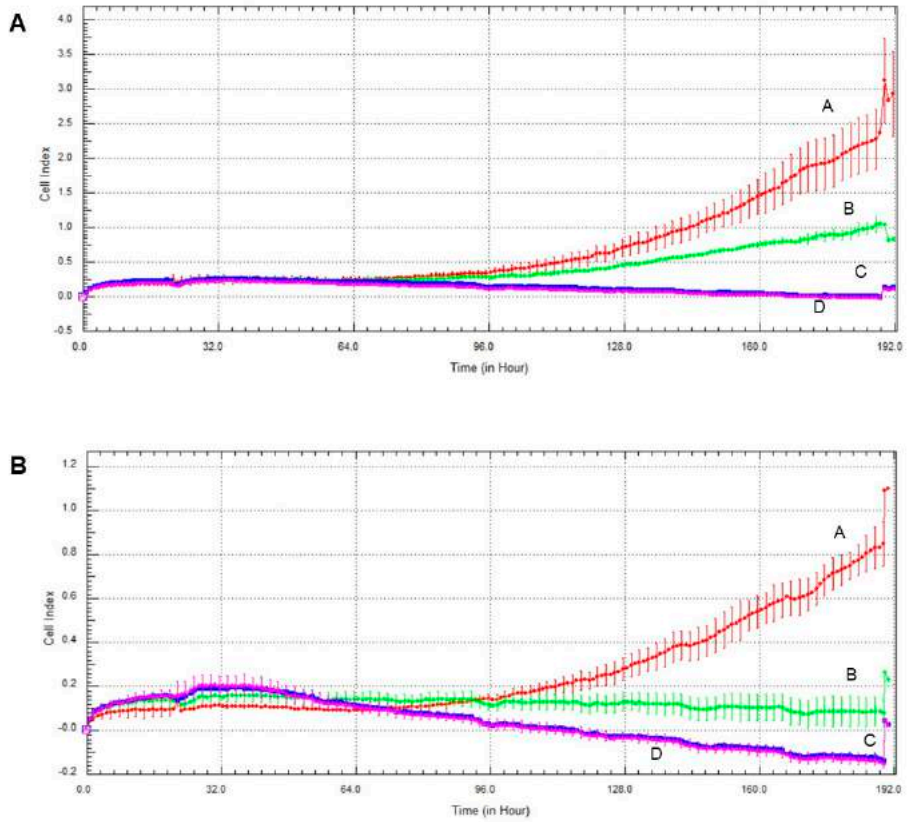

Figure 6. Effect of olaparib and oxaliplatin on invasive growth of MDA-MB-231 (**A**) and MCF7 (**B**) cells treated with 2 μM olaparib and 25 μM oxaliplatin. Line A—control, Line B—2 μM olaparib treatment, Line C—25 μM oxaliplatin treatment, Line D—combination treatment.

2.7. Effect of Olaparib, Oxaliplatin and Akt Pathway Inhibitor on Invasive Growth

The Akt pathway inhibitor decreased invasive growth, and its effect on MCF7 cells was more pronounced than on MDA-MB-231 cells (Figure 7). Both olaparib and oxaliplatin treatment augmented LY294002′s effect, decreasing invasive growth to the detection limit (Figure 7).

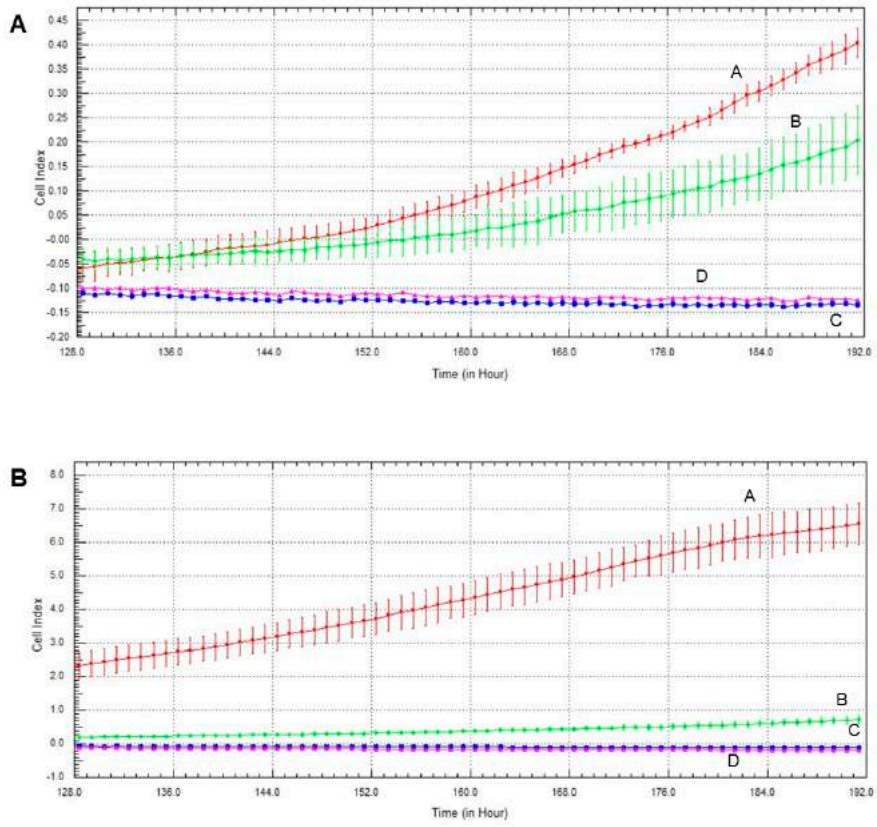

Figure 7. Effects of olaparib, oxaliplatin and LY294002 on invasive growth of MDA-MB-231 (**A**) and MCF7 (**B**) cells treated with 2 μM olaparib, 25 μM oxaliplatin and 1 μM LY294002. Line A—control, Line B—1 μM LY294002 treatment, Line C—2 μM olaparib and 25 μM oxaliplatin, Line D—combination treatment of 1 μM LY294002, 2 μM olaparib and 25 μM oxaliplatin.

3. Discussion

In breast cancer, TNBC is associated with poorer prognosis and limited targeted therapeutic options compared to the HR+ subtype [6]. Accordingly, in this study, we investigated the response of different types of breast-cancer cell lines to a combination of conventional chemotherapy [24] and synthetic lethality-based therapy [25] supplemented with Akt inhibition to prevent undesired cytoprotective effects of the latter [26]. We used the TNBC cell line MDA-MB-231 and estrogen and progesterone receptor-positive cell line MCF7, and treated these with the third-generation platinum compound oxaliplatin, the PARP inhibitor olaparib and the PI3K inhibitor LY294002.

Several studies have reported the synergistic effect of PARP inhibitors and chemotherapeutic platinum agents in various tumors. Olaparib and platinum compound carboplatin have been found to have modest activity in patients with sporadic TNBC [27]. Combination of PARP inhibitor PJ34 and antineoplastic agent cisplatin has been found to have cytotoxic synergy in non-small-cell lung-cancer line A549 [28]. Furthermore, PJ34 enhanced suppressive effect of cisplatin in liver-cancer cell line HepG2 [29]. The importance of the PI3K/Akt pathway in therapy resistance has been highlighted, demonstrating that its activation results in decreased sensitivity to chemotherapeutic agents [30]. Furthermore, PI3K/Akt pathway inhibitors have been known to cause more favorable outcomes when co-administered with usual anticancer drugs [31]. To provide experimental support for the rationale of combination therapy in TNBC, Zhao et al. investigated various combinations of olaparib, carboplatin and buparlisib, a pan-PI3K inhibitor in two human TNBC lines and a HR+ breast-cancer line [32]. By using a calculation [22] based on the median-effect equation, they found a synergistic cytostatic effect of the combination therapy in TNBC lines but not in the HR+ line [32]. We approached the question of synergy from a practical

point of view. Instead of determining dose-response effects, we used single, therapeutically relevant concentration of each drug, and applied these individually and in all possible combinations in experiments on viability, type of cell death, ROS production, cell-cycle phase, colony formation and invasive growth.

We found that 72 h of olaparib treatment decreased viability of MCF7 cells to a much greater extent than that of MDA-MB-231 cells (Figure 1). Elevated PARP-1 expressions have been reported in a wide range of human cancers including breast cancer, and an especially high PARP-1 expression has been found found in TNBC which can explain our results [23]. Furthermore, in complete agreement with our data,other studies have found the cytotoxic effect of oxaliplatin to be higher in MCF7 than in TNBC cells [30]. Several studies have reported the synergistic cytostatic effect of PARP inhibitors and platinum agents [27–29], and one study reported synergism in combined therapy comprising olaparib, carboplatin and the PI3K inhibitor buparlisib in TNBC lines but not in a HR+ breast-cancer line [32]. In contrast, under our experimental conditions, olaparib did not enhance the cytotoxic properties of oxaliplatin (Figure 1), and we could not detect synergism, nor even an additive effect between these two drugs. The PI3K inhibitor LY294002 decreased viability of the TNBC but not the HR+ line when combined with olaparib, oxaliplatin or both. However, these effects did not reach a statistically significant level (Figure 1). These data compellingly indicate that, at therapeutically relevant concentrations, cytotoxicity of the platinum compound dominated that of the PARP inhibitor and the PI3K inhibitor. At lower platinum compound and higher concentrations of PARP and PI3K a synergistic effect likely appear and a regression-based model could indicate an overall synergy that may explain the conflict between our results (Figure 1) and the findings of others [27–29,32]. Additionally, platinum compounds induce ROS production [33] and PARP inhibitors are known to protect against oxidative stress [23], what could contribute to the absence of synergy between the PARP inhibitor and the platinum agent that we observed. Accordingly, blocking the PI3K/Akt pathway by the PI3K inhibitor LY294002 increased the cytotoxicity of olaparib and oxaliplatin co-treatment, although the effect did not reach a statistically significant level (Figure 1).

We found that olaparib and oxaliplatin killed MDA-MB-231 and MCF7 cells predominantly by apoptosis (Figure 2). The apoptosis resistance of the two cell lines is different. MDA-MB-231 line has high levels of mutant p53 [34], whereas MCF7 line has wild-type p53 [35]. Additionally, TNBC cells have 10-fold greater phospholipase D (PLD) activity than MCF7 cells [34]. Mutant p53 and elevated PLD activity play a significant role in the survival of cancer cells and can contribute to the suppression of apoptosis [34]. Nevertheless, the effect of the various treatments on distribution among live, early and late-apoptotic populations was similar in both cell lines (Figure 2). In this respect it is worth noting that the washing steps before and after the staining procedure remove most non-adherent cells, and the flow cytometry method used to determine the type of cell death analyses stained cells only, regardless of the original cell number and their sensitivity to the various treatments.

Among other mechanisms, ROS-mediated processes play a prominent role in remodelling cancer phenotypes resistant to apoptosis which acquire enhanced metastatic properties [36]. In solid tumors, hypoxia and the resulting hypoxia-inducible factor (Hif)-1α mediated metabolic plasticity play a pivotal role in malignant transformation [37]. However, in cell culturing conditions, uniform oxygen partial pressure and practically inexhaustible extracellular fuel supply obscure these processes. Accordingly, we studied ROS production which reflects metabolic plasticity [38] and is compatible with cell culturing conditions. Increased ROS production by the platinum compounds [33] could induce DNA breaks that may accumulate when PARP is inhibited leading to cell death. Such a mechanism could account for the observed synergism between platinum compounds and PARP inhibitors [27–29]. In complete agreement with the literature, we found that oxaliplatin- but not olaparib or the Akt pathway inhibitor LY294002- induced ROS formation in the TNBC MDA-MB-231 line and LY294002, but olaparib did not augment oxaliplatin's effect

(Figure 3). On the other hand, the treatments alone or in combination failed to induce significant ROS production in the non-TNBC MCF7 line (Figure 3). However, increased vulnerability of MCF7 cells to the treatments resulted in a death rate, compared to that of MDA-MB-231 cells (Figure 1), leaving fewer surviving cells to produce ROS. Furthermore, MCF7 cells could produce less ROS as they represent an earlier stage of metabolic transformation than the TNBC MDA-MB-231 cell line does. Combination of these and possibly other factors could account for the observed difference between the cell lines.

Centrosome amplification occurring in the S phase of the cell cycle, is known to be associated with malignant transformation in various tissue types. Centrosome amplification is regarded as a marker for aggressiveness, even with invasive breast and prostate cancers [39]. Accordingly, we expected to find that the MDA-MB-231line had a higher percentage of cells in the S phase of their cycle than the MCF7 cells. However, we observed the opposite trend in the two cell lines (Figure 4C vs. Figure 4G) indicating that other factors, probably synchronization of cell cycles due to passages during culturing [40] dominated centrosome amplification in determining the distribution of cell-cycle phases in these two breast cancer cell lines. In both cell lines, although to a different extents, oxaliplatin arrested most of the cells in their S phase, and this was not affected by olaparib co-treatment (Figure 4C,G). These data are consistent with the DNA crosslinking effect of the platinum compound, which prevents cells from crossing the G2 checkpoint.

The TNBC cell line MDA-MB-231 represents a more aggressive, apoptosis- and therapy-resistant phenotype than the non-TNBC MCF7 line does. As measures of this aggressiveness, we assessed colony formation (Figure 5) and invasive growth (Figures 6 and 7). These data were completely consistent with the results for viability (Figure 1), with the literature and with the aforementioned view about aggressiveness of the two cell lines. They provide two additional experimental evidence for the lack of synergy between olaparib and oxaliplatin (Figures 5–7). Furthermore, they indicate (Figure 5B,D) that Akt pathway inhibition could be advantageous in combined therapy with PARP inhibitors, as it blocks their Akt-mediated cytoprotective effects [26].

In conclusion, we provided experimental evidence for the lack of synergy between olaparib, a PARP inhibitor widely used in cancer therapy, and oxaliplatin, a third-generation platinum compound. These results are in conflict with the findings of others [27–29,32], probably because, at therapeutically realistic concentrations, the cytostatic effect of the platinum compound dominates that of the PARP inhibitor. We have also demonstrated the advantage of using an Akt pathway inhibitor to augment the cytostatic properties of the platinum compound and/or to prevent the cytoprotective effects of PARP inhibition. Furthermore, we have shown the therapy resistance of the TNBC line MDA-MB-231 over the estrogen- and progesterone receptor-positive line MCF7, although we failed to advance our understanding of differences in sensitivity to chemotherapy among different types of breast cancers.

4. Materials and Methods

4.1. Drugs

Olaparib was purchased from MedChemExpress (Monmouth Junction, NJ, United States). It was dissolved in DMSO before treatment and for each treatment new solution was made. Oxaliplatin was purchased from Accord Healthcare (Munich, Germany). Akt pathway inhibitor LY294002 was purchased from Selleckchem (Houston, Texas, USA). All other reagents were of the highest purity commercially available.

4.2. Cell Cultures

MDA-MB-231 and MCF7 cell lines were obtained from American Type Culture Collection (Manassas, VA, United States). Cell lines were maintained in a humidified 5% CO_2 atmosphere at 37 °C. MDA-MB-231 cells were cultured in DMEM low glucose (Biosera, Nuaille, France) supplemented with 10% (*v/v*) FBS (Thermo Fisher, Life Technologies,

Milan, Italy). MCF7 cells were cultured in RPMI (Biosera, Nuaille, France) supplemented with 10% (*v/v*) FBS.

4.3. Survival Assay

MTT assay was used to examine cell viability. Cells were seeded at a density of 3×10^3/well in 96-well cell culture plates for 24 h before treatment. After 72 h treatment using olaparib (2 μM), oxaliplatin (25 μM) and LY294002 (1 μM), and their combination, the medium was replaced containing 0.5% MTT substrate (100 μL/well). After 2 h incubation at 37 °C the medium was discarded and DMSO was added (100 μL/well). Given the purple color of the soluble formazan product, absorbance was measured at 570 nm using the GloMax®-Multi Instrument (Promega, Madison, WI, United States). At least four parallels were used, and the experiment was repeated three times.

4.4. Apoptosis Assay

Live, early apoptotic, late apoptotic and dead cells were quantified using the MUSE Annexin V and Dead Cell Kit (Luminex Corporation, Austin, Texas, United States). The experiment was carried out according to the manufacturer's instructions. Cells were cultured in six-well plates (1.5×10^5/well) and treated with olaparib (2 μM), oxaliplatin (25 μM) and LY294002 (1 μM) and their combination for 72 h. After the treatment cells were collected and diluted in their medium to a concentration of 5×10^5/mL. Twenty minutes incubation in the dark at room temperature followed the addition of 100 μL Annexin V reagent. Annexin V-FITC positive cells were considered as apoptotic (early and late apoptotic) and were expressed as % of the total cell number examined. The MUSE Cell Analyzer device was used to assess the samples and 5000 single cell events were measured per sample. Three independent experiments were performed.

4.5. Assay for Reactive Oxygen Species

To measure intracellular reactive oxygen species (ROS) production, cells were plated (3×10^3/well) in wells of a 96-well plate, were cultured for 24 h were treated for 72 h with olaparib (2 μM), oxaliplatin (25 μM) and LY294002 (1 μM), and their combination. The medium was replaced by Krebs-Henseleit solution containing 2% FBS and 2 μM carboxy-H2DCFDA (Thermo scientific, Waltham, MA, United States). After 30 min incubation, ROS generation was measured using GloMax®-Multi Instrument (Promega, Madison, WI, United States) at respective excitation/emission wavelengths of 490/530 nm.

4.6. Cell Cycle Analysis

Cells were cultured in six-well plates (1.5×10^5/well) 24 h before treatment, and were treated with olaparib (2 μM), oxaliplatin (25 μM) and LY294002 (1 μM), and their combination, for 72 h. To assess cell cycle, flow cytometry analysis was applied. In brief, cells were harvested, washed with Dulbecco's phosphate-buffered saline (DPBS) (Biosera, Nuaille, France) and fixed with 70% ethanol (Molar Chemicals Kft., Halasztelek, Hungary) at 4 °C overnight. After fixation, the cells were centrifuged and washed twice with DPBS. Aliquots of cells (0.5×10^6) were stained with 500 μl propidium iodide (PI) (Merck KGaA, Darmstadt, Germany)/RNAse A (Thermo scientific, Waltham, MA, United States) solution containing 0.02 mg/mL PI and 10 μg/mL RNAse A in PBS-0.1% Triton-X 100 (Sigma, St. Louis, MO, United States). SONY SH800 Cell Sorter (SONY Biotechnology, San Jose, CA, United States) was used to measure fluorescent intensities. Debris and aggregates had been discriminated by gating, and at least 5000 single cell events were measured per sample. Data were analyzed and cell-cycle distribution were determined using ModFit LT (Verity software House, Topsham, ME, United States) software.

4.7. Clonogenic Assay

Cells were seeded at adensity of 3×10^3/well and were cultured for 24 h before treatment. After 14 days of treatment with 2 μM olaparib, 25 μM oxaliplatin and 1 μM

LY294002, alone and in combination, the cells were washed with 1× PBS (Biowest, Nuaille, France) and stained with 0.1% Coomassie Brilliant Blue R 250 (Merck KGaA, Darmstadt, Germany) in 30% methanol and 10% acetic acid. Plates were scanned and colonies were quantified using ImageJ program.

4.8. Growth Measurement

Cells were seeded at a density of 1×10^3/well and cultured for 24 h before treatment with 2 μM olaparib, 25 μM oxaliplatin and 1 μM LY294002, alone and in combination, in an electronic microtiter plate (E-Plate®) (ACEA Biosciences, San Diego, CA, United States). The treatment lasted 7 days. The impedance was measured every hour, using gold electrodes at the bottom of the wells. The xCELLigence Real-Time Cell Analysis (RTCA) device (ACEA Biosciences, San Diego, CA, United States) was used according to the manufacturer's protocol. The instrument was placed in a humidified incubator at 37 °C and 5% CO_2.

4.9. Statistical Analysis

Data were analyzed using OriginPro® software. For determining differences among the treatment groups, one-way ANOVA with Tukey post hoc comparison tests were performed on the row data (never on the calculated data). Results are presented as mean ± SEM of at least 3 independent experiments, as indicated in the figure legends. The differences among the groups were regarded as significant at $p < 0.05$.

Author Contributions: Conceptualization, K.A.; Data curation, K.A., B.K., D.K. and V.B.V.; Formal analysis, K.A., F.G. and K.K.; Funding acquisition, F.G.; Investigation, K.A.; Methodology, K.K.; Resources, F.G.; Supervision, K.K.; Validation, K.A.; Writing—original draft, K.A.; Writing—review & editing, F.G. and K.K. All authors have read and agreed to the published version of the manuscript.

Funding: Supported by the European Union and the State of Hungary, co-financed by the European Social Fund in the framework of GINOP-2.3.2-15-2016-00049, GINOP-2.3.3-15-2016-00025, EFOP-3.6.1-16-2016-00004.

Data Availability Statement: All data generated or analyzed during this study are included in this published article.

Acknowledgments: The authors thank Anna Pasztor, Gergo Barandi and Laszlo Giran for the technical assistance.

Conflicts of Interest: The authors declare that there are no conflict of interest regarding the publication of this article.

References

1. Ahmad, A. *Breast Cancer Metastasis and Drug Resistance*, 2nd ed.; Springer International Publishing: Cham, Switzerland, 2019; Volume 1152, p. 1.
2. Donepudi, M.S.; Kondapalli, K.; Amos, S.J.; Venkanteshan, P. Breast cancer statistics and markers. *J. Cancer Res. Ther.* **2014**, *10*, 506.
3. Dai, X.; Xiang, L.; Bai, Z. Cancer hallmarks, biomarkers and breast cancer molecular subtypes. *J. Cancer* **2016**, *7*, 1281–1294. [CrossRef] [PubMed]
4. Sareyeldin, R.M.; Gupta, I.; Al-Hashimi, I.; Al-Thawadi, H.A.; Farsi, H.F.A.; Vranic, S.; Moustafa, A.E.A. Gene expression and miRNAs profiling: Function and regulation in human epidermal growth factor receptor 2 (HER2)-positive breast cancer. *Cancers* **2019**, *11*, 646. [CrossRef] [PubMed]
5. Yao, H.; He, G.; Yan, S.; Chen, C.; Song, L.; Rosol, T.J.; Deng, X. Triple-negative breast cancer: Is there a treatment on the horizon? *Oncotarget* **2017**, *8*, 1913–1924. [CrossRef] [PubMed]
6. Masoud, V.; Pages, G. Targeted therapies in breast cancer: New challenges to fight against resistance. *World J. Clin. Oncol.* **2017**, *8*, 120–134. [CrossRef] [PubMed]
7. Hoeferlin, L.A.; Chalfant, C.E.; Park, M.A. Challenges in the treatment of triple negative and HER2-overexpressing breast cancer. *J. Surg. Sci.* **2013**, *1*, 3–7.
8. Dasari, S.; Tchounwou, P.B. Cisplatin in cancer therapy: Molecular mechanisms of action. *Eur. J. Pharmacol.* **2014**, *74*, 364–378. [CrossRef]

9. Mehmood, R.K.; Parker, J.; Ahmed, S.; Qasem, E.; Mohammed, A.A.; Zeeshan, M.; Jehangir, E. Review of cisplatin and oxaliplatin in current immunogenic and monoclonalantibody treatments. *World J. Oncol.* **2014**, *5*, 97–108. [PubMed]
10. Kang, X.; Xiao, H.H.; Song, H.Q.; Jing, X.B.; Yan, L.S.; Qi, R. Advances in drug delivery system for platinum agents based combination therapy. *Cancer Biol. Med.* **2015**, *12*, 362–374.
11. Shen, D.W.; Pouliot, L.M.; Hall, M.D.; Gottesman, M.M. Cisplatin resistance: A cellular self-defense mechanism resulting from multiple epigenetic and genetic changes. *Pharmacol. Rev.* **2012**, *64*, 706–721. [CrossRef]
12. Seetharam, R.N.; Sood, A.; Goel, S. Oxaliplatin: Pre-clinical perspectives on the mechanisms of action, response and resistance. *Ecancermedicalscience* **2009**, *3*, 153.
13. Morales, J.; Li, L.; Fattah, F.J.; Dong, Y.; Bey, E.A.; Patel, M.; Gao, J.; Boothman, D.A. Review of poly (ADP-ribose) polymerase (PARP) mechanisms of action and rationale for targeting in cancer and other diseases. *Crit. Rev. Eukaryot Gene Expr.* **2014**, *24*, 15–28. [CrossRef]
14. Turk, A.; Wisinski, K.B. PARP Inhibition in BRCA-mutant breast cancer. *Cancer* **2018**, *124*, 2498–2506. [CrossRef] [PubMed]
15. Ringley, J.T.; Moore, D.C.; Patel, J.; Rose, M.S. Poly (ADP-ribose) polymerase inhibitors in the management of ovarian cancer: A Drug Class Review. *Pharm. Ther.* **2018**, *43*, 549–556.
16. Jiang, N.; Dai, Q.; Su, X.; Fu, J.; Feng, X.; Peng, J. Role of PI3K/AKT pathway in cancer: The framework of malignant behavior. *Mol. Biol. Rep.* **2020**, *47*, 4587–4629. [CrossRef] [PubMed]
17. Lux, M.P.; Fasching, P.A.; Schrauder, M.G.; Hein, A.; Jud, S.M.; Rauh, C.; Beckmann, M.W. The PI3K pathway: Background and Ttreatment approaches. *Breast Care* **2016**, *11*, 398–404. [CrossRef]
18. Arafa, E.S.A.; Zhu, Q.; Shah, Z.I.; Wani, G.; Barakat, B.M.; Racoma, I.; El-Mahdy, M.A.; Wani, A.A. Thymoquinine up-regulates PTEN expression and induces apoptosis in doxorubicin-resistant human breast cancer cells. *Mutat. Res.* **2011**, *706*, 28–35. [CrossRef]
19. Verret, B.; Cortes, J.; Bachelot, T.; Andre, F.; Arnedos, M. Efficacy of PI3K inhibitors in advanced breast cancer. *Ann. Oncol.* **2019**, *30*, x12–x20. [CrossRef]
20. DeVita, V.T., Jr.; Chu, E. A History of cancer chemotherapy. *Cancer Res.* **2008**, *68*, 8643–8653. [CrossRef] [PubMed]
21. Makovec, T. Cisplatin and beyond: Molecular mechanisms of action and drug resistance development in cancer chemotherapy. *Radiol. Oncol.* **2019**, *53*, 148–158. [CrossRef]
22. Chou, T.C. Drug combination studies and their synergy quantification using the Chou-Talalay method. *Cancer Res.* **2010**, *70*, 440–446. [CrossRef]
23. Cseh, A.M.; Fabian, Z.; Quintana-Cabrera, R.; Szabo, A.; Eros, K.; Soriano, M.E.; Gallyas, F.; Scorrano, L.; Sumegi, B. PARP inhibitor PJ34 protects mitochondria and induces DNA-damage mediated apoptosis in combination with cisplatin or temozolomide in B16F10 melanoma cells. *Front. Physiol.* **2019**, *10*, 538. [CrossRef]
24. Garutti, M.; Pelizzari, G.; Bartoletti, M.; Malfatti, M.C.; Gerratana, L.; Tell, G.; Puglisi, F. Platinum Salts in Patients with Breast Cancer: A Focus on Predictive Factors. *Int. J. Mol. Sci.* **2019**, *20*, 3390. [CrossRef] [PubMed]
25. Pilié, P.G.; Gay, C.M.; Byers, L.A.; O'Connor, M.J.; Yap, T.A. PARP Inhibitors: Extending Benefit Beyond BRCA-Mutant Cancers. *Clin. Cancer Res.* **2019**, *25*, 3759–3771. [CrossRef] [PubMed]
26. Gallyas, F., Jr.; Sumegi, B. Mitochondrial Protection by PARP Inhibition. *Int. J. Mol. Sci.* **2020**, *21*, 2767. [CrossRef] [PubMed]
27. Lee, J.M.; Hays, J.L.; Chiou, V.L.; Annunziata, C.M.; Swisher, E.M.; Harrell, M.I.; Yu, M.; Gordon, N.; Sissung, T.M.; Ji, J.; et al. Phase I/Ib study of olaparib and carboplatin in women with triple negative breast cancer. *Oncotarget* **2017**, *8*, 79175–79187. [CrossRef]
28. Michels, J.; Vitale, I.; Senovilla, L.; Enot, D.P.; Garcia, P.; Lissa, D.; Olaussen, K.A.; Brenner, C.; Soria, J.C.; Castedo, M.; et al. Synergistic interaction between cisplatin and PARP inhibitors in non-small cell lung cancer. *Cell Cycle* **2015**, *12*, 877–883. [CrossRef]
29. Huang, S.-H.; Xiong, M.; Chen, X.-P.; Xiao, Z.-Y.; Zhao, Y.-F.; Huang, Z.-Y. PJ34, an inhibitor of PARP-1, suppresses cell growth and enhances the suppressive effects of cisplatin in liver cancer cells. *Oncol. Rep.* **2008**, *20*, 567–572. [CrossRef]
30. Movahhed-Komeili, T.; Fouladdel, S.; Barzegar, E.; Atashpour, S.; Ghahremani, M.H.; Ostad, S.N.; Madjd, Z.; Azizi, E. PI3K/Akt inhibition and down-regulation of BCRP resensitize MCF7 breast cancer cell line to mitotraxane chemotherapy. *IRAN J. Basic Med. Sci.* **2015**, *18*, 472–477.
31. Imai, Y.; Yoshimori, M.; Fukuda, K.; Yamagishi, H.; Ueda, Y. The PI3K/Akt inhibitor LY294002 reverses BCRP-mediated drug resistance without affecting BCRP translocation. *Oncol. Rep.* **2012**, *27*, 1703–1709. [CrossRef]
32. Zhao, H.; Yang, Q.; Hu, Y.; Zhang, J. Antitumor effects and mechanisms of olaparib in combination with carboplatin and BKM120 on human triple-negative breast cancer cells. *Oncol. Rep.* **2018**, *40*, 3223–3234. [CrossRef]
33. Stankovic, J.S.K.; Selakovic, D.; Mihailovic, V.; Rosic, G. Antioxidant Supplementation in the Treatment of Neurotoxicity Induced by Platinum-Based Chemotherapeutics-A Review. *Int. J. Mol. Sci.* **2020**, *21*, 7753. [CrossRef] [PubMed]
34. Hui, L.; Zheng, Y.; Yan, Y.; Bargonetti, J.; Foster, D.A. Mutant p53 in MDA-MB-231 breast cancer cells is stabilized by elevated phospholipase D activity and contributes to survival signals generated by phospholipase D. *Oncogene* **2006**, *25*, 7305–7310. [CrossRef]
35. Robinson, B.W.; Shewach, D.S. Radiosensitization by gemcitabine in p53 wild-type and mutant MCF7 breast carcinoma cell lines. *Clin. Cancer Res.* **2001**, *7*, 2581–2589.
36. Godet, I.; Shin, Y.J.; Ju, J.A.; Ye, I.C.; Wang, G.; Gilkes, D.M. Fate-mapping post-hypoxic tumor cells reveals a ROS-resistant phenotype that promotes metastasis. *Nat. Commun.* **2019**, *10*, 4862. [CrossRef] [PubMed]

37. Schito, L.; Semenza, G.L. Hypoxia-Inducible Factors: Master Regulators of Cancer Progression. *Trends Cancer* **2016**, *2*, 758–770. [CrossRef] [PubMed]
38. Ward, P.S.; Thompson, C.B. Metabolic reprogramming: A cancer hallmark even warburg did not anticipate. *Cancer Cell* **2012**, *21*, 297–308. [CrossRef]
39. Ogden, A.; Rida, P.C.G.; Aneja, R. Heading off with the herd: How cancer cells might maneuver supernumerary centrosomes for directional migration. *Cancer Metastasis Rev.* **2013**, *32*, 269–287. [CrossRef]
40. Golubev, A. Transition probability in cell proliferation, stochasticity in cell differentiation, and the restriction point of the cell cycle in one package. *Prog. Biophys. Mol. Biol.* **2012**, *110*, 87–96. [CrossRef]

International Journal of
Molecular Sciences

MDPI

Article

Cytostatic Effect of a Novel Mitochondria-Targeted Pyrroline Nitroxide in Human Breast Cancer Lines

Kitti Andreidesz [1], Aliz Szabo [1], Dominika Kovacs [1], Balazs Koszegi [1], Viola Bagone Vantus [1], Eszter Vamos [1], Mostafa Isbera [2], Tamas Kalai [2,3], Zita Bognar [1], Krisztina Kovacs [1] and Ferenc Gallyas, Jr. [1,3,4,*]

1 Department of Biochemistry and Medical Chemistry, University of Pecs Medical School, 7624 Pecs, Hungary; andreidesz.kitti@pte.hu (K.A.); aliz.szabo@aok.pte.hu (A.S.); dominika.kovacs@aok.pte.hu (D.K.); balazs.koszegi@aok.pte.hu (B.K.); viola.vantus@aok.pte.hu (V.B.V.); eszter.vamos@aok.pte.hu (E.V.); zita.bognar@aok.pte.hu (Z.B.); krisztina.kovacs@aok.pte.hu (K.K.)
2 Institute of Organic and Medicinal Chemistry, Faculty of Pharmacy, University of Pecs, 7624 Pecs, Hungary; mostafaisbera@gmail.com (M.I.); tamas.kalai@aok.pte.hu (T.K.)
3 Szentagothai Research Centre, University of Pecs, 7624 Pecs, Hungary
4 HAS-UP Nuclear-Mitochondrial Interactions Research Group, 1245 Budapest, Hungary
* Correspondence: ferenc.gallyas@aok.pte.hu; Tel.: +36-72-536-278

Abstract: Mitochondria have emerged as a prospective target to overcome drug resistance that limits triple-negative breast cancer therapy. A novel mitochondria-targeted compound, HO-5114, demonstrated higher cytotoxicity against human breast cancer lines than its component-derivative, Mito-CP. In this study, we examined HO-5114′s anti-neoplastic properties and its effects on mitochondrial functions in MCF7 and MDA-MB-231 human breast cancer cell lines. At a 10 μM concentration and within 24 h, the drug markedly reduced viability and elevated apoptosis in both cell lines. After seven days of exposure, even at a 75 nM concentration, HO-5114 significantly reduced invasive growth and colony formation. A 4 h treatment with 2.5 μM HO-5114 caused a massive loss of mitochondrial membrane potential, a decrease in basal and maximal respiration, and mitochondrial and glycolytic ATP production. However, reactive oxygen species production was only moderately elevated by HO-5114, indicating that oxidative stress did not significantly contribute to the drug's anti-neoplastic effect. These data indicate that HO-5114 may have potential for use in the therapy of triple-negative breast cancer; however, the in vivo toxicity and anti-neoplastic effectiveness of the drug must be determined to confirm its potential.

Keywords: MDA-MB-231; MCF7; mitochondrial membrane potential; mitochondrial energy metabolism; reactive oxygen species; invasive growth; Mito-CP

Citation: Andreidesz, K.; Szabo, A.; Kovacs, D.; Koszegi, B.; Bagone Vantus, V.; Vamos, E.; Isbera, M.; Kalai, T.; Bognar, Z.; Kovacs, K.; et al. Cytostatic Effect of a Novel Mitochondria-Targeted Pyrroline Nitroxide in Human Breast Cancer Lines. *Int. J. Mol. Sci.* **2021**, *22*, 9016. https://doi.org/10.3390/ijms22169016

Academic Editor: Vladimir Titorenko

Received: 30 June 2021
Accepted: 17 August 2021
Published: 20 August 2021

1. Introduction

Mitochondria have become novel targets for anti-cancer strategies [1]. While the Warburg effect states that due to defective oxidative phosphorylation, the rate of glycolysis is elevated to replace ATP loss [2], oxidative phosphorylation has been recently recognized to play an important role in oncogenesis. Furthermore, the mitochondria of cancer cells can alternate between glycolysis and oxidative phosphorylation to meet the metabolic demands of the cell and to promote survival [3]. Targeting the mitochondria shows great promise to enhance the efficiency of anti-cancer drugs. Additionally, targeting the mitochondria could mitigate treatment resistance, another crucial factor of today's anti-cancer therapy. Mitochondria-targeted nanocarriers and drugs conjugated to mitochondria-targeting ligands are the most common approaches [4].

Lipophilic cations, such as tryphenylphosphonium (TPP), are frequently used conjugates in the design of mitochondria-targeted anti-cancer drugs, and they also have antifungal, antiparasitic, and antioxidant uses. The chemical background of mitochondrial targeting by lipophilic cations, such as TPP, is that the delocalized positive charge enables

the drug to easily permeate lipid bilayers, which is an advantage compared to hydrophobic compounds that should rely on tissue-specific carriers. Lipophilic cations can achieve efficient uptake and accumulation several hundredfold within the mitochondria depending on the mitochondrial membrane potential (−150 to −180 mV) [5,6]. The mitochondrial membrane potential ($\Delta\Psi_m$) of cancer cells is higher compared to their cytosol and to non-cancer cells, and hence a selective targeting can be achieved [7]. After administration, more than 90% of the intracellular lipophilic cations was found to be located in the mitochondria [6]. When administered orally, the uptake of TPP-based drugs by the mitochondria was fast and organ-selective; they accumulated within the heart, skeletal muscle, liver, and brain of mice [6,8].

Recently, the bioenergetics of cancer cells is receiving increased interest among researchers in the field [9,10]. Breast cancer cells have profound bioenergetic, histological, and genetic differences compared to normal cells [10]. As triple-negative breast cancer (TNBC) represents about 15–20% of all cases and is associated with a poor prognosis and limited therapeutic options, the development of novel therapeutic means is needed [11]. Targeting metabolism and the mitochondria could be a useful therapeutic approach in TNBC cases because mitochondria play pivotal roles in early relapse and the metastatic spread of TNBC. Previous research has also demonstrated that targeting glycolysis might not be an effective strategy in TNBC therapy and has suggested that the mitochondrial aid-in-reserve must be selectively blocked [10].

Mito-CP, a TPP conjugated superoxide dismutase mimetic, was the first mitochondria-targeted nitroxide compound. It was used for studying the role of the mitochondrial superoxide in cancer cell proliferation [12]. Mito-CP has shown cytotoxic properties in various cancer cells, including breast cancer cells, without markedly affecting non-cancerous ones [13,14]. Recently, a novel component-derivative of Mito-CP, a pyrroline nitroxide attached dyphenylphosphine compound, HO-5114, was synthesized [15], which demonstrated markedly higher cytotoxicity against TNBC and hormone receptor positive human breast cancer (HR+BC) lines than Mito-CP. This report presents a detailed study of HO-5114′s effect on the breast cancer lines and provides evidence that the mitochondrial effects of the drug could participate in its cytotoxic and anti-proliferative effects.

2. Results

2.1. Effect of HO-5114 on Cell Viability

To assess its anti-neoplastic potential, we treated TNBC MDA-MB-231 and HR+BC MCF7 lines with 1, 2.5, 5 or 10 μM HO-5114 for 24 h and then determined their viability using the sulforhodamine B (SRB) assay. The SRB assay measures protein content that is considered to be more proportional to the cell count than metabolic activity, which can under- or over-estimate the cell count if the studied substance inhibits or uncouples mitochondrial oxidative phosphorylation [16]. We found that HO-5114 decreased viability in both breast cancer lines in a concentration- and time-dependent manner (Figure 1). Even at the lowest concentration tested, the drug substantially reduced the viability of both cell lines. In agreement with the view that TNBC is more chemotherapy-resistant than HR+BC, the MDA-MB-231 cells were more resistant against HO-5114 treatment than the MCF7 cells, although the treatment with 10 μM HO-5114 reduced viability below 10% in both cell lines (Figure 1).

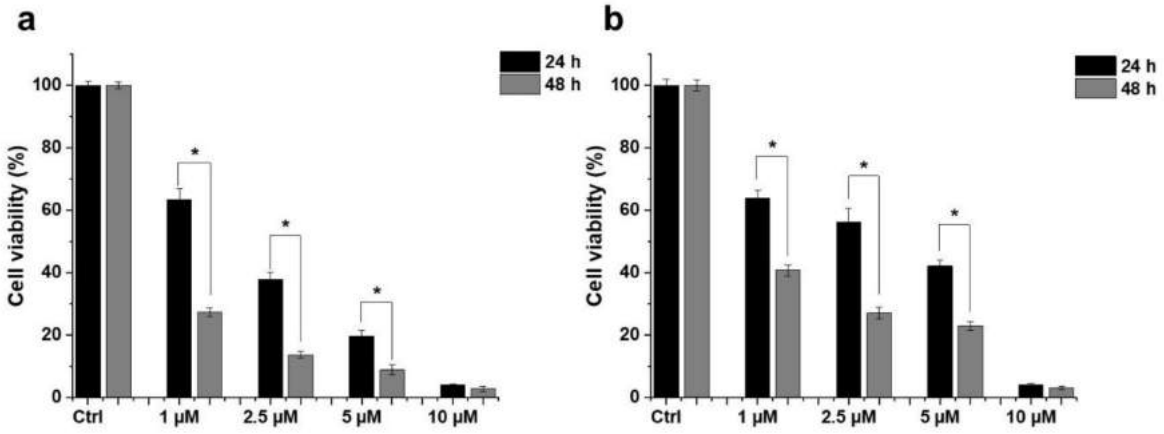

Figure 1. Effect of HO-5114 on the viability of human breast cancer lines. MCF7 (**a**) and MDA-MB-231 (**b**) cells were treated with 1, 2.5, 5 or 10 μM HO-5114 for 24 or 48 h, and then the viability was determined by the SRB assay. Data are shown as mean ± standard error of the mean (SEM) of at least three independent experiments running in three parallels each. * $p < 0.05$ compared to the cells treated for 24 h.

2.2. Determination of the Type of HO-5114-Induced Cell Death

We determined the type of HO-5114-induced cell death using flow cytometry. The cells were treated exactly as for the viability measurement, and then they were double-stained with fluorescein isothiocyanate (FITC) conjugated Annexin V and propidium iodide (PI). The latter enters the cell if the plasma membrane is disrupted, binds to the double-stranded DNA, and becomes intensely fluorescent, indicating necrosis. The former binds to phosphatidylserine, a marker of apoptosis when it is on the plasma membrane's outer layer. Double positivity indicates late apoptosis. In MCF7 cells, HO-5114 treatment increased the ratio of early—and to a much higher extent—late apoptotic cells on the expense of live cells in a concentration-dependent manner in the whole concentration range tested (Figure 2a,c). In contrast, <5 μM concentrations of HO-5114 did not have a significant effect on the MDA-MB-231 cells; however, 10 μM of HO-5114 had a pronounced effect. It lowered the live cell ratio to 25% while increasing the ratio of early and late apoptotic cells to 10% and 65%, respectively (Figure 2b,d).

2.3. Effect of HO-5114 on Reactive Oxygen Species (ROS) Generation

In many cases, anti-neoplastic agents induce ROS production in cancer cells [17]. Accordingly, we studied HO-5114-induced ROS production in human breast cancer lines using the dihydrorhodamine 123 assay. The assay is based on measuring the fluorescence of rhodamine 123 produced quantitatively from its non-fluorescent reduced form by the cellular ROS. At a 10 μM concentration, which lowered the viability of both human cancer lines to less than 10% of that of the untreated control, HO-5114 caused ROS production to the extent of about 1.7 and 2 times of the untreated control in the TNBC and HR+BC lines, respectively (Figure 3). Treatment with lower concentrations of the drug that still induced a massive decrease in the viability of both cell lines caused no or only slight cellular ROS production (Figure 3), suggesting that the induction of oxidative stress was unlikely involved among the mechanisms of HO-5114's cytotoxicity. Increasing HO-5114's concentration to 20 μM elevated ROS production proportionally in both cell lines (Figure 3), indicating that ROS production was likely far from the saturation level under these conditions.

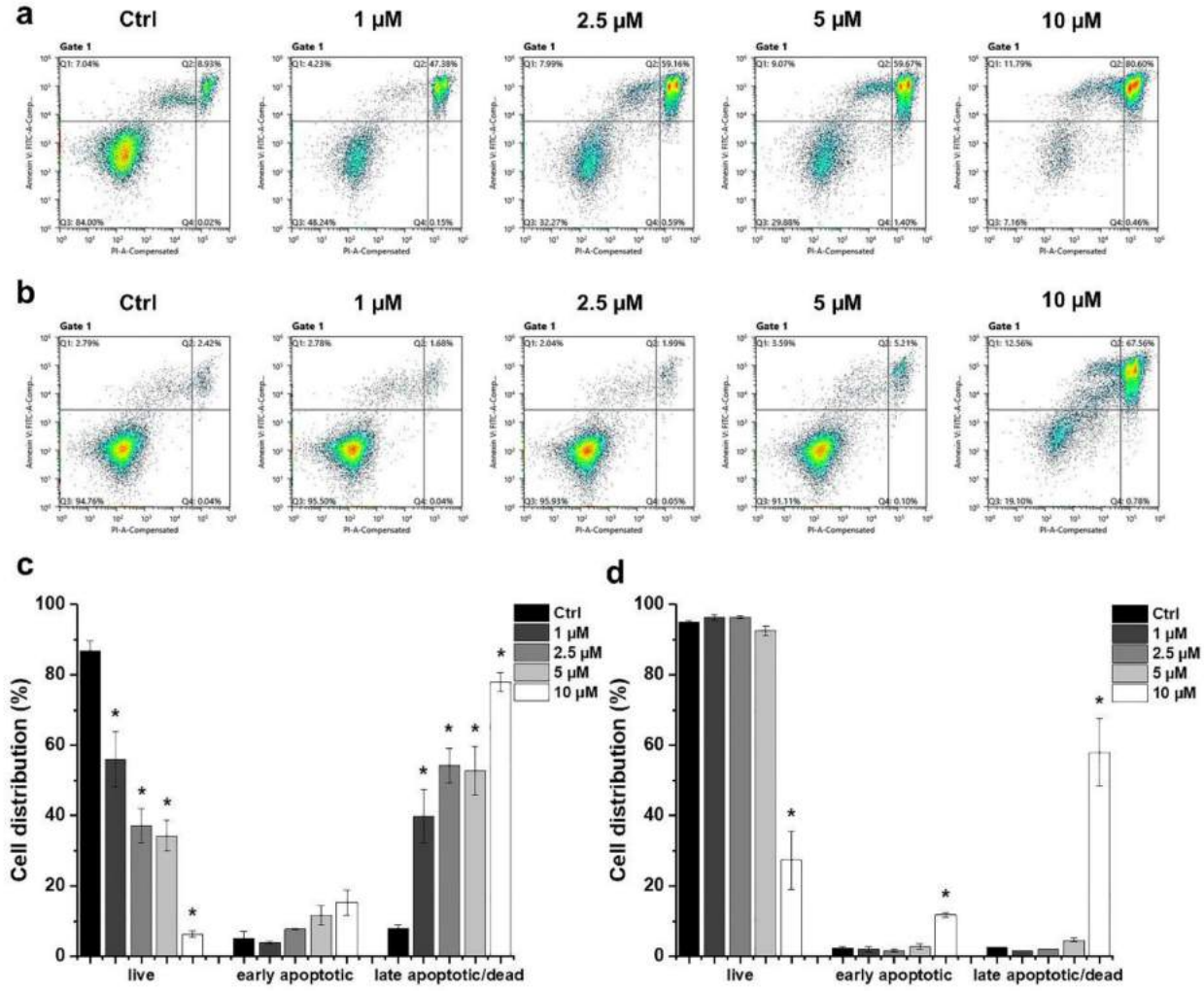

Figure 2. Effect of HO-5114 on the apoptosis of human breast cancer lines. MCF7 (**a**,**c**) and MDA-MB-231 (**b**,**d**) cells were treated with 1, 2.5, 5 or 10 μM HO-5114 for 24 h, and then the cells were double-stained with FITC-Annexin V and PI and were exposed to a flow cytometry analysis. Dot plots (**a**,**b**) show the distribution of early apoptotic, late apoptotic, and live cells (Q1, Q2 and Q3 quadrants, respectively). Bar charts (**c**,**d**) represent the results of at least three independent experiments. The results are shown as mean ± SEM. * $p < 0.05$ compared to the untreated cells.

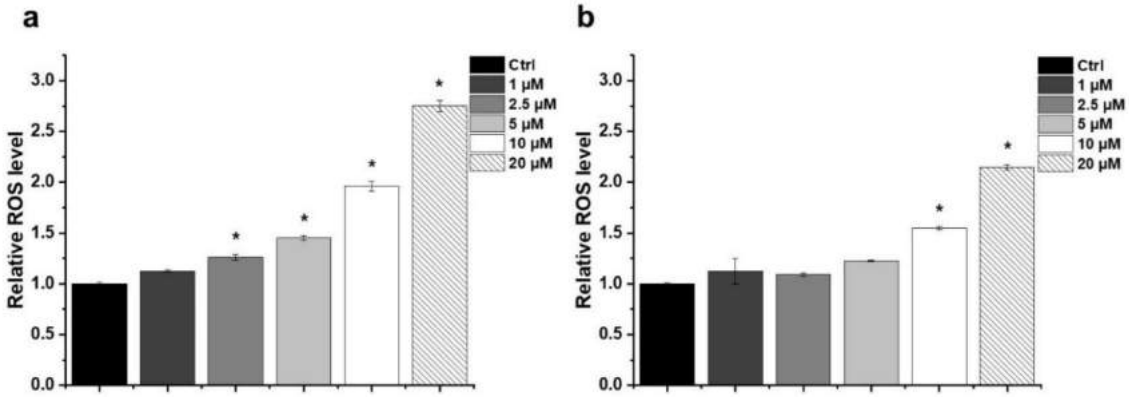

Figure 3. Effect of HO-5114 on cellular ROS production in human breast cancer lines. MCF7 (**a**) and MDA-MB-231 (**b**) cells were treated with 1, 2.5, 5, 10 or 20 μM HO-5114 for 4 h, and then ROS accumulation was assessed by the quantitative formation of fluorescent rhodamine 123 oxidized by the ROS from its non-fluorescent reduced precursor. The results are shown as mean ± SEM of at least three independent experiments. * $p < 0.05$ compared to the untreated cells.

To investigate the role of oxidative stress induction in the anti-neoplastic effect of HO-5114, we studied how an antioxidant affects HO-5114′s cytotoxicity in BC cells. To this end, we treated the MCF7 and MDA-MB-231 cells with 1, 2.5, 5 or 10 µM HO-5114 for 24 h in the presence or absence of 1 mM N-acetylcysteine (NAC) and then measured the viability using the SRB assay. We could not observe any effect of NAC on HO-5114′s cytotoxicity in the case of the HR+BC line MCF-7 (Figure 4a). In contrast, in the TNBC line MDA-MB-231, NAC significantly increased the viability of the control cells as well as the cells treated with up to 5 µM HO-5114; however, at a 10 µM HO-5114 concentration, there was no difference in viability between cells treated in the presence and absence of NAC (Figure 4b).

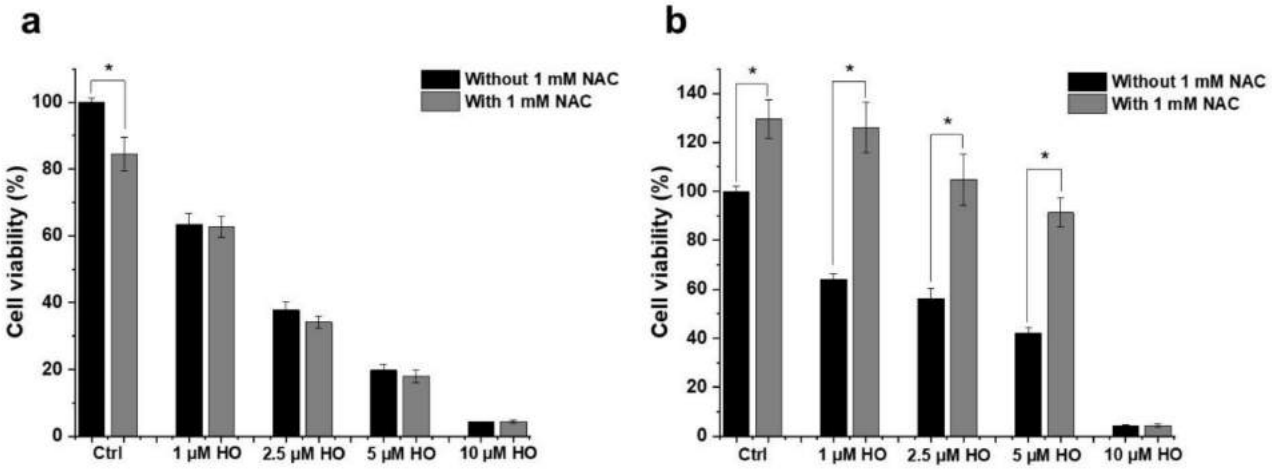

Figure 4. Effect of NAC on HO-5114′s cytotoxicity in human breast cancer lines. MCF7 (**a**) and MDA-MB-231 (**b**) cells were treated with 1, 2.5, 5 or 10 µM HO-5114 for 24 h in the absence or presence of 1 mM NAC, and then the viability was determined using the SRB assay. Data are shown as mean ± SEM of at least three independent experiments running in three parallels each. * $p < 0.05$ compared to the cells untreated with NAC.

2.4. Effect of HO-5114 on $\Delta\Psi_m$

HO-5114 is targeted to the mitochondria due to its diphenylphosphonium component. Therefore, we studied whether it affects $\Delta\Psi_m$ by measuring the JC-1 fluorescence. Based on its cationic properties, JC-1 is taken up by the mitochondria in a $\Delta\Psi_m$-dependent manner. In healthy mitochondria, it forms red fluorescent J-aggregates. Mitochondrial damage results in decreased $\Delta\Psi_m$, leading to a lower accumulation of JC-1 in the form of green fluorescent monomers, while the fluorescence disappears when the $\Delta\Psi_m$ dissipates completely. After merely a 1 h treatment, HO-5114 at the concentration of 1 µM caused a significant drop in the $\Delta\Psi_m$ of MCF7 cells, while increasing the drug's concentration to 2.5 µM resulted in a massive $\Delta\Psi_m$ loss indicated by the almost complete disappearance of the red fluorescence of JC-1 (Figure 5a,c). The MDA-MB-231 line was more resistant to HO-5114; the same concentrations triggered basically the same changes in the $\Delta\Psi_m$ that were observed for the MCF7 cells, but it necessitated 2.5 h of treatment rather than 1 h only (Figure 5b,d).

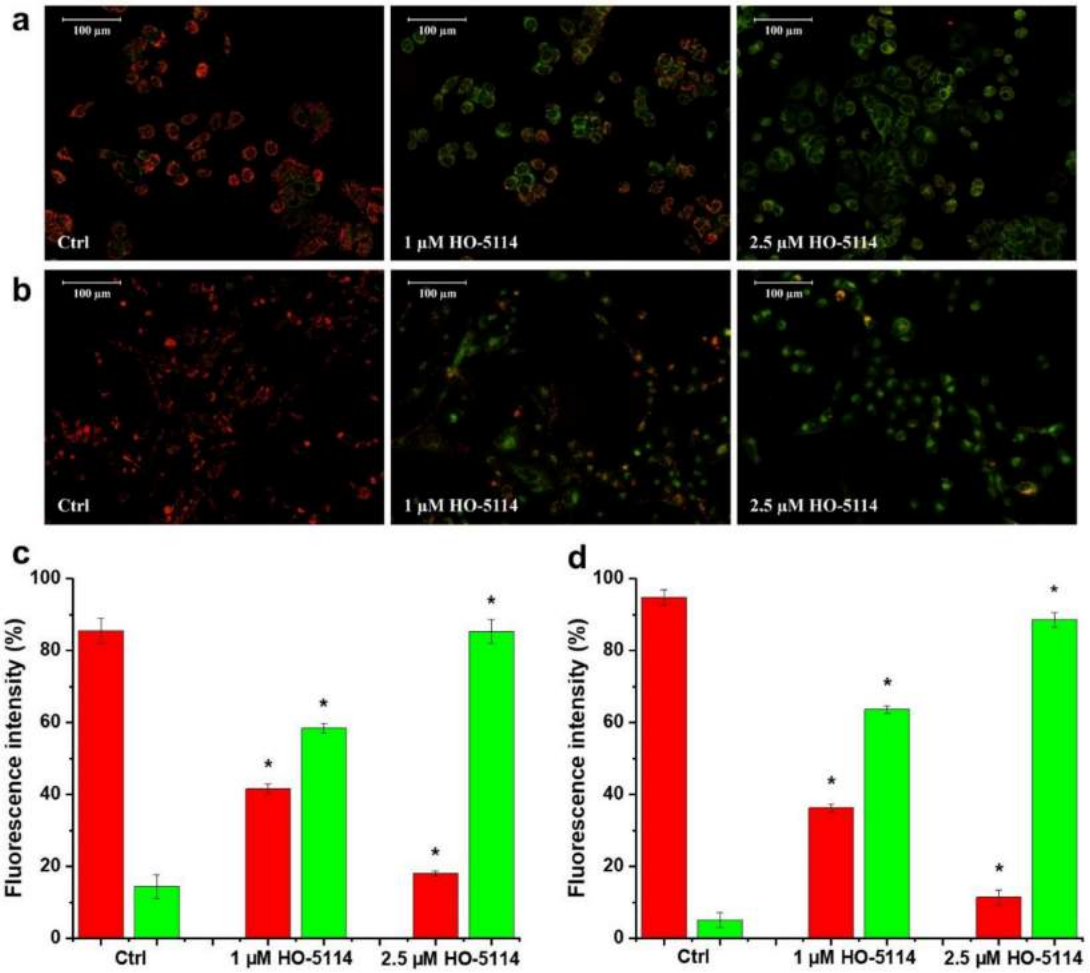

Figure 5. Effect of HO-5114 on the viability of human breast cancer lines. MCF7 (**a**,**c**) and MDA-MB-231 (**b**,**d**) cells were treated with 1 or 2.5 µM HO-5114 for 1 (**a**,**c**) or 2.5 (**b**,**d**) h, and then $\Delta\Psi_m$ was assessed by fluorescence microscopy after loading the cells with the lipophilic, cationic fluorescent dye, JC-1. Red and green fluorescence indicates normal and depolarized $\Delta\Psi_m$, respectively. Representative merged images of the same field acquired from the microscope's red and green channels separately are presented (**a**,**b**). Quantitative assessment of $\Delta\Psi_m$, (**c**,**d**) expressed as the % of fluorescence intensity, means ± SEM of three independent experiments. Quantitative comparisons are true within the same color only. Red and green bars denote red and green fluorescence, respectively. * $p < 0.05$ compared to the untreated cells.

2.5. Effect of HO-5114 on Mitochondrial Energy Production

Due to the increasing importance of energy metabolism among the pathomechanisms of cancer [3], we studied the effect of HO-5114 on the mitochondrial energy production of MDA-MB-231 and MCF7 lines using the Seahorse XFp Cell Mito Stress Test Kit. The device simultaneously measures the real-time cellular oxygen consumption rate (OCR) and extracellular acidification rate (ECAR), indicators of mitochondrial respiration and aerobic glycolysis, respectively. The cells were treated with 1 or 2.5 µM HO-5114 for 4 h, while OCR and ECAR were monitored during the last 75 min of treatment. Basal respiration was recorded for 15 min (Figure 6a; 1), and then the F_oF_1 ATPase inhibitor oligomycin was administered to assess ATP production (Figure 6a; 4). After another 20 min of recording, mitochondrial electron transport and ATP synthesis were uncoupled from each other by adding carbonyl cyanide 4-(trifluoromethoxy) phenylhydrazone (FCCP) to determine maximal respiration (Figure 6a; 3). After an additional further 20 min of recording, mitochondrial respiration was blocked by adding rotenone and antimycin A, inhibitors of Complex I and III of the mitochondrial respiratory chain, to determine proton leak and non-mitochondrial oxygen consumption (Figure 6a; 2 and 5).

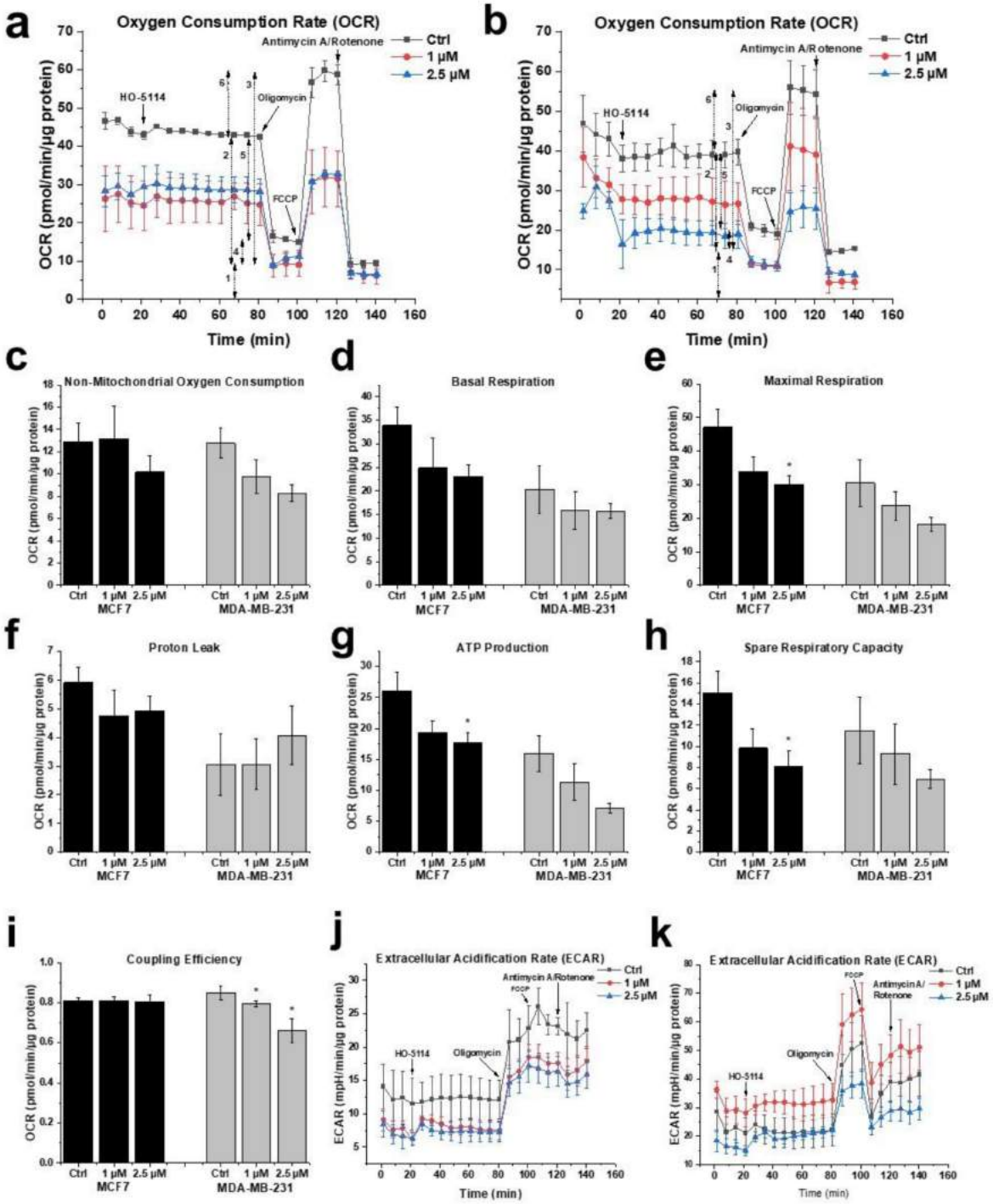

Figure 6. Effect of HO-5114 on the energy metabolism of human breast cancer lines. The cells were treated with 1 or 2.5 μM HO-5114 for 4 h, while OCR and ECAR were monitored during the last 75 min of treatment. The F_oF_1 ATP synthase inhibitor oligomycin (o), the uncoupler FCCP, and the respiratory inhibitors rotenone and antimycin A (R+AmA) were added at the bold arrows. (**a**) OCR recordings in the MCF7 line. The double-headed arrows with numbers next to them indicate: (1) basal respiration, (2) proton leak, (3) maximal respiration, (4) ATP production, (5) non-mitochondrial oxygen consumption, and (6) spare respiratory capacity. (**b**) OCR recordings in the MDA-MB-231 line. (**c**–**i**) Parameters derived from (**a**,**b**); for explanation, see the text and (**a**). (**c**) Non-mitochondrial oxygen consumption. (**d**) Basal respiration. (**e**) Maximal respiration. (**f**) Proton leak. (**g**) Mitochondrial ATP production. (**h**) Spare respiratory capacity. (**i**) Coupling efficiency. (**j**) ECAR recordings in the MCF7 line. (**k**) ECAR recordings in the MDA-MB-231 line. OCR and ECAR data were normalized to mg protein content and presented as means ± standard deviation (SD) of three independent experiments running in two parallels. * $p < 0.05$ compared to the untreated cells.

From the recorded raw data (Figure 6a,b), the Seahorse instrument generated multiple parameters of cellular energy metabolism (Figure 6c–i) that were all diminished by HO-5114 treatment except the proton leak, which was not affected in either cell line (Figure 6f). Furthermore, coupling efficiency that indicates how tightly respiration is coupled to ATP synthesis was not affected in the MCF7 line but was decreased in the MDA-MB-231 line (Figure 6i). The parameters of cellular energy metabolism associated with mitochondrial oxygen consumption, such as basal respiration, maximal respiration, and ATP production, were lower in the TNBC cells than in the HR+BC cells. Furthermore, 1 and 2.5 μM HO-5114 decreased these parameters to about the same extent for the latter cell line, while it affected them in a concentration-dependent manner for the former (Figure 6d,e,g). Administration of the ATP synthesis inhibitor oligomycin diminished OCR, which was accompanied by an elevation in ECAR in both cell lines (Figure 6j,k). HO-5114 at a concentration of 1 and 2.5 μM reduced ECAR to about the same extent in the MCF7 line, while it increased and decreased ECAR compared to the untreated control at 1 and 2.5 μM, respectively (Figure 6j,k).

Similar to the viability studies, we investigated the effect of NAC on the energy metabolism of untreated and HO-5114-treated BC cells. To this end, we included 1 mM NAC in a set of HO-5114-treated cells throughout the experiment. In the presence of NAC, the effect of HO-5114 on all parameters of cellular energy metabolism except the proton leak was reversed, in a higher extent for the MDA-MB-231 line than for the MCF7 line (Figure 7). In the MCF7 cells, HO-5114 decreased the proton leak that was further decreased in the presence of NAC. In contrast, HO-5114 increased the proton leak of the MDA-MB-231 cells that was further increased in the presence of NAC (Figure 7f).

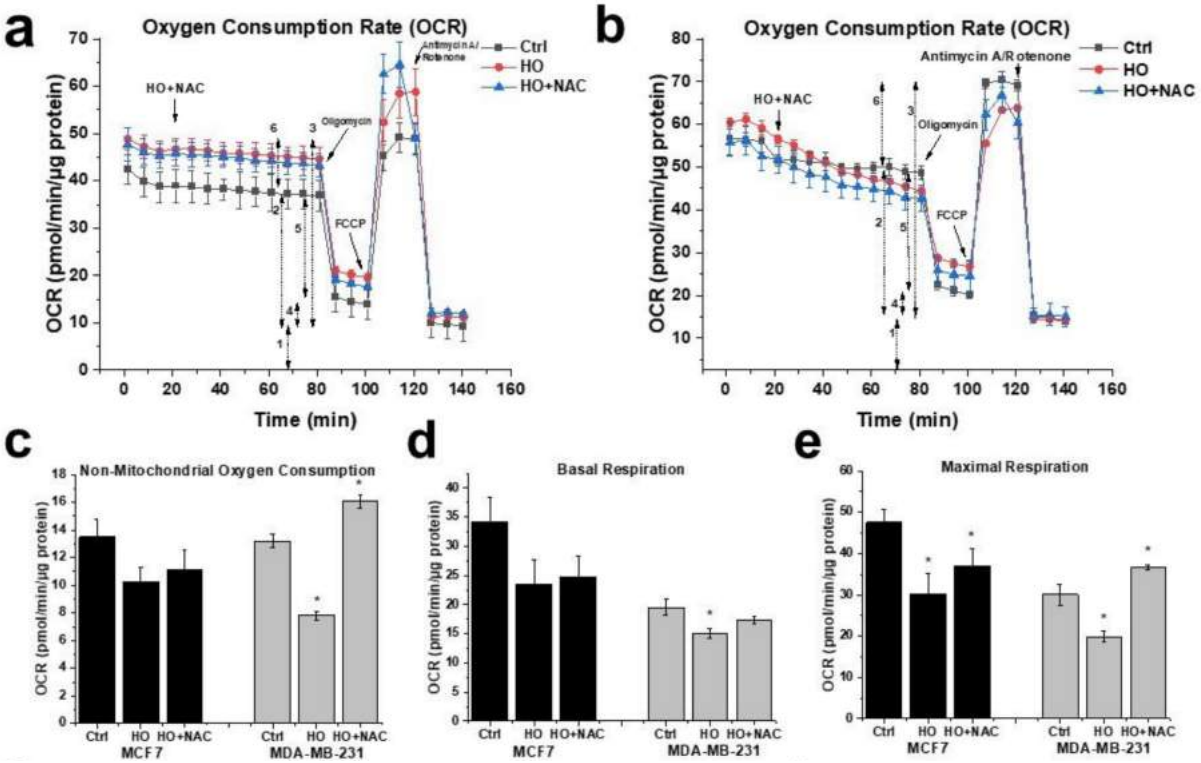

Figure 7. *Cont.*

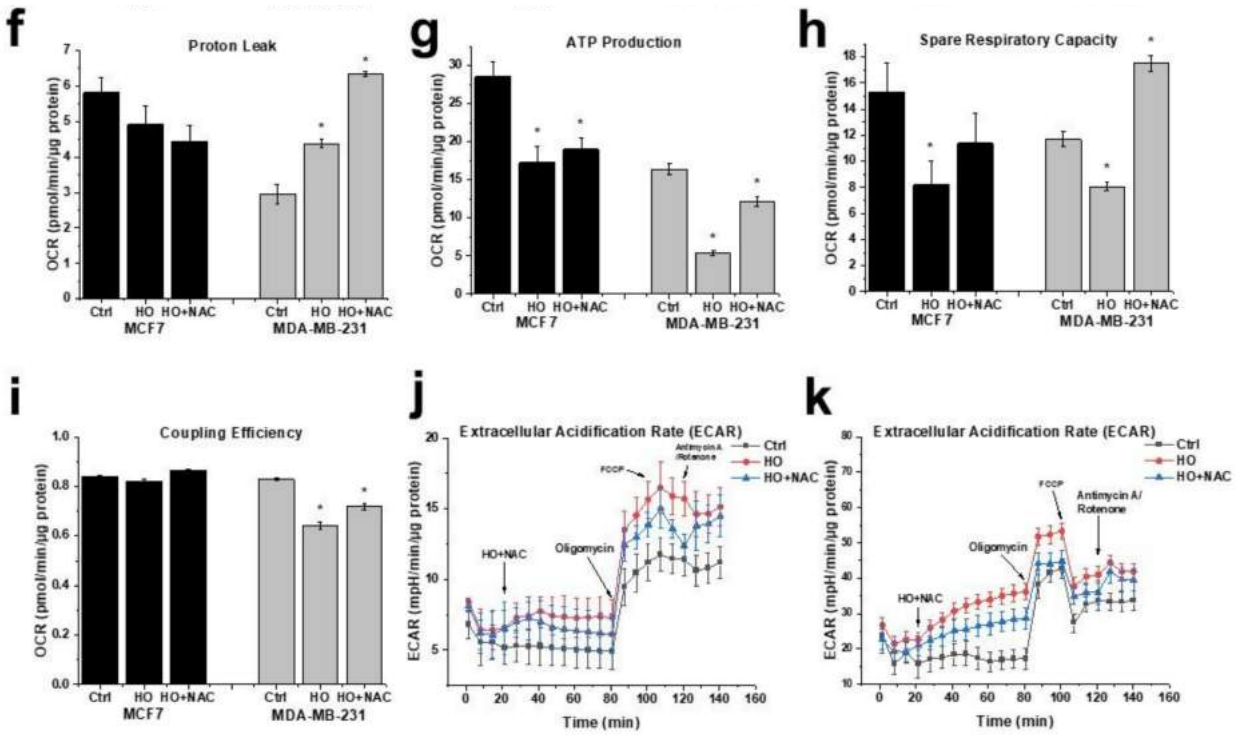

Figure 7. Effect of HO-5114 and NAC on the energy metabolism of human breast cancer lines. The cells were treated with 2.5 µM HO-5114 in the presence (blue line) and absence (red line) of 1 mM NAC for 4 h, while OCR and ECAR were monitored during the last 75 min of treatment. The F_oF_1 ATP synthase inhibitor oligomycin (o), the uncoupler FCCP, and the respiratory inhibitors rotenone and antimycin A (R + AmA) were added at the bold arrows. (**a**) OCR recordings in the MCF7 line. The double-headed arrows with numbers next to them indicate: (1) basal respiration, (2) proton leak, (3) maximal respiration, (4) ATP production, (5) non-mitochondrial oxygen consumption, and (6) spare respiratory capacity. (**b**) OCR recordings in the MDA-MB-231 line. (**c**–**i**) Parameters derived from (**a**,**b**); for explanation, see the text and (**a**). (**c**) Non-mitochondrial oxygen consumption. (**d**) Basal respiration. (**e**) Maximal respiration. (**f**) Proton leak. (**g**) Mitochondrial ATP production. (**h**) Spare respiratory capacity. (**i**) Coupling efficiency. (**j**) ECAR recordings in the MCF7 line. (**k**) ECAR recordings in the MDA-MB-231 line. OCR and ECAR data were normalized to mg protein content and presented as means ± SD of three independent experiments running in two parallels. * $p < 0.05$ compared to the untreated cells.

2.6. Effect of HO-5114 on Colony Formation

A colony formation assay was performed to assess the proliferation capacity of MCF7 and MDA-MB-231 cells treated with different concentrations of HO-5114. The cells were cultured in the presence of 50, 75, 100 or 250 nM of HO-5114 for seven days, and then the colonies were stained and counted. The drug effectively reduced colony formation in a concentration-dependent manner in both cell lines (Figure 8). Interestingly, the TNBC line was more sensitive to the treatment than the HR+BC line; 250 nM HO-5114 completely eradicated the MDA-MB-231 cells, while it allowed the survival of about 10 colonies of MCF7 cells (Figure 8).

2.7. Effect of HO-5114 on Invasive Growth

Cell proliferation, migration, and invasion are important in understanding tumor progression and metastasis formation [18]. We used the xCELLigence Real-Time Cell Analysis method to assess the effect of HO-5114 on the invasive growth characteristics of MCF7 and MDA-MB-231 cells. The instrument measures electron flow transmitted between gold microelectrodes fused to the bottom surface of a microtiter plate in the presence of an electrically conductive culturing medium. Adherent cells cultured in the plates change the impedance expressed as arbitrary units called the cell index, the magnitude of which is dependent on number, morphology, size, and attachment properties of the cells. The cells were cultured in the presence of 75, 100 or 250 nM of HO-5114 for seven days, while

the cell index was monitored in real-time. The drug effectively reduced the cell index in a concentration-dependent manner in both cell lines (Figure 9). At the highest concentration (250 nM), HO-5114 decreased invasive growth close to the detection limit in both cell lines. Similar to the colony formation experiments, the TNBC line was more sensitive to the treatment than the HR+BC line (Figure 9).

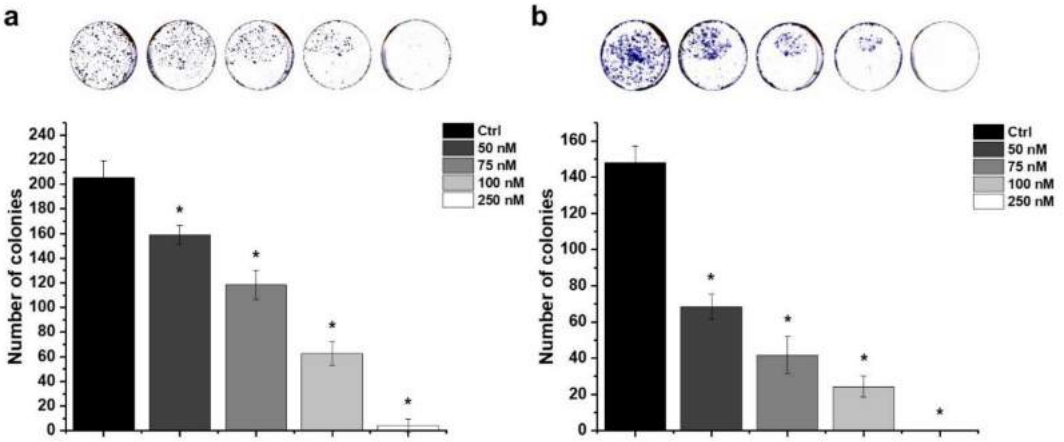

Figure 8. Effect of HO-5114 on the colony formation of human breast cancer lines. MCF7 (**a**) and MDA-MB-231 (**b**) cells were cultured in the presence of 0, 50, 75, 100 or 250 nM of HO-5114 for seven days and then were stained with Coomassie Blue, and the colonies were counted. The results are shown as mean ± SEM of at least three independent experiments. * $p < 0.05$ compared to the untreated cells.

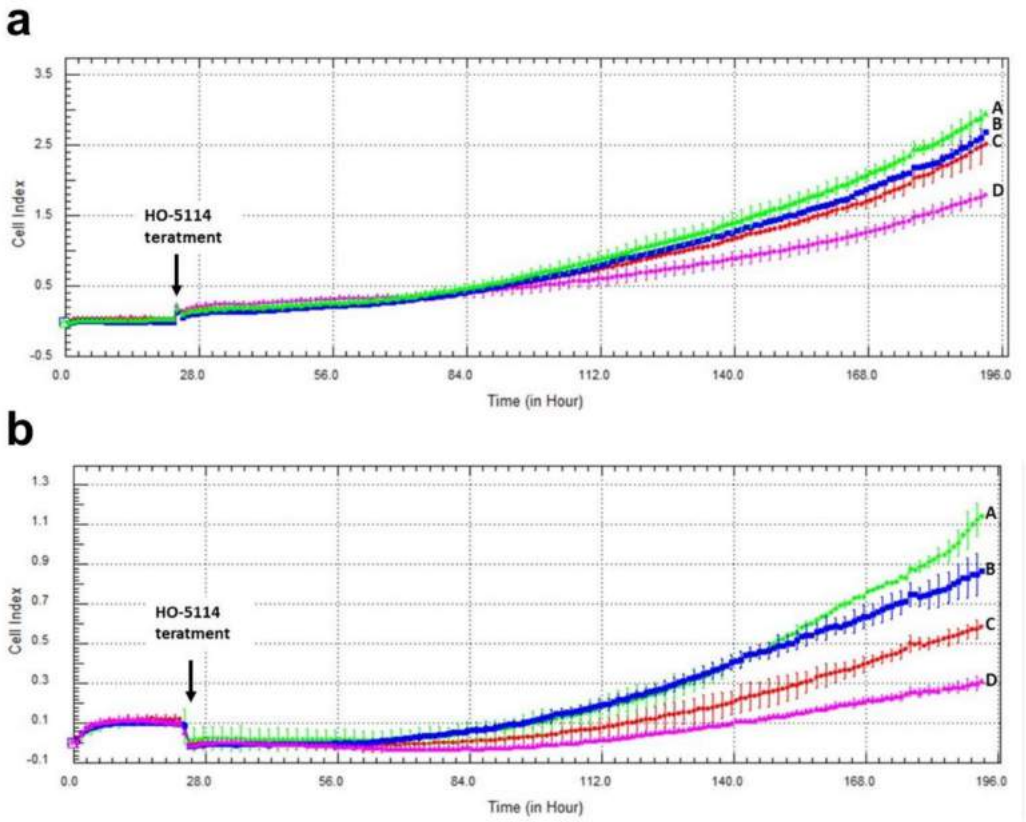

Figure 9. Effect of HO-5114 on the invasive growth of human breast cancer lines. MCF7 (**a**) and MDA-MB-231 (**b**) cells were cultured in the presence of 0 (line A), 75 (line B), 100 (line C), or 250 (line D) nM of HO-5114 for seven days, while the cell index was monitored in real-time. The results are shown as mean ± SEM of at least three independent experiments. * $p < 0.05$ compared to the untreated cells.

3. Discussion

TNBC is considered to have a poorer prognosis and a more limited targeted therapy repertoire than the HR+ subtype [19]. Additionally, the energy metabolism of the two breast cancer subtypes differs profoundly, which is indicated by the opposite effect of mitochondrial rescue on glycolytically inhibited HR+BC and TNBC cells; it is negative for the former and positive for the latter [10]. Accordingly, mitochondria-targeted compounds that compromise mitochondrial energy production may prove effective in the therapy of TNBC [13]. Mito-CP was reported to deplete the cellular ATP level, to inhibit mitochondrial oxygen consumption, to affect mitochondrial morphology, and to dissipate $\Delta\Psi_m$ [14]. As a component-derivative of Mito-CP [15], HO-5114 was expected to have similar mitochondrial effects. The drug exceeded these expectations because 10 μM of HO-5114 suppressed viability to about the same extent as 50 μM Mito-CP during a 24 h exposure [15]. In complete agreement with these previous results, in the present study, we found that even 1 μM of HO-5114 decreased the viability of both human breast cancer lines by more than 35%, while it almost completely suppressed it at a 10 μM concentration (Figure 1). At a longer exposure time (48 h), the drug's anti-proliferative effect became more pronounced in both the HR+ and the TNBC lines (Figure 1).

Mitochondria affect cancer cell survival through at least three major mechanisms: energy production, the intrinsic apoptotic pathway, and ROS generation [20]. These three pathways are interrelated because apoptosis is an energy-dependent process, while energy shortage and the resulting decrease in $\Delta\Psi_m$ leads to the release of pro-apoptotic intermembrane proteins, such as cytochrome c, an apoptosis-inducing factor, and endonuclease G [21]. ROS damages the mitochondrial electron-transport chain and thus the ATP production, while the compromised electron-transport chain produces more ROS [2]. ROS activates apoptosis via damaging macromolecules and interfering with the pro-apoptotic signaling pathways [22]. We observed a substantial induction of apoptosis after a 24 h exposure to 10 μM of HO-5114 in the TNBC line, while lower concentrations of the drug were ineffective in this respect (Figure 2b). In contrast, and in full agreement with the widely accepted view that TNBC is more apoptosis-resistant than HR+BC [11], even 1 μM of HO-5114 induced massive apoptosis in the MCF7 line (Figure 2a).

ROS participates in mediating cancer phenotype remodeling that manifests in apoptosis resistance and increased metastatic properties [23]. The chronic hypoxia prevalent in solid tumors results in the constant activation of the hypoxia-inducible factor-1α transcription factor that induces a malignant transformation associated metabolic remodeling [24]; however, we found a very similar extent of HO-5114-induced ROS formation in the MCF7 and MDA-MB-231 lines (Figure 3), although the latter represents a higher stage of metabolic transformation than the former [23]. The moderate increase in ROS accumulation in response to an increased HO-5114 concentration to 20 μM (Figure 3) also indicated that ROS production in the BC lines was insensitive to HO-5114 treatment, contrary to the expectation. The difference in conditions between solid tumors and the cell culture, where uniform oxygen and fuel supply is provided, may account for the discrepancy between the expected and observed ROS production. Elevated ROS production is considered to be necessary for survival and growth of TNBC cells [25], therefore, antioxidants are expected to hinder their survival [26]. However, we found that the antioxidant NAC increased the viability of control MDA-MB-231, while it did not affect MCF7 cells, indicating a higher ROS level that impeded proliferation in the former (Figure 4). The viability promoting effect of NAC overcompensated for the cytotoxic effect of HO-5114 at the concentration of up to 5 μM, but at 10 μM, it failed to do so (Figure 4b). The absence of NAC's effect on HO-5114′s cytotoxicity in the HR+BC line (Figure 4a) indicated not only a reduced chronic oxidative stress in it compared to the TNBC line but also suggested differences in metabolic reprogramming between the two BC cell lines [27].

The driving force for ATP synthesis is provided by $\Delta\Psi_m$; however, it has additional essential roles, such as transporting nuclearly encoded mitochondrial proteins [28], transporting K^+, Ca^{2+}, and Mg^{2+} [29], generating ROS [30], mitochondrial quality control [31],

and the regulation of pro-apoptotic intermembrane protein release [32–34]. Cell survival essentially relies on the maintenance of $\Delta\Psi_m$. Accordingly, in ischemic situations, the F_oF_1 ATPase can operate in reverse mode and consume ATP to maintain $\Delta\Psi_m$ to rescue the cell. The ATP is supplied by the substrate-level phosphorylation of non-glucose substrates under these conditions; however, considering the amount of the available non-glucose substrate pool, this survival attempt is often futile [35–37]. In solid tumors, the cancer cells must adapt their metabolism to the chronic hypoxia and partially ischemic situation [38,39]. In contrast to ROS induction, we observed a very sensitive response of $\Delta\Psi_m$ loss to HO-5114 treatment. Even 1 μM of the drug induced significant changes in $\Delta\Psi_m$ during as short a treatment as 1 h for the MCF7 line and 2.5 h for the MDA-MB-231 line (Figure 5).

Cancer cells face a double challenge in producing enough energy and a sufficient metabolic intermediate for proliferation in a predominantly hypoxic and partially ischemic environment [40]. Mostly, they rely on glycolysis rather than mitochondrial oxidative phosphorylation, even if sufficient oxygen is available for the latter [41]. Accordingly, increased glucose uptake is a characteristic feature of tumors that is used to identify them by ^{18}F-deoxyglucose positron emission tomography [42,43] for diagnostic purposes. On the other hand, the most malignant cancer types, such as metastatic tumor cells, therapy-resistant tumor cells, and cancer stem cells, rely on mitochondrial ATP synthesis [44,45]. The survival, proliferation, and metastasis of these cells depend on the oxidative phosphorylation and form the basis of their therapy resistance [46,47]. Accordingly, for the most malignant cancer types, oxidative phosphorylation is an emerging therapeutic target [48], and drugs significantly affecting tumor cell metabolism may have therapeutic value [38]. Considering its effects on energy metabolism in human breast cancer lines, HO-5114 fulfills this criterion. At a 1 and 2.5 μM concentration, it significantly diminished all OCR-related parameters in both cell lines except coupling efficiency (Figure 6). HO-5114 at a 2.5 μM concentration reduced ATP production that could contribute to the drug's anti-metastatic property. In complete agreement with its effect on the viability of BC lines, NAC counteracted the inhibitory effect of HO-5114 on the various parameters of cellular energy metabolism except the proton leak (Figure 7). These data support the conclusion that HO-5114 affects the energy metabolism of the BC lines. The proton leak can indicate damage to the mitochondrial respiratory chain or regulation of mitochondrial ATP synthesis via uncoupling proteins (UCPs) [49]. Indeed, the role of UCP2 in regulating the balance between substrate-level and oxidative phosphorylation has recently been reported [50]. We found that both BC lines increased ECAR, i.e., substrate-level phosphorylation when oxidative ATP production was blocked by oligomycin (Figures 6 and 7). ECAR in the MDA-MB-231 line even returned to its initial rate when the oxidative phosphorylation was uncoupled by FCCP (Figures 6 and 7), demonstrating that the balance between the two ATP producing machinery is more responsive in the TN than in the HR+BC cells.

The hormone receptor status determines the cell proliferation, differentiation, and cancer progression properties of breast cancers [51]. Accordingly, the MDA-MB-231 line represents a more aggressive, apoptosis- and therapy-resistant phenotype than the HR+ MCF7 line. The results of the aforementioned experiments that involved 1–24 h exposure to HO-5114 were in line with this view; however, in the colony formation (Figure 8) and invasive growth (Figure 9) experiments, where the cells were exposed to a 50–250 nM concentration of the drug for seven days, MDA-MB-231 proved to be more sensitive to the treatment than the MCF7 line. The reason for this difference in sensitivity to HO-5114 treatment between short- and long-term exposure is not clear based on the experiments.

In conclusion, all data acquired in this study indicated that HO-5114 had a robust anti-neoplastic effect on cultured BC cells. Furthermore, resistance to HO-5114 treatment did not differ markedly between the HR+ and TNBC lines. The latter even seemed to be more sensitive to the drug in models involving long-term treatment; however, in vitro cell culture effects translate poorly to human therapy. Accordingly, to establish the therapeutic potentiality of HO-5114, follow up experiments have to be performed in animal models for determining its in vivo toxicity and anti-neoplastic effectiveness.

4. Materials and Methods

4.1. Reagents

Hexadecyl (1-oxyl-2,2,5,5-tetramethyl-2,5-dihydro-1H-pyrrol-3-yl) diphenylphosphonium bromide (HO-5114) was synthesized and purified by us (MI and TK). All other reagents were of the highest purity commercially available.

4.2. Cell Cultures

MCF7 and MDA-MB-231 cell lines were purchased from American Type Culture Collection (Manassas, VA, USA). Cells were grown and maintained in a humidified incubator at 37 °C with 5% CO_2. Estrogen and progesterone receptor-positive MCF7 cells were cultured in RPMI (Biosera, Nuaille, France) supplemented with 10% fetal bovine serum (FBS). Triple-negative MDA-MB-231 cells were cultured in DMEM Low Glucose (Biosera, Nuaille, France) augmented with 10% FBS (Thermo Fisher, Life Technologies, Milan, Italy).

4.3. Viability Assay

Cells were seeded at a density of an 8×10^3/well in 96-well cell culture plates 24 h before the treatment. After 24 h of treatment with 1, 2.5, 5, or 10 μM of HO-5114, the medium was discarded, and the cells were washed with phosphate buffered saline (PBS; Biowest, Nuaille, France) and fixed in 100 μL of a cold 10% trichloroacetic acid (TCA) solution (Sigma-Aldrich Co., Budapest, Hungary) for 30 min at 4 °C. After TCA was discarded, the cells were washed with a 1% acetic acid solution (Sigma-Aldrich Co., Budapest, Hungary) and dried overnight at room temperature. The next day, 70 μL 0.1% sulforhodamine B (SRB) (Sigma-Aldrich Co., Budapest, Hungary) in a 1% acetic acid solution was added to the wells for 20 min at room temperature. The plates were washed 5 times with a 1% acetic acid solution and dried for at least 2 h. Added to the cell was 200 μL of a 10 mM TRIS solution (Sigma-Aldrich Co., Budapest, Hungary) and the samples were incubated at room temperature on a plate shaker for 3 h. Absorbance was measured at 560 and 600 nm simultaneously using the GloMax®-Multi Instrument (Promega, Madison, WI, USA). OD_{600} was subtracted as the background from the OD_{560} values.

4.4. Flow Cytometric Analysis of Cell Death

A flow cytometry analysis was applied to quantify the ratio of live, early apoptotic, and late apoptotic/dead cell populations. The cells were seeded into 6-well plates at a starting density of 10^5/well 24 h before they were treated with 1, 2.5, 5, or 10 μM of HO-5114 for 24 h. The FITC-Annexin V Apoptosis Detection Kit with PI (BioLegend, San Diego, CA, USA) was used to label cells according to the manufacturer's instructions. The samples were measured with a SONY SH800 Cell Sorter (SONY Biotechnology, San Jose, CA, USA). Debris and aggregates had been eliminated by gating, and at least 20,000 single cell events were acquired per sample. The analysis was carried out with Cell Sorter Software (SONY Biotechnology, San Jose, CA, USA). Double negative (Annexin V−/PI−) cells were considered live. Annexin V positive (Annexin V+/PI−) and double positive (Annexin V+/PI+) cells were identified as early and late apoptotic, respectively. PI positive (Annexin V−/PI+) necrotic cells were not detected. They were likely eliminated during the washing steps prior to staining.

4.5. Measurement of ROS Production

To measure intracellular ROS production, the cells were seeded at a starting density of 1.5×10^4/well into 96-well plates and were cultured for 24 h. The cells were treated with 1, 2.5, 5, 10, or 20 μM of HO-5114 in a Krebs-Henseleit solution supplemented with 10% FBS and containing dihydrorhodamine 123 (Sigma-Aldrich Co., Budapest, Hungary). ROS generation was monitored from 0 min until 4 h using the GloMax®-Multi Instrument (Promega, Madison, WI, USA) at respective excitation/emission wavelengths of 490/525 nm.

4.6. Measurement of Mitochondrial Bioenergetics

To analyze respiratory and glycolytic energy production, OCR and ECAR were measured simultaneously by a Seahorse XFp Extracellular Flux Analyzer (Agilent Technologies, Santa Clara, CA, USA). The cells were plated at a starting density of 1.5×10^4/well into Seahorse XFp Cell Culture Miniplates 24 h before treatment. The medium was replaced to the Seahorse XF Assay Media (pH 7.4) containing 10 mM glucose, 2 mM L-glutamine, and 1 mM pyruvate. After measuring the basal respiration for 18 min, HO-5114 was added to the medium at a final concentration of 1 or 2.5 μM, and the cells were further incubated for 4 h. In the final 75 min of incubation, recording of OCR and ECAR was resumed, and the following modulators were injected sequentially: oligomycin (1.5 μM final concentration), FCCP (1 μM final concentration), and rotenone and antimycin A (0.5 μM final concentration each). The OCR and ECAR data were normalized to total cellular protein, which was determined by the Micro BCA Protein Assay kit (Thermo Fisher Scientific, Waltham, MA, USA).

4.7. Measurement of Mitochondrial Membrane Potential

The cells were seeded to glass coverslips in 6-well plates at a starting density of 1.5×10^5 cells/well and were cultured for 24 h. They were treated with 1 and 2.5 μM HO-5114 for 1 or 2.5 h for the MCF7 or MDA-MB-231 lines, respectively. After treatment, the cells were washed in PBS and incubated for 15 min at 37 °C in a modified Krebs-Henseleit solution containing 100 ng/mL of the cationic carbocyanine dye JC-1 (5,5′,6,6′-tetrachloro-1,1′,3,3′tetraethylbenzimidazolylcarbocyanine iodide). Following incubation, the cells were washed once with a modified Krebs-Henseleit solution and then visualized by a Nikon Eclipse Ti-U fluorescent microscope equipped with a Spot RT3 camera using a 20× objective lens and epifluorescent illumination. The same microscopic fields were imaged with a 490 nm bandpass excitation and >590 nm (red) or <546 nm (green) emission filters, consecutively. For quantifying red and green fluorescent intensities, their respective greyscale images were normalized to three randomly chosen spots of their backgrounds. Red and green fluorescent intensities were calculated as the percentage of their sum.

4.8. Colony Formation Assay

The cells were seeded at a starting density of 2×10^3/well into 6-well plates and were cultured for 24 h before they were exposed to 50, 75, 100, or 250 nM of HO-5114 for seven days. Then, the cells were washed with PBS and were stained with 0.1% Coomassie Brilliant blue R 250 (Merck KGaA, Darmstadt, Germany) in 30% methanol (Sigma-Aldrich Co., Budapest, Hungary) and 10% acetic acid. The tissue culture plates were imaged using a GE Healthcare ImageScanner II (AP Hungary Co., Budapest, Hungary) set for 600 dpi. The colonies were quantified using ImageJ software.

4.9. Measurement of Invasive Growth

To monitor the effects of HO-5114 on the growth of MCF7 and MDA-MB-231 cells, we used the xCELLigence system that allows for the real-time, quantitative analysis of adherent cells. The measurement method is based on the use of electronic microtiter plates (E-Plate®), in the xCELLigence Real-Time Cell Analysis (RTCA) device (ACEA Biosciences, San Diego, CA, USA); both were used according to the manufacturer's protocol. The instrument was placed in a humidified incubator at 37 °C and 5% CO_2. Cells were seeded at the starting density of 1×10^3/well and were cultured for 24 h. Then, the cells were exposed to 75, 100, and 250 nM HO-5114 for seven days in the E-Plate®, during which the impedance was measured each hour.

4.10. Statistical Analysis

The results are presented as mean ± standard error of the mean (SEM) of at least three independent experiments. The statistical differences between the groups were analyzed by a one-way ANOVA with the Tukey post-hoc test using OriginPro® software (Originlab

Corp., Northampton, MA, USA). The differences among the groups were regarded as significant at $p < 0.05$.

Author Contributions: Conceptualization, T.K. and F.G.J.; methodology, K.K. and Z.B.; software, V.B.V.; formal analysis, K.A., K.K. and A.S.; data acquisition, K.A., A.S., D.K., B.K., E.V. and M.I.; writing—original draft preparation, K.A. and F.G.J.; writing—review and editing, F.G.J.; visualization, K.A. and D.K.; funding acquisition, Z.B., T.K. and F.G.J. All authors have read and agreed to the published version of the manuscript.

Funding: This project was supported within the framework of 2020-4.1.1.-TKP2020 (T.K.), by EFOP 3.6.1.-16-2016-00004 and the Excellence Programme of the Ministry of Human Resources, Hungary (T.K., F.G.J.), and the János Bolyai Research Scholarship of the Hungarian Academy of Sciences (Z.B.).

Institutional Review Board Statement: Not applicable.

Informed Consent Statement: Not applicable.

Data Availability Statement: All data are presented in the paper.

Conflicts of Interest: The authors declare no conflict of interest. The funders had no role in the design of the study, in the collection, analyses, or interpretation of data, in the writing of the manuscript, or in the decision to publish the results.

Abbreviations

ANOVA	Analysis of variance
ΔΨm	Mitochondrial membrane potential
ECAR	Extracellular acidification rate
FBS	Fetal bovine serum
FCCP	Carbonyl cyanide 4-(trifluoromethoxy) phenylhydrazone
FITC	Fluorescein isothiocyanate
HR+BC	Hormone receptor positive breast cancer
NAC	N-acetylcysteine
OCR	Oxygen consumption rate
PI	Propidium iodide
R + AmA	Rotenone and antimycin A
ROS	Reactive oxygen species
SD	Standard deviation
SEM	Standard error of the mean
SRB	Sulforhodamine B
TCA	Trichloroacetic acid
TNBC	Triple-negative breast cancer
TPP	Tryphenylphosphonium

References

1. Dong, L.; Gopalan, V.; Holland, O.; Neuzil, J. Mitocans Revisited: Mitochondrial Targeting as Efficient Anti-Cancer Therapy. *Int. J. Mol. Sci.* **2020**, *21*, 7941. [CrossRef]
2. Weinberg, F.; Hamanaka, R.; Wheaton, W.W.; Weinberg, S.; Joseph, J.; Lopez, M.; Kalyanaraman, B.; Mutlu, G.M.; Budinger, G.R.; Chandel, N.S. Mitochondrial metabolism and ROS generation are essential for Kras-mediated tumorigenicity. *Proc. Natl. Acad. Sci. USA* **2010**, *107*, 8788–8793. [CrossRef]
3. Dong, L.; Neuzil, J. Targeting mitochondria as an anticancer strategy. *Cancer Commun.* **2019**, *39*, 63. [CrossRef]
4. Battogtokh, G.; Cho, Y.Y.; Lee, J.Y.; Lee, H.S.; Kang, H.C. Mitochondrial-Targeting Anticancer Agent Conjugates and Nanocarrier Systems for Cancer Treatment. *Front. Pharmacol.* **2018**, *9*, 922. [CrossRef] [PubMed]
5. Murphy, M.P. Selective targeting of bioactive compounds to mitochondria. *Trends Biotechnol.* **1997**, *15*, 326–330. [CrossRef]
6. Smith, R.A.; Porteous, C.M.; Gane, A.M.; Murphy, M.P. Delivery of bioactive molecules to mitochondria in vivo. *Proc. Natl. Acad. Sci. USA* **2003**, *100*, 5407–5412. [CrossRef] [PubMed]
7. Zielonka, J.; Joseph, J.; Sikora, A.; Hardy, M.; Ouari, O.; Vasquez-Vivar, J.; Cheng, G.; Lopez, M.; Kalyanaraman, B. Mitochondria-Targeted Triphenylphosphonium-Based Compounds: Syntheses, Mechanisms of Action, and Therapeutic and Diagnostic Applications. *Chem. Rev.* **2017**, *117*, 10043–10120. [CrossRef]

8. Porteous, C.M.; Logan, A.; Evans, C.; Ledgerwood, E.C.; Menon, D.K.; Aigbirhio, F.; Smith, R.A.; Murphy, M.P. Rapid uptake of lipophilic triphenylphosphonium cations by mitochondria in vivo following intravenous injection: Implications for mitochondria-specific therapies and probes. *Biochim. Biophys. Acta* **2010**, *1800*, 1009–1017. [CrossRef] [PubMed]
9. Schulze, A.; Harris, A.L. How cancer metabolism is tuned for proliferation and vulnerable to disruption. *Nature* **2012**, *491*, 364–373. [CrossRef]
10. Reda, A.; Refaat, A.; Abd-Rabou, A.A.; Mahmoud, A.M.; Adel, M.; Sabet, S.; Ali, S.S. Role of mitochondria in rescuing glycolytically inhibited subpopulation of triple negative but not hormone-responsive breast cancer cells. *Sci. Rep.* **2019**, *9*, 13748. [CrossRef] [PubMed]
11. Collignon, J.; Lousberg, L.; Schroeder, H.; Jerusalem, G. Triple-negative breast cancer: Treatment challenges and solutions. *Breast Cancer* **2016**, *8*, 93–107. [CrossRef]
12. Dhanasekaran, A.; Kotamraju, S.; Karunakaran, C.; Kalivendi, S.V.; Thomas, S.; Joseph, J.; Kalyanaraman, B. Mitochondria superoxide dismutase mimetic inhibits peroxide-induced oxidative damage and apoptosis: Role of mitochondrial superoxide. *Free Radic. Biol. Med.* **2005**, *39*, 567–583. [CrossRef] [PubMed]
13. Cheng, G.; Zielonka, J.; Dranka, B.P.; McAllister, D.; Mackinnon, A.C., Jr.; Joseph, J.; Kalyanaraman, B. Mitochondria-targeted drugs synergize with 2-deoxyglucose to trigger breast cancer cell death. *Cancer Res.* **2012**, *72*, 2634–2644. [CrossRef]
14. Boyle, K.A.; Van Wickle, J.; Hill, R.B.; Marchese, A.; Kalyanaraman, B.; Dwinell, M.B. Mitochondria-targeted drugs stimulate mitophagy and abrogate colon cancer cell proliferation. *J. Biol. Chem.* **2018**, *293*, 14891–14904. [CrossRef] [PubMed]
15. Isbera, M.; Bognár, B.; Gallyas, F.; Bényei, A.; Jekő, J.; Kálai, T. Syntheses and Study of a Pyrroline Nitroxide Condensed Phospholene Oxide and a Pyrroline Nitroxide Attached Diphenylphosphine. *Molecules* **2021**, *26*, 4366. [CrossRef]
16. Vichai, V.; Kirtikara, K. Sulforhodamine B colorimetric assay for cytotoxicity screening. *Nat. Protoc.* **2006**, *1*, 1112–1116. [CrossRef] [PubMed]
17. Ghoneum, A.; Abdulfattah, A.Y.; Warren, B.O.; Shu, J.; Said, N. Redox Homeostasis and Metabolism in Cancer: A Complex Mechanism and Potential Targeted Therapeutics. *Int. J. Mol. Sci.* **2020**, *21*, 3100. [CrossRef]
18. Dowling, C.M.; Herranz Ors, C.; Kiely, P.A. Using real-time impedance-based assays to monitor the effects of fibroblast-derived media on the adhesion, proliferation, migration and invasion of colon cancer cells. *Biosci. Rep.* **2014**, *34*, e00126. [CrossRef]
19. Masoud, V.; Pages, G. Targeted therapies in breast cancer: New challenges to fight against resistance. *World J. Clin. Oncol.* **2017**, *8*, 120–134. [CrossRef]
20. Guerra, F.; Arbini, A.A.; Moro, L. Mitochondria and cancer chemoresistance. *Biochim. Biophys. Acta Bioenerg.* **2017**, *1858*, 686–699. [CrossRef] [PubMed]
21. Burke, P.J. Mitochondria, Bioenergetics and Apoptosis in Cancer. *Trends Cancer* **2017**, *3*, 857–870. [CrossRef]
22. Redza-Dutordoir, M.; Averill-Bates, D.A. Activation of apoptosis signalling pathways by reactive oxygen species. *Biochim. Biophys. Acta* **2016**, *1863*, 2977–2992. [CrossRef]
23. Godet, I.; Shin, Y.J.; Ju, J.A.; Ye, I.C.; Wang, G.; Gilkes, D.M. Fate-mapping post-hypoxic tumor cells reveals a ROS-resistant phenotype that promotes metastasis. *Nat. Commun.* **2019**, *10*, 4862. [CrossRef]
24. Schito, L.; Semenza, G.L. Hypoxia-Inducible Factors: Master Regulators of Cancer Progression. *Trends Cancer* **2016**, *2*, 758–770. [CrossRef]
25. Sarmiento-Salinas, F.L.; Delgado-Magallon, A.; Montes-Alvarado, J.B.; Ramirez-Ramirez, D.; Flores-Alonso, J.C.; Cortes-Hernandez, P.; Reyes-Leyva, J.; Herrera-Camacho, I.; Anaya-Ruiz, M.; Pelayo, R.; et al. Breast Cancer Subtypes Present a Differential Production of Reactive Oxygen Species (ROS) and Susceptibility to Antioxidant Treatment. *Front. Oncol.* **2019**, *9*, 480. [CrossRef]
26. Kwon, Y. Possible Beneficial Effects of N-Acetylcysteine for Treatment of Triple-Negative Breast 555 Cancer. *Antioxidants* **2021**, *10*, 169. [CrossRef]
27. Martinez-Reyes, I.; Chandel, N.S. Cancer metabolism: Looking forward. *Nat. Rev. Cancer* **2021**. [CrossRef] [PubMed]
28. Neupert, W.; Herrmann, J.M. Translocation of proteins into mitochondria. *Annu. Rev. Biochem.* **2007**, *76*, 723–749. [CrossRef] [PubMed]
29. Zorova, L.D.; Popkov, V.A.; Plotnikov, E.Y.; Silachev, D.N.; Pevzner, I.B.; Jankauskas, S.S.; Babenko, V.A.; Zorov, S.D.; Balakireva, A.V.; Juhaszova, M.; et al. Mitochondrial membrane potential. *Anal. Biochem.* **2018**, *552*, 50–59. [CrossRef]
30. Korshunov, S.S.; Skulachev, V.P.; Starkov, A.A. High protonic potential actuates a mechanism of production of reactive oxygen species in mitochondria. *FEBS Lett.* **1997**, *416*, 15–18. [CrossRef]
31. Srinivasan, S.; Guha, M.; Kashina, A.; Avadhani, N.G. Mitochondrial dysfunction and mitochondrial dynamics—The cancer connection. *Biochim. Biophys. Acta Bioenerg.* **2017**, *1858*, 602–614. [CrossRef]
32. Green, D.R.; Reed, J.C. Mitochondria and apoptosis. *Science* **1998**, *281*, 1309–1312. [CrossRef] [PubMed]
33. Tait, S.W.; Green, D.R. Mitochondrial regulation of cell death. *Cold Spring Harb. Perspect. Biol.* **2013**, *5*, a008706. [CrossRef] [PubMed]
34. Fatokun, A.A.; Dawson, V.L.; Dawson, T.M. Parthanatos: Mitochondrial-linked mechanisms and therapeutic opportunities. *Br. J. Pharmacol.* **2014**, *171*, 2000–2016. [CrossRef] [PubMed]
35. Baxter, P.; Chen, Y.; Xu, Y.; Swanson, R.A. Mitochondrial dysfunction induced by nuclear poly(ADP-ribose) polymerase-1: A treatable cause of cell death in stroke. *Transl. Stroke Res.* **2014**, *5*, 136–144. [CrossRef] [PubMed]

36. Chinopoulos, C.; Seyfried, T.N. Mitochondrial Substrate-Level Phosphorylation as Energy Source for Glioblastoma: Review and Hypothesis. *ASN Neuro* **2018**, *10*, 1759091418818261. [CrossRef] [PubMed]
37. Chinopoulos, C. Acute sources of mitochondrial NAD(+) during respiratory chain dysfunction. *Exp. Neurol.* **2020**, *327*, 113218. [CrossRef]
38. Weinberg, S.E.; Chandel, N.S. Targeting mitochondria metabolism for cancer therapy. *Nat. Chem. Biol.* **2015**, *11*, 9–15. [CrossRef] [PubMed]
39. Ashley, N.; Poulton, J. Mitochondrial DNA is a direct target of anti-cancer anthracycline drugs. *Biochem. Biophys. Res. Commun.* **2009**, *378*, 450–455. [CrossRef]
40. Bennett, N.K.; Nguyen, M.K.; Darch, M.A.; Nakaoka, H.J.; Cousineau, D.; Ten Hoeve, J.; Graeber, T.G.; Schuelke, M.; Maltepe, E.; Kampmann, M.; et al. Defining the ATPome reveals cross-optimization of metabolic pathways. *Nat. Commun.* **2020**, *11*, 4319. [CrossRef]
41. Warburg, O. On respiratory impairment in cancer cells. *Science* **1956**, *124*, 269–270.
42. Gatenby, R.A.; Gillies, R.J. Why do cancers have high aerobic glycolysis? *Nat. Rev. Cancer* **2004**, *4*, 891–899. [CrossRef] [PubMed]
43. Kroemer, G.; Pouyssegur, J. Tumor cell metabolism: Cancer's Achilles' heel. *Cancer Cell* **2008**, *13*, 472–482. [CrossRef] [PubMed]
44. LeBleu, V.S.; O'Connell, J.T.; Gonzalez Herrera, K.N.; Wikman, H.; Pantel, K.; Haigis, M.C.; de Carvalho, F.M.; Damascena, A.; Domingos Chinen, L.T.; Rocha, R.M.; et al. PGC-1alpha mediates mitochondrial biogenesis and oxidative phosphorylation in cancer cells to promote metastasis. *Nat. Cell Biol.* **2014**, *16*, 992–1003, 1001–1015. [CrossRef]
45. Lin, C.S.; Liu, L.T.; Ou, L.H.; Pan, S.C.; Lin, C.I.; Wei, Y.H. Role of mitochondrial function in the invasiveness of human colon cancer cells. *Oncol. Rep.* **2018**, *39*, 316–330. [CrossRef]
46. Hirpara, J.; Eu, J.Q.; Tan, J.K.M.; Wong, A.L.; Clement, M.V.; Kong, L.R.; Ohi, N.; Tsunoda, T.; Qu, J.; Goh, B.C.; et al. Metabolic reprogramming of oncogene-addicted cancer cells to OXPHOS as a mechanism of drug resistance. *Redox. Biol.* **2019**, *25*, 101076. [CrossRef]
47. Zhang, G.; Frederick, D.T.; Wu, L.; Wei, Z.; Krepler, C.; Srinivasan, S.; Chae, Y.C.; Xu, X.; Choi, H.; Dimwamwa, E.; et al. Targeting mitochondrial biogenesis to overcome drug resistance to MAPK inhibitors. *J. Clin. Investig.* **2016**, *126*, 1834–1856. [CrossRef]
48. Ashton, T.M.; McKenna, W.G.; Kunz-Schughart, L.A.; Higgins, G.S. Oxidative Phosphorylation as an Emerging Target in Cancer Therapy. *Clin. Cancer Res.* **2018**, *24*, 2482–2490. [CrossRef] [PubMed]
49. Baffy, G. Mitochondrial uncoupling in cancer cells: Liabilities and opportunities. *Biochim. Biophys. Acta Bioenerg.* **2017**, *1858*, 655–664. [CrossRef]
50. Vozza, A.; Parisi, G.; De Leonardis, F.; Lasorsa, F.M.; Castegna, A.; Amorese, D.; Marmo, R.; Calcagnile, V.M.; Palmieri, L.; Ricquier, D.; et al. UCP2 transports C4 metabolites out of mitochondria, regulating glucose and glutamine oxidation. *Proc. Natl. Acad. Sci. USA* **2014**, *111*, 960–965. [CrossRef]
51. Karamanou, K.; Franchi, M.; Vynios, D.; Brezillon, S. Epithelial-to-mesenchymal transition and invadopodia markers in breast cancer: Lumican a key regulator. *Semin. Cancer Biol.* **2020**, *62*, 125–133. [CrossRef] [PubMed]